

**Fluctuations**  
in  
**Quantum Optical Systems:**  
From  
**Bose-Einstein Condensates**  
to  
**Squeezed States of Light**

Von der Fakultät für Mathematik und Physik der  
Gottfried Wilhelm Leibniz Universität Hannover  
zur Erlangung des Grades

**Doktor der Naturwissenschaften**

Dr. rer. nat.

genehmigte

**Dissertation**

von

**Alem Mebrahtu Tesfamariam**

**2006**



Referent: Prof. Dr. Maciej Lewenstein  
Korreferent: Prof. Dr. Luis Santos

Tag der Promotion: 26.10.2006



# Abstract

In this Thesis we study the theory of fluctuations in quantum optical systems: from Bose-Einstein condensates to squeezed states of light. The Thesis is divided into three parts, which, although dealing with different areas of quantum optics have a joint aspect in that they concern fluctuations.

In the first part we consider the problem of evaporative cooling of an atomic gas towards high phase space densities. Thermal fluctuations in such a gas may be very well described by classical Monte Carlo methods and molecular dynamics. Nevertheless, the described process of evaporative cooling leads to the realization of a quantum degenerate regime. Applying molecular dynamics simulation we study the dynamics of evaporative cooling of cold gaseous  $^{87}\text{Rb}$  atoms in an anisotropic trap loaded continuously from an incoming atomic beam. Based on this simulation, we show that it is possible to continuously trap more than  $10^8$  atoms with a relatively high phase space density exceeding 0.011 at an equilibrium temperature of nearly  $20 \mu\text{K}$ .

In the second part of the Thesis we deal with the physics of Bose-Einstein condensates. We present an introduction to the basics of Bose-Einstein condensation (BEC), including the quantum description of fluctuations at zero temperature via Bogoliubov-de Gennes equations. We describe the problem of 1D BEC (quasi-BEC) in detail and study the problem of splitting and merging process at finite temperature. Fluctuations are described by quantum quasi-particle modes that are highly occupied, allowing us to simulate phase fluctuations using a classical approach. We show that, at zero temperature and for a sufficiently adiabatic process, coherent splitting and merging with a constant relative phase between the initial and the final merged condensates is possible. At finite temperature our results show that there are strong phase fluctuations during the process but the pattern of the Thomas-Fermi density profile is preserved although the “overall” phase of the condensate is not. We study also nonlinear effects in 1D BEC, and in particular solitons and their dynamical behaviour. After presenting the basics of solitons in BEC, we investigate methods of realising quantum switches/memories with bright matter wave lattice solitons using “effective” potential barrier/well cor-

responding to defects in an optical lattice. In the case of "effective" potential barrier, when the kinetic energy of the soliton is of the order of the barrier height, we show that the system can be used as a quantum switch. On the other hand, when the defect is of an "effective" well type, in the limit where the well depth is much larger than the kinetic energy and in a trapping regime, it is possible to release the solitons at will keeping most of the atoms within the solitonic structure opening possibilities for applications as quantum memories.

The last part of the Thesis deals with squeezing phenomena in non-degenerate parametric oscillator which, under favourable conditions, generates squeezed states of light. This part concerns fully with quantum fluctuations that have no classical analogy. The description of the optical system is based on solving Fokker Planck equation for the quantum Q-representation. When the optical system operates below threshold, we show that it is possible to significantly suppress, or squeeze quantum fluctuations in one quadrature below the standard quantum limit at the expense of highly enhanced fluctuations at the other.

In this way the Thesis covers several levels and methods of description of fluctuations in quantum optics: classical, semi-classical, semi-quantum and purely quantum.

**keywords:**

fluctuations, molecular dynamics, Bose-Einstein condensation, phase and density fluctuations, matter wave solitons, quantum switch and memory, parametric oscillator, squeezed states of light, Q-function.

# Zusammenfassung

In dieser Arbeit untersuchen wir Fluktuationseffekte in quantenoptischen Systemen: von Bose-Einstein Kondensaten zu gequetschten Lichtzuständen. Die Arbeit gliedert sich in drei Teile, welche zwar in verschiedenen Bereichen der Quantenoptik anzusiedeln sind, jedoch im Kernaspekt stets durch Fluktuationsphänomene bestimmt sind.

Im ersten Abschnitt betrachten wir die evaporative Kühlung eines atomaren Gases hin zu hohen Phasenraumdichten. In solch einem Ensemble lassen sich thermische Fluktuationen hinreichend gut im Rahmen klassischer Monte-Carlo-Methoden und molekularer Dynamik beschreiben. Nichtsdestotrotz mündet der beschriebene Prozess letztendlich im quantenentarteten Regime. Mittels dieser molekulardynamischen Simulation studieren wir das evaporative Kühlverhalten atomaren  $^{87}\text{Rb}$  Gases in einer anisotropen Falle, die kontinuierlich von einem einfallenden atomaren Strahl geladen wird. Auf diese Weise demonstrieren wir die Möglichkeit, mehr als  $10^8$  Atome mit einer Phasenraumdichte oberhalb von 0.011 bei einer Gleichgewichtstemperatur von ungefähr  $20\mu\text{K}$  kontinuierlich zu laden.

Im zweiten Teil der Arbeit untersuchen wir das physikalische Verhalten von Bose-Einstein Kondensaten. Wir stellen in diesem Rahmen die grundlegenden Konzepte der Bose-Einstein-Kondensation vor, insbesondere die Quantenbeschreibung von Fluktuationen am absoluten Nullpunkt mittels Bogoliubov-de Gennes Gleichungen.

Wir beschreiben detailliert das Problem eindimensionaler (Quasi-)Kondensate und untersuchen den Prozess des Trennens und Verschmelzens bei endlicher Temperatur. Fluktuationen werden hierbei durch hochbesetzte Quantenmoden von Quasiteilchen beschrieben, die einen klassischen Simulationzugang der auftretenden Phasenfluktuationen ermöglichen. Einen hinreichend adiabatischen Prozeß vorausgesetzt, zeigen wir, dass eine kohärente Trennung und Verschmelzung mit einer konstanten relativen Phase zwischen anfänglichem und reformiertem Kondensat bei  $T = 0$  möglich ist. Bei endlicher Temperatur zeigt sich, dass trotz starker Phasenfluktuationen die Struktur des Thomas-Fermi-Dichteprofiles erhalten ist, jedoch nicht die Gesamtphase des Kondensates. Zudem analysieren wir nichtlineare Effekte in 1D

Kondensaten, insbesondere Solitonen und ihr dynamisches Verhalten. Nach einer Einführung in das Thema ergründen wir Methoden zur Realisierung von Quantenschaltern und -speichern durch Materiewellen heller Gittersolitonen unter Hinzunahme effektiver Potentialbarrieren beziehungsweise -töpfe, die durch Defekte im optischen Gitter erzeugt werden. Im Fall einer effektiven Potentialschwelle zeigen wir, dass das System als Quantenschalter nutzbar ist, wenn die kinetische Energie des Solitons in der Größenordnung der Barrierenhöhe liegt. Im anderen Szenario eines effektiven Potentialtopfes eröffnen sich im Fallenregime unter gleichzeitigem Limes großer Potentialtiefe im Vergleich zur kinetischen Energie Möglichkeiten, Solitonen kontrolliert auszukoppeln, so dass ein Großteil der Atome in solitonischer Struktur erhalten bleibt. Solch ein System könnte daher zur Umsetzung eines Quantenspeichers herangezogen werden.

Der letzte Teil der Arbeit beschäftigt sich mit Quetschphänomenen in nichtentarteten parametrischen Oszillatoren, welche unter geeigneten Bedingungen gequetschte Lichtzustände generieren. Die dabei auftretenden Quantenfluktuationen besitzen kein klassisches Analogon. Die Beschreibung des optischen Systems basiert auf der Lösung der Fokker-Planck-Gleichung in der quantenmechanischen Darstellung der Q-Funktion. Wenn das System unter schwellig betrieben wird, zeigen wir, dass Quantenfluktuationen signifikant unterdrückt beziehungsweise in einer Quadratur unter das Standardquantenlimit gequetscht werden können. Die jeweiligen Fluktuationen in der anderen Quadratur werden dabei merklich verstärkt.

Zusammenfassend behandelt diese Arbeit verschiedene methodische Ebenen zur Beschreibung von Fluktuationsphänomenen in der Quantenoptik: klassische, semi-klassische, semi-quantenmechanische und rein quantenmechanische.

**Schlageworte:**

Fluktuationen, Moleculardynamik, Bose-Einstein Kondensation, Phasenfluktuationen und Dichtenfluktuationen, Materiewellensolitonen, Quantenschalter und -speichern, parametrischer Oszillator, gequetschte Zustände von Licht, Q-Funktion.

# Contents

<b>Abstract</b>	<b>v</b>
<b>1 Introduction</b>	<b>1</b>
1.1 Fluctuations in Quantum Physics . . . . .	3
1.2 Thermal and Quantum Fluctuations . . . . .	3
1.3 Fluctuations and the Uncertainty Principle . . . . .	4
1.4 Vacuum Fluctuations . . . . .	5
1.5 Outline of the Thesis . . . . .	6
<b>2 Evaporative Cooling for High Phase Space Density</b>	<b>9</b>
2.1 Cooling and Trapping Techniques . . . . .	9
2.1.1 Laser Cooling . . . . .	9
2.1.2 Atomic trapping . . . . .	10
2.1.3 Evaporative Cooling . . . . .	12
2.2 Molecular Dynamics Simulation for Evaporative Cooling . . .	12
2.2.1 Molecular Dynamics . . . . .	12
2.2.2 The Dynamics of Evaporative Cooling . . . . .	14
2.3 Summary . . . . .	21
<b>3 The Basics of Ultracold Degenerate Quantum Gases</b>	<b>23</b>
3.1 Mathematical Description of Bose-Einstein Condensation . . .	23
3.2 Historical Development of Bose-Einstein Condensates . . . . .	28
3.3 Mean-field Theory of Ultracold Bosonic Gases . . . . .	30
3.3.1 The Gross-Pitaevskii Equation . . . . .	30
3.3.2 Ground State Energy of Condensates . . . . .	33
3.3.3 The Bogoliubov-de Gennes Equations . . . . .	33
3.3.4 The Thomas-Fermi Approximation . . . . .	35
3.4 Summary . . . . .	36

<b>4</b>	<b>Splitting and Merging Elongated BEC at Finite Temperature</b>	<b>37</b>
4.1	Description of the Model . . . . .	41
4.2	Splitting and Merging at Zero Temperature . . . . .	44
4.3	Splitting and Merging at Finite Temperature . . . . .	46
4.4	Summary . . . . .	50
<b>5</b>	<b>Quantum Switches and Memories for Matter Wave Lattice Solitons</b>	<b>53</b>
5.1	The Physical System . . . . .	54
5.2	"Effective" Potential Barrier . . . . .	56
5.3	"Effective" Potential Well . . . . .	61
5.4	Control of the Collisions . . . . .	65
5.5	Summary . . . . .	66
<b>6</b>	<b>Parametric Oscillation with Squeezed Vacuum Reservoirs</b>	<b>67</b>
6.1	The Master Equation . . . . .	68
6.2	The Fokker-Planck Equation . . . . .	74
6.3	Solution of the Fokker-Planck Equation . . . . .	76
6.4	Quadrature Squeezing . . . . .	83
6.4.1	Quadrature Squeezing in a DPO . . . . .	83
6.4.2	Quadrature Squeezing in a NDPO . . . . .	87
6.5	Summary . . . . .	91
<b>7</b>	<b>Conclusion</b>	<b>93</b>
<b>A</b>	<b>The Bogoliubov-de Gennes Equations</b>	<b>95</b>
<b>B</b>	<b>Derivation of Master Equation for the NDPO</b>	<b>97</b>
<b>C</b>	<b>Expectation Values of Squeezed Vacuum Reservoir Modes</b>	<b>109</b>
<b>D</b>	<b>Acknowledgements</b>	<b>113</b>
<b>E</b>	<b>Dedication</b>	<b>117</b>
<b>F</b>	<b>List of Publications</b>	<b>119</b>
<b>G</b>	<b>Curriculum Vitae</b>	<b>121</b>
	<b>Bibliography</b>	<b>123</b>
	<b>Index</b>	<b>135</b>

# List of Figures

2.1	Scheme of a Magneto-optical trap . . . . .	11
2.2	Continuous loading of an anisotropic atom trap for a high phase space density . . . . .	15
2.3	Continuous trapping of atoms in an anisotropic trap . . . . .	17
2.4	Determination of equilibrium temperature of trapped atoms . . . . .	18
2.5	Phase space density of trapped atoms in an anisotropic trap . . . . .	19
2.6	Evolution of radial and axial truncation parameters . . . . .	20
3.1	Cooling toward Bose-Einstein condensation . . . . .	28
3.2	The first experimentally observed BEC of $^{87}\text{Rb}$ . . . . .	29
3.3	Thomas-Fermi density profile of 1D BEC of $^{87}\text{Rb}$ . . . . .	35
4.1	Double-well potential for splitting and merging 1D BEC . . . . .	42
4.2	Model for switching on and off a double-well potential . . . . .	44
4.3	Adiabatic splitting and merging of 1D BEC at $T = 0$ . . . . .	45
4.4	Non-adiabatic splitting and merging at zero temperature . . . . .	46
4.5	Phase fluctuations in 1D BEC at finite temperature . . . . .	49
4.6	Splitting and merging 1D BEC at finite temperature . . . . .	50
5.1	Transmission and reflection coefficients of solitons with an “effective” potential barrier . . . . .	57
5.2	Reflection, transmission and trapping of lattice solitons . . . . .	59
5.3	Delay time in transmission as a function ‘barrier’ amplitude . . . . .	60
5.4	Temporal evolution of trapped fraction density of the soliton interacting with an “effective” well and a contour of the space-time evolution of the lattice soliton . . . . .	62
5.5	Time evolution of trapped of trapped fraction density of solitons interacting with an “effective” potential well . . . . .	64
5.6	Collision between two identical solitons in the presence of a defect . . . . .	65
6.1	Scheme for generating squeezed states of light from a NDPO . . . . .	72

6.2	A simple description of quadrature squeezing of quantum fluctuations . . . . .	84
-----	--	----

# Chapter 1

## Introduction

Quantum physics defines fluctuations as temporary variations in the amount of energy in a point in space that arise from the uncertainty principle. In this Chapter we present a general introduction to the Thesis and a brief description about fluctuations. We verify thermal, quantum and vacuum fluctuations, and explore their relations with the uncertainty principle [1–4]. We conclude this Chapter by presenting the outline of the Thesis.

In every physical process there are always some sort of fluctuations. The level of manifestation of these fluctuations on different systems depends mainly on the type of the system considered (micro/macro) and also on different aspects such as temperature, the nature of the particles and their interactions, and the environment of the system under consideration. Regardless of the level of their manifestation, fluctuations do always exist intrinsically. Hence they can not be avoided completely by any means. However they can be minimised or suppressed to a certain extent by different mechanisms. Therefore, it is highly crucial to study their nature and effects in different physical systems, and the mechanisms used to suppress or squeeze them. It is with this motive that we study the role of fluctuations in cold atomic gases and squeezed states of light in this Thesis.

The field of quantum atom optics combines quantum optics with atom optics, which is currently a very active field of study. It treats the quantum properties of light and matter. Since both ultracold bosonic gases (Bose-Einstein condensates) and optical fields are composed of bosons, the majority of the processes which have long been studied in non-linear optics and quantum optics for photons have equivalents in the field of ultracold atomic gases.

The matter surrounding us consists of atoms (particles) that obey the laws of quantum mechanics. These laws do not often reveal themselves on the macroscopic level of our everyday life. In the case of atomic gases for in-

stance, they begin to play an important role when the de Broglie wavelength of the gas particles of the system under consideration is made to be very big. This happens when the temperature of the system is significantly lowered using different cooling mechanisms such as laser cooling and trapping, and evaporative cooling. Such system of particles at very low temperature comprises the new field of ultracold atomic physics, in which the thermal de Broglie wavelength of the particles is of the order of, or larger than their mean inter-particle distance.

Bose-Einstein condensation [5–7] is a quantum phenomenon which is formed by bosonic atoms that are cooled down to extremely low temperatures approaching to the absolute zero. It is a very unique phenomenon that has brought different areas of physics together and opened an interdisciplinary field of research. Since the observation of the first Bose-Einstein condensation in 1995, the field of ultracold atomic gases has been growing very rapidly and led to the realization of many other quantum phenomena. Still many novel ideas are currently under investigation. These include, among others, the search for an atom laser, the manipulation of low dimensional Bose-Einstein condensates using optical lattice potentials, and the study of matter wave solitons in one dimensional condensates making use of the non-linearity in the Gross-Pitaevskii equation.

The foundation of the field of ultracold atomic physics has opened many new possibilities for studying the effects of quantum mechanics in experimentally and theoretically accessible systems. The advantage of such ultralow temperature systems is that the complexity of the system is reduced by reducing the possible states the system can occupy. This allows for a more complete understanding of the system.

Another topic of study in this Thesis is squeezing of quantum fluctuations in optical systems. Squeezing in the quantum world has no classical analogy and refers to the reduction or suppression of quantum fluctuations or noise. Squeezed states of light [8–12] are non-classical states, in which quantum fluctuations in one quadrature are suppressed below the minimum level of fluctuations that can be achieved by vacuum or coherent states. In this sense squeezed states of light may provide lesser fluctuations or noise than that of vacuum, or coherent states. Squeezing is thus highly useful, as it may be employed to improve precision measurements and interferometric applications, and gravitational wave detection techniques.

## 1.1 Fluctuations in Quantum Physics

The term fluctuation is used commonly to indicate some sort of variation/s from an average or an expected value. But it is not a trivial concept, particularly, when its usage is extended to the quantum world. For instance a laser light is commonly considered to be highly coherent. However, any light (even laser) from a real optical system is never, strictly speaking, monochromatic, nor does it emanate from a single point in space. This implies that there are always some sort of fluctuations that can affect the coherence of the laser beam.

In recent years, there has been significant progress in the theoretical and experimental study of fluctuations in different areas of physics. Even quantum fluctuations are now observed and measured in experiments and also modified and manipulated using different techniques (cf. [4, 12]).

The concept of fluctuations plays an important role in the more general context of statistical mechanics and quantum optics relating to one of the intriguing questions associated with the field of ultracold atomic gases and non-classical states of light. Thermal and quantum fluctuations have been studied both theoretically and experimentally by several authors in optical systems [1, 4, 12–16] and in Bose-Einstein condensates (cf. [17–30]).

## 1.2 Thermal and Quantum Fluctuations

Although thermal fluctuations are of course more relevant at large temperatures, they may play a significant role even at very low temperatures, and particularly around the critical temperature for condensation [13, 25].

Usually condensates are described as coherent states eventhough fluctuations are always present, since for many situations these fluctuations are negligible. However, when fluctuations increase Bose-Einstein condensation cannot be considered to be 'pure'. If big enough, these fluctuations may destroy any condensation. This is specially more relevant for one- and two-dimensional systems since for a homogeneous system Bose-Einstein condensation is prevented in 1D, and in 2D is only possible at zero temperature [31, 32].

It is also important to stress that thermal fluctuations in Bose-Einstein condensates are indirectly connected to the intrinsic quantum nature of the condensates, and follow the quantum thermal statistics of Bose-Einstein condensates.

Quantum fluctuations are a result of the uncertainty principle [2–4] and may drive phase transitions even at  $T = 0$  (quantum phase transitions), as

e.g. the superfluid to Mott insulator transition, recently observed in ultracold lattice gases [33].

In contrast to quantum phase transitions, classical phase transitions are characteristically driven by thermal fluctuations and the trade-off between energy and entropy in the free energy. However, at absolute zero, all thermal fluctuations are frozen out and the entropy becomes zero [1]. This implies that, at very low temperature, quantum fluctuations dominate over thermal fluctuations.

Quantum fluctuations are fundamental properties of all physical systems. They do exist even if all classical sources of error and/or thermal fluctuations were to be eliminated from the measurement process. Quantum fluctuations play an important role in ultracold atomic gases and squeezed states of light. They reveal themselves as unavoidable barriers to accuracy and limit the sensitivity of detectors and measuring devices. Such a limit is sometimes referred to as the standard quantum limit. The search for light fields and physical systems with reduced, or even completely suppressed fluctuations is an active field of study in quantum optics. The possibility to overcome the quantum limit with squeezed states of light is the special focus of the last Chapter of this Thesis.

## 1.3 Fluctuations and the Uncertainty Principle

As stated earlier, quantum fluctuations are the consequence of the uncertainty principle. The Heisenberg uncertainty principle, or in short the uncertainty principle, is the basis of zero-point energy or the quantum vacuum as stated in Refs. [3, 14]. It is one of the fundamental laws of quantum physics and states that the values of certain pairs of conjugate variables, such as position and momentum, energy and time, phase and amplitude, phase and occupation number, or phase and density cannot be determined simultaneously with an absolute precision. It also states that everything one can measure is subject to truly random fluctuations. This indicates that quantum fluctuations are not the result of human limitations. Using more accurate measuring devices, uncertainty or fluctuations in measurements could be made as small as possible, but cannot be eliminated completely, even as a theoretical idea.

More generally, the uncertainty principle concerns non-commuting quantum mechanical operators, and can be described mathematically with the help of operators. Taking an arbitrary operator  $\hat{A}$ , one can define its fluctu-

ations as

$$\begin{aligned}
 (\Delta\hat{A})^2 &= \langle(\hat{A} - \langle\hat{A}\rangle)^2\rangle \\
 &= \langle\hat{A}^2\rangle - 2\langle\hat{A}\rangle\langle\hat{A}\rangle + \langle\hat{A}\rangle^2 \\
 &= \langle\hat{A}^2\rangle - \langle\hat{A}\rangle^2.
 \end{aligned}
 \tag{1.1}$$

We are going to use equation (1.1) throughout this Thesis for describing quantum and thermal fluctuations.

In view of Eq. (1.1), the uncertainty principle for a pair of observables represented by their respective operators, say  $\hat{A}$  and  $\hat{B}$ , can be described as

$$\Delta\hat{A}\Delta\hat{B} = \sqrt{(\Delta\hat{A})^2}\sqrt{(\Delta\hat{B})^2} \geq \frac{1}{2}|\langle[\hat{A}, \hat{B}]\rangle|
 \tag{1.2}$$

where  $\Delta\hat{A}$  and  $\Delta\hat{B}$  represent the fluctuations of  $\hat{A}$  and  $\hat{B}$  relative to their corresponding expectation values  $\langle\hat{A}\rangle$  and  $\langle\hat{B}\rangle$  respectively, and the two operators fulfill the commutation relation:

$$[\hat{A}, \hat{B}] = \hat{A}\hat{B} - \hat{B}\hat{A}.
 \tag{1.3}$$

Based on relation (1.2), one can say that the uncertainty principle is highly related with fluctuations. In this regard Raymer [3] stated that the uncertainty principle is not about measurements at all, but instead about actual fluctuations within an elementary particle as to its energy, or momentum.

The equality in Eq. (1.2) holds true for coherent and squeezed vacuum states. In this case the standard quantum limit takes into consideration that the fluctuations in the two conjugate variables satisfy the relation  $\Delta\hat{A} = \Delta\hat{B} = \sqrt{\hbar/2}$  or  $\Delta\hat{A}^2 = \Delta\hat{B}^2 = \hbar/2$ . States which satisfy this criterion are called minimum uncertainty states. This equality is however not a requirement for the uncertainty principle. The necessary condition for the uncertainty principle (1.2) is that the product of the two conjugate variables should always fulfil the relation (1.2). Either of the them can take much smaller value of fluctuations than the other, but this should be compensated by largely enhanced fluctuations on the other so that the relation (1.2) or the uncertainty principle to be precise remains always valid. Note that it is where the role of squeezing of quantum fluctuations enters into the play in which suppression of fluctuations below the standard quantum limit is possible for one of the two conjugate variables.

## 1.4 Vacuum Fluctuations

Quantum mechanics predicts that vacuum or ground state energy can never be exactly zero [34]. There is always some sort of lowest possible energy state

called ground state or the zero-point energy. As an analog of the uncertainty principle, one of the implications of the basic formalism of quantum theory is that an ordinary quantum field cannot maintain precisely zero value, but must always show certain fluctuations even in vacuum. Such fluctuations are termed as vacuum fluctuations [34, 35].

The best example for vacuum fluctuations is the Casimir effect (a review is available at [34]). Casimir first predicted that zero point quantum fluctuations of the electromagnetic field give rise to an attractive force between two closely spaced perfect conductors [36]. In this idealised situation, a macroscopic physical manifestation, i.e., a force, arises purely from electromagnetic quantum fluctuations [37].

Similarly, one can expect an analogous force to arise from quantum fluctuations in quasi-particle vacuum in zero temperature dilute Bose-Einstein condensates [29]. Indirect effects from such fluctuations have been observed, including the shift of collective frequencies [38], the existence of a quantum phase transition in an optical lattice [33], and the correlations of these quantum fluctuations as a source for entangled atoms [39].

## 1.5 Outline of the Thesis

The Thesis is organised in the following way. In Chapter 1 we have already started the Thesis by presenting a short general introduction which is followed by a brief description of fluctuations. We have verified three types of fluctuations namely: thermal, quantum and vacuum fluctuations, and discussed their relations with the uncertainty principle.

In Chapter 2 we investigate the dynamics of evaporative cooling of  $^{87}\text{Rb}$  cold atoms continuously trapped in an anisotropic (cigar-shaped) trap for high phase space density using molecular dynamics.

Chapter 3 focuses on the basics of ultracold bosonic gases. We give the statistical description of Bose gases, discuss the Bose-Einstein condensation (BEC) as a phase transition, and introduce the historical development, realization and prospects of Bose-Einstein condensates. In this Chapter we also present the theoretical description of weakly interacting Bose gases at extremely low temperatures, and the derivation of the Gross-Pitaevskii equation and the Bogoliubov-de Gennes equations.

In Chapter 4 we investigate the manipulation of elongated condensates using optical potentials and study the effect of finite temperature on the phase and density fluctuations. We explore splitting and merging of an elongated 1D Bose condensate of  $^{87}\text{Rb}$  atoms at zero and finite temperature by simulating the phase and density fluctuations.

---

In Chapter 5 we study matter wave solitons in 1D Bose-Einstein condensates by means of the 1D non-linear Schrödinger equation. In this chapter we investigate different possibilities of control of the dynamics of bright lattice matter wave solitons by using their interaction with defects of arbitrary amplitude and width. We verify the application of matter wave solitons for quantum switches and quantum memories using defects as “effective” potential barrier and well respectively.

Chapter 6 studies the phenomenon of squeezing in non-degenerate parametric oscillator (NDPO) coupled with two independent squeezed vacuum reservoirs. In this Chapter we show that it is possible to squeeze quantum fluctuations in a particular quadrature component below the standard quantum limit at the expense of highly enhanced fluctuations in the conjugate quadrature without violating the uncertainty principle.

In Chapter 7 we present a conclusion of the main results of our study. In Appendix A a more explicit derivation of the Bogoliubov-de Gennes equations addressed in Sec. 3.3.3 is presented. We present also a detailed derivation of the master equation describing the NDPO of Chapter 6. In Appendix C we give a derivation of the expectation values of squeezed vacuum reservoir modes associated with the NDPO.



# Chapter 2

## Evaporative Cooling for High Phase Space Density

Cooling and trapping of atoms are basic steps necessary for any further research on cold atoms. In this Chapter we study numerically the dynamics of evaporative cooling of cold gaseous  $^{87}\text{Rb}$  atoms in an anisotropic trap loaded continuously from an incoming atomic beam. The numerical simulations, based on a method known as molecular dynamics [40–43], allow us for determining the time evolution of the number, temperature and phase space density of atoms in the trap, as well as the axial and transversal truncation parameters of the trap.

### 2.1 Cooling and Trapping Techniques

In this section we shall very briefly introduce the concepts of laser cooling, atomic trapping and evaporative cooling.

#### 2.1.1 Laser Cooling

Laser cooling employs the mechanical effects of laser light on atoms to reduce their momentum spreading, and hence cool the samples. Several mechanisms have been proposed (which eventually could even lead to quantum degeneracy [44]), but we shall just describe the simplest of them, namely the so-called Doppler cooling [45, 46]. To verify this cooling process, let us assume a two-level atom with a ground state  $|g\rangle$  and an excited state  $|e\rangle$ , separated by a transition energy  $\hbar\omega_{eg}$ . We further consider that the atom is affected by two counter-propagating laser beams of equal frequency  $\omega_L$  which is quasi-resonant with the transition frequency, but red-detuned with respect to the transition frequency, i.e. the detuning  $\delta = \omega_L - \omega_{eg} < 0$ . When

the atom moves with a velocity  $\mathbf{v}$ , it observes an effective laser frequency of  $\omega'_L = \omega_L - \mathbf{k}_L \cdot \mathbf{v}$ , due to the Doppler effect, where  $\mathbf{k}_L$  is the vector wavenumber of the laser. In other words, the absorbed photons transfer a momentum opposite to the moving direction, while the emission goes in an arbitrary direction and has on average no effect. On the other hand an atom moving away from the red detuned laser is shifted out of resonance and will unlikely absorb a photon. A laser beam pointing from all directions have the effect of a viscous damping force. Hence the atom will be more in resonance with the laser opposed to its motion, and therefore the radiation pressure damps the velocity of the atom. In summary, the laser acts as a very viscous medium which is referred to as optical molasses. Besides the viscous effect, there is an stochastic contribution due to the momentum fluctuations produced by the recoil of the spontaneously emitted photons which produces heating (broadening of the momentum distribution) which is in competition with the Doppler cooling and finally leads to an equilibrium distribution characterised by the so-called Doppler temperature  $T_D = \hbar\Gamma/2k_B$ , where  $\Gamma$  is line-width of the atomic transition [47, 48]. This temperature in the case alkali atoms is typically of the order of hundred microkelvins. Laser cooling of alkali atoms has led to yet another discovery of polarisation gradient cooling and the Sisyphus effect [49], that allow to reach microkelvin temperatures, even though it was not sufficient to obtain a BEC.

### 2.1.2 Atomic trapping

Of course, the experiments of cold atoms need a reliable way of trapping the samples under investigation. Different trapping mechanisms have been employed. On one side, the mechanical effects of laser light may be used to directly trap the atoms in the so-called dipole traps [50]. The principle of a dipole trap is based on the interaction of an electric field  $\mathbf{E}(\mathbf{r}, t)$  with a two-level atom ( $|g\rangle, |e\rangle$ )

$$H_I = -\mathbf{d} \cdot \mathbf{E}(\mathbf{r}, t), \quad (2.1)$$

where  $\mathbf{d}$  is the dipole moment associated with the corresponding transition.

Additionally, one may employ an inhomogeneous magnetic field, and via the Zeeman effect construct a magnetic trap [51]. In such a situation, the magnetic potential energy experienced by an atom is given by

$$U_{\text{mag}}(\mathbf{r}) = \mu_B g_F m_F B(\mathbf{r}), \quad (2.2)$$

where  $\mu_B$  is the Bohr magneton,  $g_F$  is the gyromagnetic ratio or the Landé g-factor of the chosen Zeeman sublevels ( $F, m_F$ ),  $F$  is the total angular momentum of the given atomic level and  $m_F$  is the magnetic quantum number. A

given atomic level is referred to as *weak-field (strong-field) seeker* if  $g_F m_F > 0$  ( $g_F m_F < 0$ ), since in such a case the atoms are driven towards regions of minimum (maximum) magnetic field. Note that, since it is impossible to create a local maximum with a static magnetic field, only *weak-field seeking* states can be trapped by the inhomogeneous magnetic field  $B(\mathbf{r})$  with a local minimum. In  $^{87}\text{Rb}$ , the  $|F = 2, m_F = 2\rangle$  is taken as an example a *weak-field seeker*.

A third possibility combines both lasers and magnetic fields, the so-called magneto-optical trap or MOT [52]. The basics of this trap, in the case of one-dimensional configuration, can be illustrated as shown in Fig. 2.1. To verify such a trap, following a similar approach to that in [53], let us

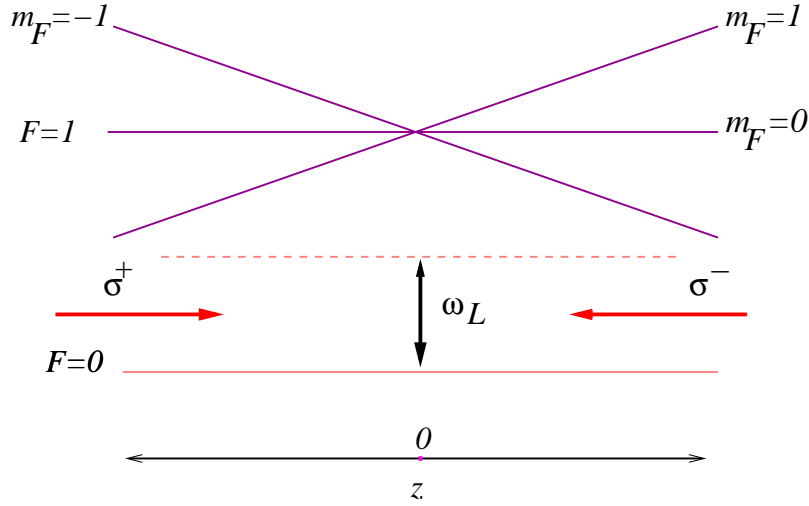


Figure 2.1: (Color online) Description of a magneto-optical trap.

consider an atom with a zero-spin ground level ( $F = 0$ ) and a spin-one excited level ( $F = 1$ ) having the Zeeman sublevels  $m_F = \pm 1, 0$ . When a weak inhomogeneous magnetic field  $B(z) = bz$  along the  $z$ -axis is applied, the Zeeman sublevels are split by an amount of energy given by  $\Delta E(z) = \mu_B g_F m_F b z$ . The atom is affected by two counter-propagating laser beams with opposite circular polarisation,  $\sigma^-$  and  $\sigma^+$  along the  $-z$  and  $+z$  directions respectively (Fig. 2.1). When the laser is red-detuned with respect to the  $B = 0$  transition, the atom at  $z > 0$  absorbs more  $\sigma^-$  than  $\sigma^+$  photons, and consequently feels an average force towards the origin ( $z = 0$ ). On the other hand, for the  $z < 0$  the Zeeman effect is opposite, i.e. the atom is directed again towards the  $z = 0$ . Hence, the atom is trapped around the  $z = 0$ . Note that the scheme is easily extended to the usual three dimensional magneto-optical trap (3D-MOT) by using three-pairs of counter-propagating

laser beams. It is also possible to have a MOT which is capable of effectively operating in a 2D structure (2D-MOT) using four laser beams instead of six.

### 2.1.3 Evaporative Cooling

Evaporative cooling is a well known cooling technique in every day life such as in the cooling of a cup of coffee. For the purpose of obtaining degenerate ultracold atomic gases (BECs), it was proposed by Hess [54] (1986) for the cooling of a gas of spin-polarised atomic hydrogen. After adapted for alkali atoms, evaporative cooling quickly led to the realization of BEC (see Chapter 3). A detailed review on evaporative cooling is found in [55].

Evaporative cooling works by letting the most energetic atoms escape from the trap. Subsequently the remaining relatively less energetic atoms undergo collisional rethermalization towards a lower temperature [55, 56]. By repeating this process it is possible to build up phase space densities large enough for achieving BEC (see Chapter 3). However, evaporative cooling also leads to a decrease in the number of atoms, which, if strong enough, may prevent the atomic gas sample from attaining the critical phase space density (Eq. 3.20) required for condensation. By minimising loss mechanisms the required quantum degeneracy of the atoms can be achieved.

## 2.2 Molecular Dynamics Simulation for Evaporative Cooling

### 2.2.1 Molecular Dynamics

In the following we shall analyse the evaporative cooling of a  $^{87}\text{Rb}$  sample by means of a molecular dynamics program developed and provided to us by J. Dalibard/D. Guéry-Odelin group. Molecular dynamics simulation (MDS) is a standard computational technique, where the time evolution of a system of weakly interacting particles is followed by integrating their equation of motion according to the laws of classical mechanics. This method requires fewer simplifications and assumptions than other methods, such as the direct solution of the Boltzmann equation. The MDS, as originally proposed by Bird [40], is used for decoupling the motion of the particles and the interparticle collisions, circumventing the difficulties of direct physical modelling over a small time step  $\Delta t \ll \tau_c$ , where  $\tau_c$  is the mean collision time. Of course, and since the particles are assumed to obey classical mechanics, we should always compare the thermal de Broglie wavelength  $\lambda_{dB}$  and the mean interparticle separation ( $d$ ). In this regard, the MDS is justified if  $\lambda_{dB} \ll d$ , which

in turn limits the regime of temperatures for which MDS may be employed.

In the MDS method, the positions ( $\mathbf{r}$ ) and the velocities ( $\mathbf{v}$ ) of each atom are stored. Actually, in practice the concept of a macro-atom is employed [40, 42, 57, 58], i.e.  $\mathcal{M}$  real atoms are represented by a single particle with the same mass and that experiences the same trapping potential as the real ones. However, the scattering cross section between two macro-atoms is considered  $\mathcal{M}$  times larger than between two real atoms with the same velocity. In our simulation  $\mathcal{M}$  is typically  $\sim 10^4$ .

The position space is divided into many cells. The size of the cell ( $\Delta\mathbf{r}$ ) must be small compared to the scale of changes in the gas properties. In particular one has to compare the cell size with the correlation lengths of the spatial correlations of interest. Since correlation lengths diverge at phase transitions, MDS cannot be reliably employed in that case.

The time is advanced in discrete steps ( $\Delta t$ ). The simulation time must be much longer than the relaxation time of the quantities we are interested in. These times became very large when approaching phase transitions, and hence once more MDS cannot be reliably employed for those cases.

The atoms are considered to move through distances appropriate to their velocities ( $\mathbf{v} \cdot \Delta t$ ). In addition, the trapping potential  $U(\mathbf{r})$  induces a force

$$\mathbf{F}(\mathbf{r}) = -\nabla U(\mathbf{r}) \quad (2.3)$$

on each atom which leads to the velocity change

$$\Delta\mathbf{v} = \frac{\mathbf{F}(\mathbf{r})}{m} \Delta t. \quad (2.4)$$

In order to conveniently deal with an atom number which varies by 8 orders of magnitude we use a duplication technique as described in [42]. We evolve the distribution of the atoms initially present in the trap and the those continuously entering the trap in terms of  $\mathcal{M}$ . Each time a macro-atom collides with another from the residual gas or the incoming atoms, it is replaced by a new macro-atoms, each representing only  $\mathcal{M}/2$  atoms. If the parent macro-atom is in  $(x, y, z)$  with velocity  $(v_x, v_y, v_z)$ , one of two new macro-atoms is placed at the same point with the same velocity, and the other one is placed in  $(-x, -y, z)$  with the velocity  $(-v_x, -v_y, v_z)$ . This duplication, which exploits the symmetry of the trap, guarantees that these two new macro-atoms will not undergo a collision with each other immediately after the duplication process.

The size  $\Delta\mathbf{r}$  is adjusted as the cloud cools down, so that the probability for having two particles in the same box is much smaller than 1. When two macro-atoms are found in the same box, a collision may take place between

them. The probability for this collision is  $\mathcal{M} \sigma(\mathbf{k}) \mathbf{v} \delta t / \delta^3 \mathbf{r}$ , where  $\mathbf{k}$  and

$$\mathbf{v} = 2\hbar\mathbf{k}/m \quad (2.5)$$

are the relative wave vector and velocity of the colliding particles, and  $\sigma(\mathbf{k})$  the collisional cross section between two real atoms. The time step  $\Delta t$  is chosen such that this probability is small compared to 1. The occurrence of a collision is then randomly decided. The collision is isotropic since only the  $l = 0$  partial wave contributes at these ultralow temperatures. In this approach

$$\sigma(\mathbf{k}) = \frac{8\pi a_s^2}{1 + k^2 a_s^2} \quad (2.6)$$

but at very low relative velocity ( $k^2 a_s^2 \ll 1$ ) one recovers the well known limit  $\sigma = 8\pi a_s^2$  (which we employ in our calculations), while one obtains for higher velocities the unitary limit  $\sigma(\mathbf{k}) = 8\pi/k^2$ , corresponding to the result for a zero-energy resonance. The collisions are considered in the center-of-mass reference. After a collision occurs the relative velocity maintains its absolute value, but its angular dependence is randomly modified. In this way we calculate the new velocities after a collision.

## 2.2.2 The Dynamics of Evaporative Cooling

In the following we shall consider the dynamics of the evaporative cooling of a cold  $^{87}\text{Rb}$  sample in an anisotropic (cigar-shaped) trap, as described in Fig. 2.2 [43]. In this scheme, particles from a continuously incoming atomic beam are injected into the trapping potential, and can be trapped by undergoing elastic collisions with the particles already present in the trap. After the collisions, evaporation of the hottest atoms occurs either when the longitudinal energy of the atoms exceeds the axial height of the trap,  $U_z$ , or when their transverse energy exceeds the actual trap depth (the transverse evaporation threshold  $U_\perp$ ). It is at an optimal value of the transverse trap depth  $U_\perp$  that a relatively efficient evaporative cooling is obtained. The scheme (Fig. 2.2) takes advantage of the different evaporation rates along the axial and the transverse directions. This leads to the possibility of accumulating particles in the well even if their incident energy notably exceeds the trap depth. Such a method also enables accumulation of relatively colder atoms with relatively higher phase space density. The balance between the continuous arrival of new particles and the evaporation of the hottest atoms finally leads a saturation level on the number, temperature and phase space density of the trapped atoms as well as the radial and axial truncation parameters of the trap as shown in Figs. 2.3 (b), 2.4 (b), 2.5 (b) and 2.6 respectively.

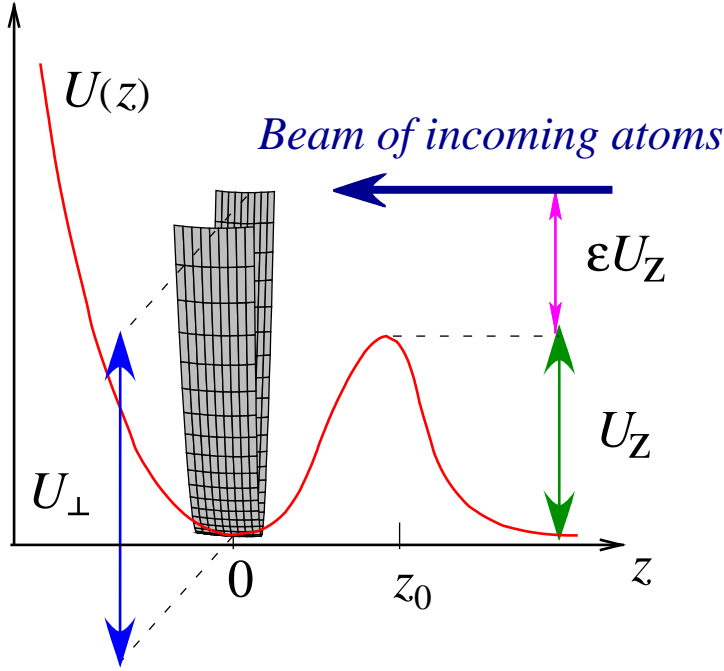


Figure 2.2: (Color online) Continuous loading of an anisotropic atom trap from an incoming atomic beam for a high phase space density.

In our simulations we consider  $^{87}\text{Rb}$  which has cross section  $\sigma = 8\pi a_s^2 = 7.1 \times 10^{-16} \text{m}^2$ . The radial and axial frequencies of the trap are  $\omega_\perp/2\pi = \omega_x/2\pi = \omega_y/2\pi = 1 \text{kHz}$  and  $\omega_z/2\pi = 10 \text{Hz}$  respectively. In addition, the incoming atoms possess a total flux  $\Phi \sim 10^8 \text{atoms/s}$ , with an average velocity  $v_0 = 0.20 \text{m/s}$  and a velocity dispersion  $\delta v_0 = 0.04 \text{m/s}$  along the axial and the radial directions (temperature of  $T_i \sim 17 \mu\text{K}$ ). The flux passing the point  $z = z_0$  is assumed to be about 85% of the total incoming flux, i.e.,  $\Phi_{\text{in}} = 0.85\Phi$ . In the trap about  $N_0 \sim 10^6$  atoms with an average temperature of  $T_0 = 31 \mu\text{K}$  are assumed to be present initially. The incoming atoms collide with the atoms already in the trap and with themselves in the potential well (Fig. 2.2). Under these conditions the initial phase space density is  $\rho_{PS0} \sim 10^{-5}$  and the axial trap depth or the barrier height at the point  $z = z_0$  is given by  $U_z(z = z_0)/k_B = \frac{1}{2}m(v_0 - \delta v_0)^2/k_B \sim 135 \mu\text{K}$ . This barrier is chosen in such a way that only atoms with an incident velocity larger than  $v_0 - \delta v_0$  reach the trap.

Using the MDS [43] one determines the probability  $p_z$  that an atom reaches  $z = z_0$  after a collision, being thus evaporated. One also determines the average energy  $U_z + \kappa_z k_B T$  carried away by an evaporated atom, where

$\kappa_z$  (and  $\kappa_\perp$ ) are dimensionless coefficients that depend on the axial (and transversal) truncation parameters  $\eta_z = U_z/k_B T$  ( $\eta_\perp = U_\perp/k_B T$ ). Similarly one determines the probability  $p_\perp$  of radial evaporation, as well as the energy  $U_\perp + \kappa_\perp k_B T$  by the evaporated atom. One obtains in this way i) for  $\eta_z$  between 4 and 7,  $\omega_z \ll \gamma$ , and  $\kappa_z \simeq 2.9$ , that

$$p_z \simeq 0.14 e^{\eta_z} \frac{\omega_z}{\gamma}, \quad (2.7)$$

and ii) for  $\eta_\perp$  in the range from 8 to 13, and radial frequency between  $\omega_\perp \gg \gamma$  and  $\gamma \geq 5\omega_\perp$  and  $\kappa_\perp \approx 2.0$

$$p_\perp \simeq 2.0 e^{\eta_\perp} \frac{\omega_\perp}{\omega_\perp + 1.4\gamma}, \quad (2.8)$$

where  $\gamma = \sqrt{2k_B T}/\pi m n_0 \sigma$  is the average collision rate of each particle before escaping from the trap. Here  $n_0$  is the atomic density at the trap centre.

Once the coefficients are determined for a given  $U_\perp$ ,  $U_z$  and  $T$ , the dynamics of the system can be described by the time evolution of the number  $N$  and of the total energy  $E = 3Nk_B T$  (we assume at any time equilibrium)

$$\frac{dN}{dt} = \Phi_{\text{in}} - (p_z + p_\perp)\gamma N \quad (2.9)$$

and

$$\frac{dE}{dt} = \Phi_{\text{in}}(1 + \varepsilon)U_z - p_z \gamma N (U_z + \kappa_z k_B T) - p_\perp \gamma N (U_\perp + \kappa_\perp k_B T) \quad (2.10)$$

where,  $\varepsilon$  is a very small dimensionless coefficient inversely related with the truncation parameter of the trap ( $\varepsilon \sim \kappa(\eta)/\eta$ ).

The steady state values of  $N$  and  $T$  are determined after solving the time-independent version Eqs. (2.9) and (2.10). These results are plotted as a function of the transverse trap depth ( $U_\perp$ ) as shown in Figs. 2.3 (a), 2.4 (a) and 2.5 (a) from which the optimal transverse trap depth is deduced to be  $U_\perp/k_B \approx 274\mu\text{K}$  which is same result with that of [43]. This value is obtained for  $U_\perp \sim (1 + \varepsilon)U_z$  and  $p_\perp/p_z \sim 2$ . We use this potential for our simulation [59].

After fixing the optimal potential we solve for the time evolution. In principle, one could directly simulate equations (2.9) and (2.10) using the approximations (2.7) and (2.8) for  $p_z$ ,  $p_\perp$ ,  $\kappa_z$  and  $\kappa_\perp$ . However, these approximated values could lead to quantitative deviations from the correct results. Hence, we analyze the time evolution using directly the MDS, obtaining  $N(t)$ ,  $T(t)$ , the phase space density  $\rho_{PS}(t)$  of trapped atoms and the truncation parameters  $\eta_\perp(t)$  and  $\eta_z(t)$ . Note that for different values of  $T$ ,  $U_z$  and  $U_\perp$  we must determine the coefficients of the equations (2.9) and (2.10).

From Fig. 2.3 (b) we can deduce that, at the optimal transverse potential depth, it is possible to trap more than  $10^8$  atoms continuously. Here we want to stress that it is due to the continuous loading from the atomic beam that the number of the atoms in the trap show no decrease as it is usually the case in most evaporative cooling processes due to the different lose mechanisms.

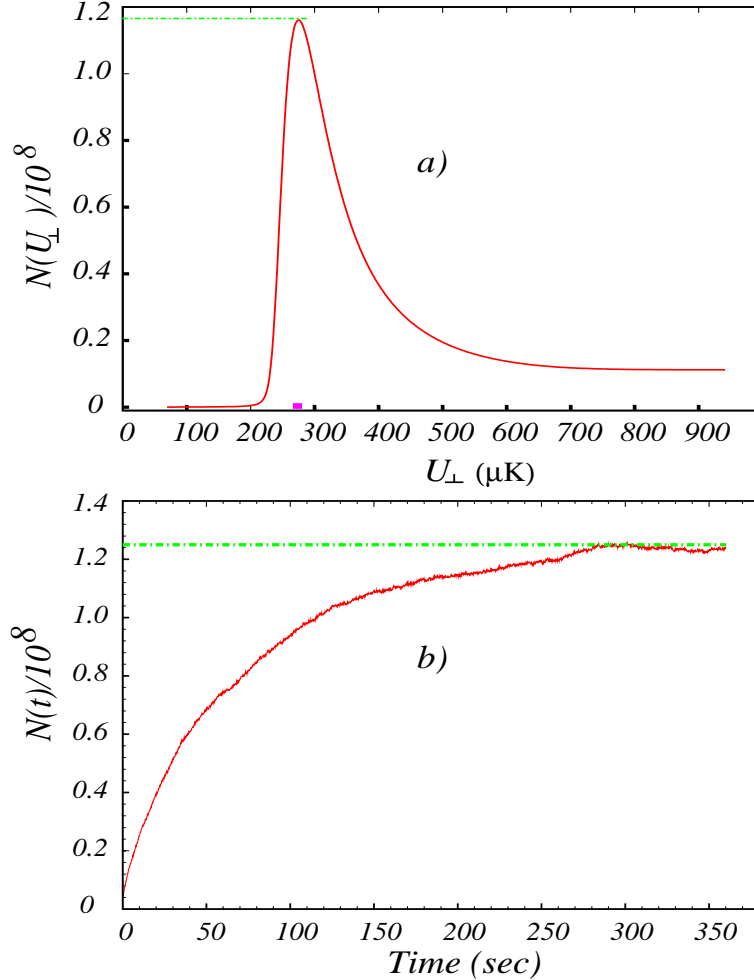


Figure 2.3: (Color online) (a) Number of trapped atoms as a function of a transversal trap depth, and (b) Time evolution of the number of atoms in an anisotropic trap.

The achievement of a BEC requires a systematic cooling of the atoms while they are in the trap, i.e. the reduction of the temperature without reducing the number of atoms trapped. For this purpose, we need to look for parameters that optimise the cooling process. A comparison between

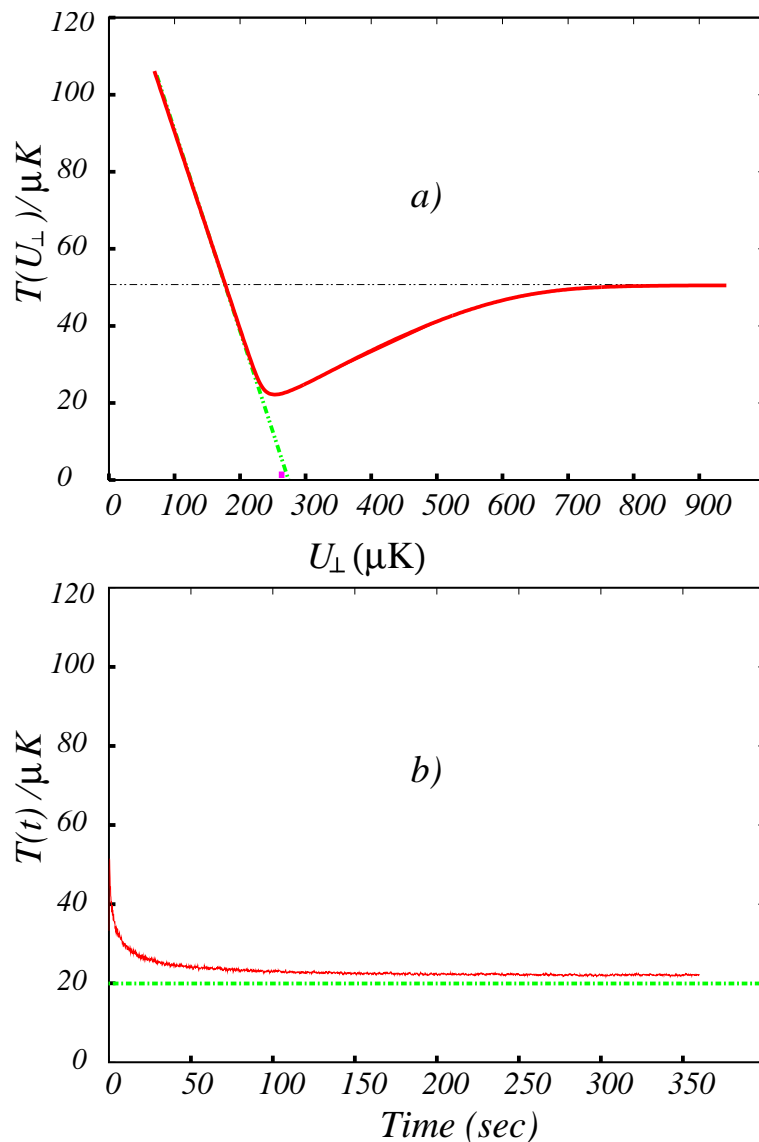


Figure 2.4: (Color online) Determination of average equilibrium temperature of atoms trapped in an anisotropic trap at an optimal transverse trap depth. (a) Temperature as a function of transverse trap depth, and (b) time evolution of the temperature.

the steady state (Fig. 2.4 (a)) and numerical (Fig. 2.4 (b)) results leads to the conclusion that the optimal potential leads to a decrease in the temperature until it reaches a saturation level. Hence, based on the numerical results in Fig. 2.4 (b), we can conclude that it is possible to achieve an equi-

librium temperature of  $T \sim 20\mu\text{K}$ . This is of course done by determining the average energy of the atoms in the trap after collision, evaporation and rethermalization. Although the temperature achieved is still about two orders of magnitude higher than the critical temperature for the condensation of  $^{87}\text{Rb}$ , maintaining the atoms at such temperature for long time can be useful by itself.

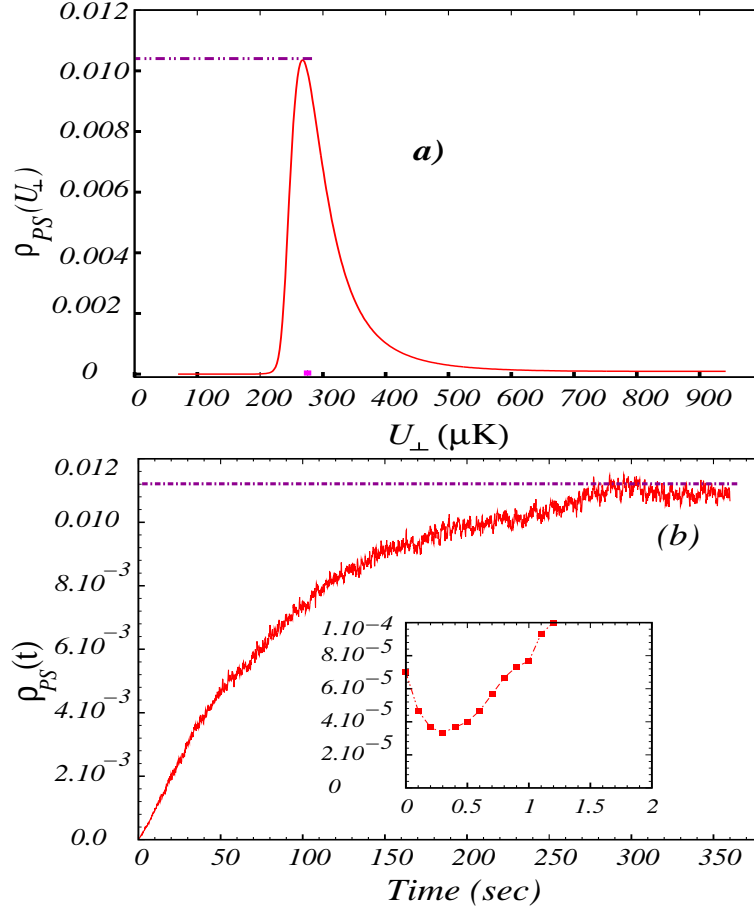


Figure 2.5: (Color online) Maximising phase space density of atoms in an anisotropic trap: (a) phase space density as a function of transversal trap depth, and (b) time evolution of the phase space density.

As it will be verified latter in Chapter 3, the phase space density is proportional to  $\frac{N}{T^{3/2}}$ . Hence an increase in this quantity during the process of evaporative cooling is to be traded off between the decreasing number of atoms and the temperature. In our simulation, the possible decrease of the trapped atoms is compensated by the continuous injection of atoms into the

trap from the incoming atomic beam. Therefore, the phase space density continues to increase until a saturation level is reached as shown in Fig. 2.5 (b). From the simulation (Fig. 2.5 (b)), we can see that a maximum phase space density of  $\rho_{PS} \sim 0.011$  is achieved. Again, even though this is still about two orders of magnitude lower than the critical value for condensation the gain is significant, since we began our simulation from an initial phase space density of  $\rho_{PS0} \sim 10^{-5}$ .

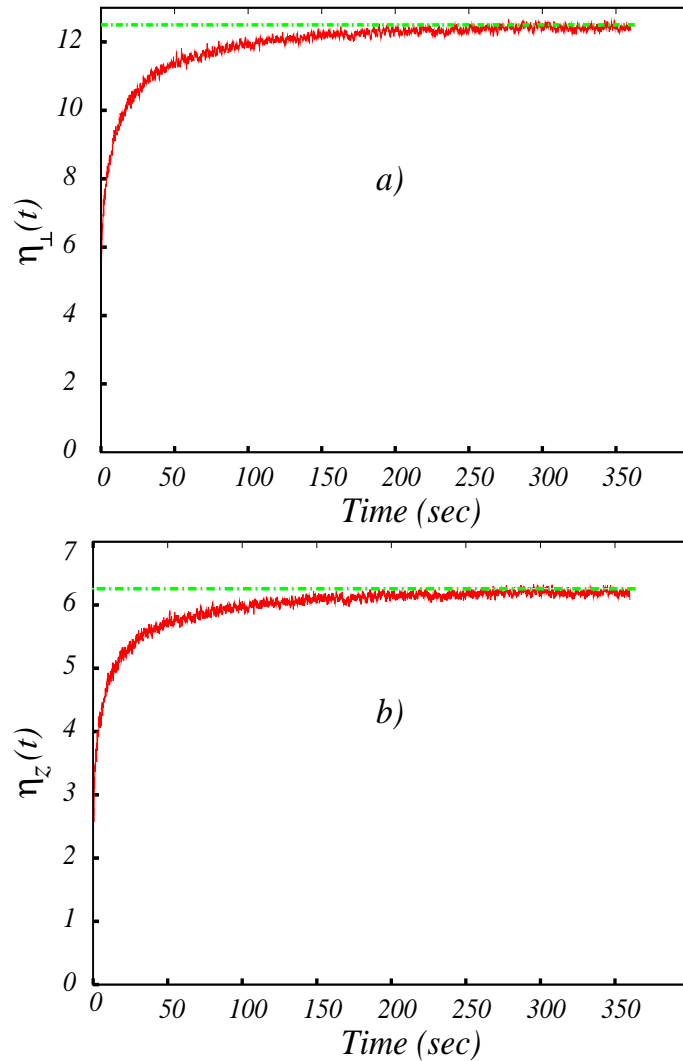


Figure 2.6: (Color online) Time evolution of (a) radial and (b) axial truncation parameters or trap depth coefficients.

Since the trap depth and its truncation play an important role throughout

the cooling process, we show in Fig. 2.6 how the truncation parameters along the radial and axial directions evolve in time. For the given parameters the simulation indicates that the axial and radial trap coefficients are estimated to be  $\eta_{\perp} = U_{\perp}/k_B T \sim 12.3$  and  $\eta_z = U_z/k_B T \sim 6.4$  respectively.

## 2.3 Summary

In this Chapter we have studied the dynamics of evaporative cooling which is required for achieving degenerate ultracold atomic gases. With the intention to determine some relevant parameters for the dynamics of evaporative cooling in order to generate ultracold atoms at higher phase space density, we have applied a molecular dynamics simulation for atoms in a realistic anisotropic trap experiment continuously injected by an incoming atomic beam. With the help of this simulation, we have shown that it is possible to trap more than  $10^8$  atoms at a temperature of  $20 \mu\text{K}$  with a phase space density of slightly exceeding 0.011. These results are obtained using an optimal transverse trap depth of  $274 \mu\text{K}$ . Making use of this optimal potential, we have also determined the values for the axial and radial trap truncation parameters to be 6.4 and 12.3 respectively.

In all the numerical results displayed in the Figs. 2.3 (b), 2.4 (b), 2.5 (b) and Fig. 2.6, it is shown that the time evolution of the number of trapped atoms, the temperature, the phase space density and the truncation parameters have reached saturation levels. These results confirm that it is possible to achieve an optimum value for each of the required quantities and maintain it for long time by continuously pumping atoms into the trap. Although the results achieved with this program for the temperature and the phase space density are still orders of magnitude away from the required values for quantum degeneracy, we are of the opinion that this approach can be useful for continuously trapping and cooling atoms, and can be used for the generation of a continuous matter wave, or an atom laser.



# Chapter 3

## The Basics of Ultracold Degenerate Quantum Gases

The physics of ultracold atomic gases is interesting because of two main reasons. The first is that interactions of such dilute atomic gases are characterised usually by small number of parameters: the three dimensional s-wave scattering length  $a_s$  and the mass  $m$  of the atoms. This may allow for the analytical analysis of the system of these gases. The second reason is that ultracold atomic gases are convenient for various trapping and manipulation mechanisms.

One of the important aspects of ultracold degenerate atomic gases is their interaction. In BECs, the atoms do interact, but very weakly. These interactions do allow for detailed theoretical understanding about the nature and behaviour of the interacting particles. On top of that, these interactions can be dynamically controlled, i.e. it is possible to dictate the strength of the interactions. It is also possible to control the type of interactions (attractive or repulsive) between the atoms by changing the force between them from an attractive to a repulsive or vice-versa, via the method known as Feshbach resonance [60]. This flexibility in controlling the strength and type of interactions is one of the main reasons, why tremendous breakthroughs are continuously emerging in the field of ultracold atoms at a remarkable rate.

### 3.1 Mathematical Description of Bose-Einstein Condensation

Bose-Einstein condensation is the result of a phase transition which occurs as a consequence of the Bose-Einstein statistics. In this section we shall discuss how this remarkable phenomenon is possible.

We begin our discussion by considering a macroscopic system of  $N$  non-interacting bosonic atoms of mass  $m$  in a box of volume  $V$  in thermal equilibrium (at a finite temperature  $T$ ) with its surroundings (in the derivation here we follow a similar approach as that of Ref. [61]). Such a system is described by the well known Bose-Einstein distribution function

$$f_{BE}(\epsilon_k, \mu, T) = \frac{1}{z^{-1}e^{\beta\epsilon_k} - 1} \quad (3.1)$$

where  $\epsilon_k$  is energy of a single quantum state  $k$  occupied by a mean number of particles  $N(\epsilon_k)$ ,  $\beta = (k_B T)^{-1}$  is inversely proportional to  $T$  with  $k_B$  being the Boltzmann constant,  $z = e^{\beta\mu}$  is called fugacity of the bosonic gas, and  $\mu$  is the chemical potential. The chemical potential is the energy required to add a particle to the system while keeping the entropy and volume fixed. It can be determined from the constraint (particle number conservation):

$$N = \sum_k f_{BE}(\epsilon_k, \mu, T) = \sum_k \frac{1}{z^{-1}e^{\beta\epsilon_k} - 1}. \quad (3.2)$$

Since the occupation number (3.1) should be positive, we need  $0 < z < 1$  at  $\epsilon_k(k=0) = 0$ . This means that

$$N(k=0) = N_0 = \frac{1}{z^{-1} - 1} = \frac{z}{1 - z} > 0 \quad (3.3)$$

which implies  $\mu < 0$ . The chemical potential of the Bose gas, being negative, increases as the temperature drops, and approaches zero at the critical temperature denoted by  $T_c$ , indicating a phase transition to a condensed state. In addition, the chemical potential should always be smaller than the lowest energy level  $\epsilon_0$  in order to avoid a negative occupation number.

If the Bose-Einstein distribution (3.1) varies slowly on the scale of the energy level spacing, then the summation in Eq. (3.2) can be replaced by integration over all the density of states of the bosonic particles. However, if  $\mu \rightarrow 0$  the distribution has a singularity at the ground state ( $k=0$ ). This singularity can be avoided by singling out the ground state contribution and use the density of states for the remaining levels. Accordingly, Eq. (3.2) can be written as

$$N = N_0 + \int \rho(\epsilon) f_{BE} d\epsilon, \quad (3.4)$$

where  $N_0$  is the condensate population at  $T=0$ ,  $N_{ex}$  is the number of excited atoms, and  $\rho(\epsilon)$  is 3D density of states. For an ideal Bose gas with a large volume,  $\rho(\epsilon)$  is assumed to be continuous (see for example [61, 62]) and reads

$$\rho(\epsilon) = \frac{2\pi(2m)^{3/2} V}{h^3} \epsilon^{1/2} = \frac{2}{\sqrt{\pi}} V \left( \frac{m}{2\pi\hbar^2} \right)^{3/2} \epsilon^{1/2}. \quad (3.5)$$

The second term in Eq. (3.4) gives the number of particles in the excited states which can be calculated as

$$\begin{aligned}
N_{ex} &= \int_0^{\infty} \rho(\epsilon) f_{BE}(\epsilon_k, \mu, T) d\epsilon \\
&= \frac{2}{\sqrt{\pi}} V \left( \frac{m}{2\pi\hbar^2} \right)^{3/2} \int_0^{\infty} \frac{\epsilon^{1/2}}{z^{-1}e^{\beta\epsilon} - 1} d\epsilon \\
&= \frac{2}{\sqrt{\pi}} V \left( \frac{m}{2\pi\hbar^2} \right)^{3/2} \int_0^{\infty} \frac{\epsilon^{1/2}}{z^{-1}e^{\epsilon/k_B T} - 1} d\epsilon. \tag{3.6}
\end{aligned}$$

Setting  $x = \epsilon/k_B T$  and

$$\lambda_{dB} = \sqrt{\frac{2\pi\hbar^2}{mk_B T}} \propto T^{-\frac{1}{2}} \tag{3.7}$$

where  $\lambda_{dB}$  is called thermal de Broglie wavelength, Eq. (3.6) can be further expressed as

$$N_{ex} = \frac{2}{\sqrt{\pi}} V \lambda_{dB}^{-3} \int_0^{\infty} \frac{x^{1/2}}{z^{-1}e^x - 1} dx = \frac{2}{\sqrt{\pi}} V \lambda_{dB}^{-3} \Gamma(3/2) g_{3/2}(z) \tag{3.8}$$

where  $\Gamma(3/2) = \int_0^{\infty} e^{-x} x^{1/2} dx = \sqrt{\pi}/2$  is the Gamma function and  $g_{3/2}(z)$  is a Bose function which reduces to the Riemann zeta function for  $z = 1$  and has the value of

$$g_{3/2}(\mu \rightarrow 0) = \zeta(3/2) = \sum_{n=1}^{\infty} n^{-3/2} \approx 2.612. \tag{3.9}$$

Note that the Riemann zeta function diverges at  $z = 1$  which corresponds to the ground state occupation. In this case (for  $\mu \rightarrow 0$ ), Eq. (3.8) leads to

$$N_{ex} = V \frac{g_{3/2}(z(\mu \rightarrow 0))}{\lambda_{dB}^3}. \tag{3.10}$$

For a non-zero chemical potential and for a general value of  $\alpha$ , Eq. (3.8) can be expressed as

$$N_{ex} = \frac{2}{\sqrt{\pi}} V \lambda_{dB}^{-3} \sum_{n=1}^{\infty} \int_0^{\infty} x^{\alpha-1} e^{-nx} z^n dx = \frac{2}{\sqrt{\pi}} V \lambda_{dB}^{-3} \Gamma(\alpha) g_{\alpha}(z), \tag{3.11}$$

where now

$$\Gamma(\alpha) = \int_0^{\infty} x^{\alpha-1} e^{-x} dx \quad (3.12)$$

and

$$g_\alpha(z) = \frac{1}{\Gamma(\alpha)} \int_0^{\infty} \frac{x^{\alpha-1}}{z^{-1}e^x - 1} dx = \sum_{k=1}^{\infty} \frac{z^k}{k^\alpha}. \quad (3.13)$$

When the bosonic gas system is cooled, its energy  $\epsilon_k$  decreases and, consequently  $\mu$  must increase in order to conserve the total number of particles. Since  $\mu < 0$ , an upper limit for the number of particles in the excited states can be deduced by setting the maximum value of the chemical potential in the integral (3.11) to be zero. Denoting this upper limit by  $N_{\text{ex}}^{\text{max}}$ , and making use of Eqs. (3.8) and (3.9), one can arrive at

$$N_{\text{ex}}^{\text{max}} = V\zeta(3/2)\lambda_{dB}^{-3} = 2.612V \left( \frac{2\pi\hbar^2}{mk_B T} \right)^{-\frac{3}{2}}. \quad (3.14)$$

At high temperature where  $\mu \ll 0$ , all the particles are essentially in the excited states and hence  $N_{\text{ex}}^{\text{max}} \gg N_0$ . When the temperature of the system decreases, the value of the chemical potential increases from the negative towards zero, and eventually reaches the critical temperature at which  $N_{\text{ex}}^{\text{max}}(T) \rightarrow N_{\text{ex}}(T_c)$ . This leads, upon making use of Eq. (3.14), to

$$T_c = \frac{2\pi\hbar^2}{mk_B} \left( \frac{N_{\text{ex}}}{2.612V} \right)^{2/3}. \quad (3.15)$$

Below the critical temperature, the particles can no longer be accommodated in the excited states but continue to fall down to the ground state. Further cooling of the system leads to more and more particles in the ground state forming a macroscopic population.

Now using Eqs. (3.4) and (3.15), the condensate fraction as a function of temperature for a general system can be expressed as

$$\frac{N_0}{N} = \frac{N - N_{\text{ex}}}{N} = 1 - \left( \frac{T}{T_c} \right)^\alpha. \quad (3.16)$$

At this level the number of excited particles at temperatures below the critical temperature can be rewritten as

$$N_{\text{ex}} = N \left( \frac{T}{T_c} \right)^\alpha. \quad (3.17)$$

For bosonic particles in a 3D box, where  $\alpha = 3/2$ , the condensate fraction is turned out to be

$$\frac{N_0}{N} = 1 - \left(\frac{T}{T_c}\right)^{3/2}. \quad (3.18)$$

For a 3D harmonic oscillator potential on the other hand,  $\alpha = 3$  and hence the condensate fraction becomes

$$\frac{N_0}{N} = 1 - \left(\frac{T}{T_c}\right)^3. \quad (3.19)$$

From Eqs. (3.16, 3.18, 3.19), one can easily see that the condensate fraction explicitly depends on temperature and has a maximum value of unity when all the particles did fall down to the ground state at zero temperature ( $T = 0$ ). We can also verify that below the critical temperature a finite fraction of the total number of particles occupy a single quantum state. This is one of the defining features of Bose-Einstein condensation. Note that the critical (or transition) temperature  $T_c$  is defined as the highest temperature at which there may exist a macroscopic occupation of the ground state as described in Fig 3.1.

As can be seen from Fig 3.1 and the above derivation, BEC occurs when a collection of identical bosonic particles are cooled down to a very low temperature such that their quantum mechanical de Broglie waves overlap [63]. Hence for  $T \leq T_c$  we have

$$n \lambda_{dB}^3 \geq 2.612, \quad (3.20)$$

where  $n = N/V$  is the density of the Bose gas. Relation (3.20) is a crucial criterion for the occurrence of Bose-Einstein condensates. The equality holds true at the phase transition for Bose-Einstein condensation. When the temperature lowers further below the critical point, the de Broglie wavelength of the atoms becomes larger than the atomic separation.

BEC is indeed an extraordinary kind of phase transition, because unlike other phase transitions, it does not need necessarily interactions between atoms. In the case of BEC, the underlying ingredient is the quantum mechanical indistinguishability of atoms of the same element. In every other kind of phase transition, real forces between the atoms or particles may cause a sudden change of state, say from a gas to a liquid. However this is not the case for Bose-Einstein condensates. The BEC transition occurs when bosonic gases of a thermal cloud become cold enough so that their de Broglie wavelength becomes of the order of or greater than their mean inter-particle spacing as shown in Fig. 3.1.

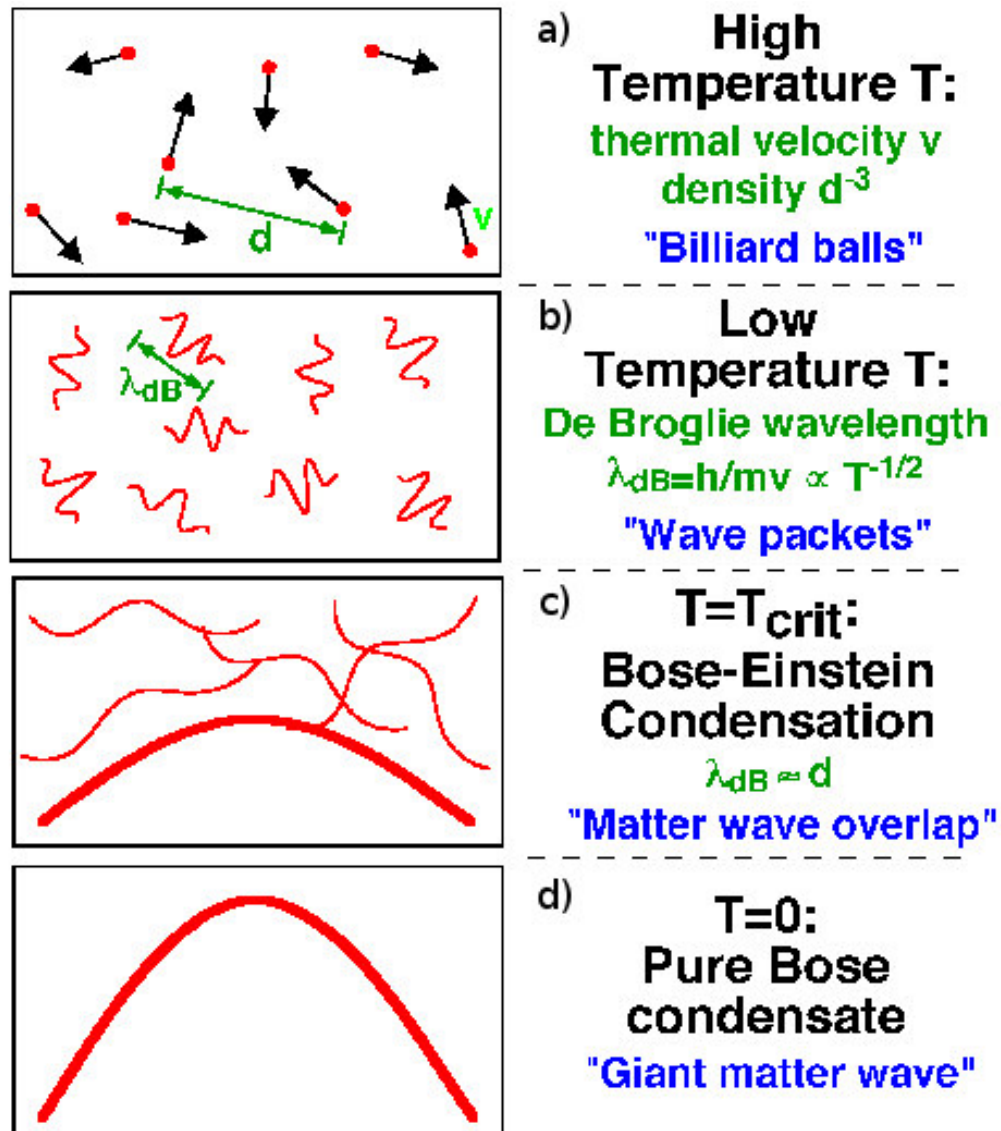


Figure 3.1: (Color online) Simplified matter wave interpretation [63] at different temperatures: (a) At high temperature,  $T \gg T_c$ ,  $\lambda_{dB} \ll d$  and the particles are in thermal motion; (b) at  $T \rightarrow T_c$ ,  $\lambda_{dB} \rightarrow d$  and wave packets appear; (c) at  $T = T_c$ ,  $\lambda_{dB} = d$  and BEC is emerged; (d) at  $T \ll T_c$  or  $T = 0$ ,  $\lambda_{dB} \gg d$  and BEC with coherent phase is created (Courtesy of [http://cua.mit.edu/ketterle\\_group/Nice\\_pics.htm](http://cua.mit.edu/ketterle_group/Nice_pics.htm)).

### 3.2 Historical Development of Bose-Einstein Condensates

The history of BEC began in 1925 during the early days of quantum mechanics, when Einstein, based on the initial work of Bose [64] on the statistics

of photons, generalised the idea to non-interacting massive bosonic particles [65].

Initially Einstein's prediction was subject of many controversies mainly due to the lack of opportunity to observe this phenomenon experimentally. One of the reasons for the pessimism at that time was the fact that the BEC phase transition is usually masked by inter-particle interactions.

Indeed, although BEC played a fundamental role in the analysis of superfluidity in  $^4\text{He}$  [66–68], it was not until the mid 90's that a pure BEC was obtained in alkali atoms, following the extraordinary developments on atomic cooling and trapping discussed in Chapter 2.

The long awaited Bose-Einstein condensation was realised experimentally (Fig. 3.2) for the first time in 1995 by the group of E. Cornell and C. Wieman in  $^{87}\text{Rb}$  atoms [5]. Rapidly after that, BEC was observed in  $^{23}\text{Na}$  by the

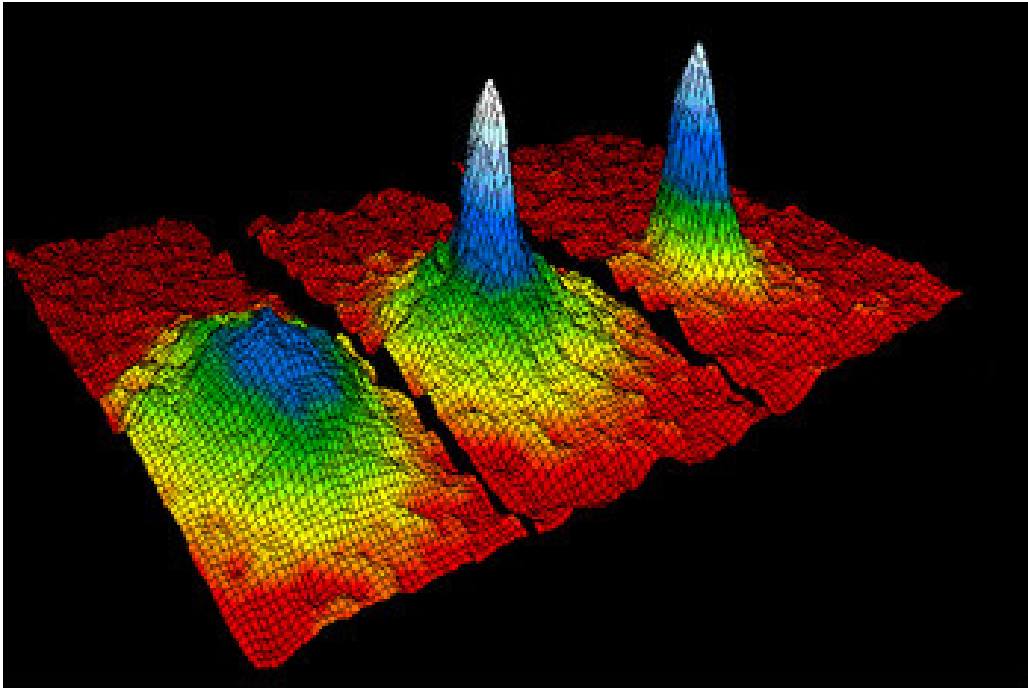


Figure 3.2: (Color online) Diagram of the first experimental observation of BEC [5] in  $^{87}\text{Rb}$ . It depicts velocity distribution at different temperatures. The one to left is bosonic cloud just before condensation ( $T > T_c$ ), the central is at  $T = T_c$  where condensation appears, and the one to the right is pure BEC ( $T \ll T_c$ ) (Courtesy of [http://en.wikipedia.org/wiki/Bose-Einstein\\_condensation](http://en.wikipedia.org/wiki/Bose-Einstein_condensation)).

group of W. Ketterle [6] and in  $^7\text{Li}$  by the group of R. Hulet [7].

Initially there was a strong hope to observe BEC in spin polarised hydrogen due to the pioneering work of Hecht [69]. However, it was almost after 40 years since Hecht's work and three years after the first BEC in  $^{87}\text{Rb}$  that the first experimental observation of condensation in atomic hydrogen was reported by Fried *et al.* in 1998 [70]. More recently condensation has been achieved in  $^{85}\text{Rb}$  [71], metastable  $^4\text{He}$  [72],  $^{41}\text{K}$  [73],  $^{133}\text{Cs}$  [74],  $^{174}\text{Yb}$  [75] and  $^{52}\text{Cr}$  [76]. Ytterbium and Chromium are notably different from the others condensates. This is because Ytterbium is the only atom condensed so far with two valence electrons, and Chromium has a large magnetic dipole moment. Recently  $\text{Li}_2$  [77] and  $\text{K}_2$  [78] molecules have been also condensed.

### 3.3 Mean-field Theory of Ultracold Bosonic Gases

#### 3.3.1 The Gross-Pitaevskii Equation

The Gross-Pitaevskii equation (GPE), developed in the early 60s by Pitaevskii [79] and Gross [80, 81], describes successfully most of the BEC properties at very low temperatures. Since we are going to make use of the GPE in the next two Chapters, we include here the basic derivation of this equation. The Hamiltonian of a system of  $N$  weakly interacting spinless bosons, interacting through a pair potential,  $V_1(\mathbf{r}, \mathbf{r}')$ , and immersed in an external trapping potential,  $V_{\text{trap}}(\mathbf{r})$ , reads

$$\begin{aligned} \hat{H}(\mathbf{r}, t) = & \int d^3\mathbf{r} \hat{\Psi}^\dagger(\mathbf{r}, t) \left( -\frac{\hbar^2}{2m} \nabla^2(\mathbf{r}) + V_{\text{trap}}(\mathbf{r}) \right) \hat{\Psi}(\mathbf{r}, t) \\ & + \frac{1}{2} \int d^3\mathbf{r} \int d^3\mathbf{r}' \hat{\Psi}^\dagger(\mathbf{r}, t) \hat{\Psi}^\dagger(\mathbf{r}', t) V_1(\mathbf{r}, \mathbf{r}') \hat{\Psi}(\mathbf{r}', t) \hat{\Psi}(\mathbf{r}, t), \end{aligned} \quad (3.21)$$

where  $\hat{\Psi}(\mathbf{r}, t)$  and  $\hat{\Psi}^\dagger(\mathbf{r}, t)$  are the bosonic field operators that, respectively, represent the annihilation and creation of a bosonic particle at the position  $\mathbf{r}$  and satisfy the crucial bosonic commutation relations shown in Eqs. (3.24) and (3.25).

If the gas is dilute and cold enough, the characteristic de Broglie wavelength of the particles and the mean inter-particle separation are usually much larger than the characteristic radius of the inter-particle interaction. For typical condensates (with the exception of Chromium whose dipole interactions play a significant role) the interaction between these extremely low energetic particles is characterised by the s-wave scattering length  $a_s$ , and hence the true potential can be substituted by a contact pseudo-potential

$$V_1(\mathbf{r}, \mathbf{r}') = g\delta(\mathbf{r} - \mathbf{r}'), \quad (3.22)$$

where

$$g = \frac{4\pi\hbar^2 a_s}{m} \quad (3.23)$$

is the 3D coupling constant.

Making use of Eq. (3.22) and integrating over all  $\mathbf{r}'$ , as well as applying the bosonic commutation relations,

$$[\hat{\Psi}(\mathbf{r}', t), \hat{\Psi}(\mathbf{r}, t)] = [\hat{\Psi}^\dagger(\mathbf{r}', t), \hat{\Psi}^\dagger(\mathbf{r}, t)] = 0 \quad (3.24)$$

and

$$[\hat{\Psi}(\mathbf{r}', t), \hat{\Psi}^\dagger(\mathbf{r}, t)] = \delta(\mathbf{r}' - \mathbf{r}), \quad (3.25)$$

the many-body Hamiltonian (3.21) takes the form

$$\begin{aligned} \hat{H}(\mathbf{r}, t) &= \int d^3\mathbf{r} \hat{\Psi}^\dagger(\mathbf{r}, t) \left( -\frac{\hbar^2}{2m} \nabla^2(\mathbf{r}, t) + V_{\text{trap}}(\mathbf{r}) \right) \hat{\Psi}(\mathbf{r}, t) \\ &\quad + \frac{g}{2} \int d^3\mathbf{r} \hat{\Psi}^\dagger(\mathbf{r}, t) \hat{\Psi}^\dagger(\mathbf{r}, t) \hat{\Psi}(\mathbf{r}, t) \hat{\Psi}(\mathbf{r}, t). \end{aligned} \quad (3.26)$$

Using the Heisenberg time evolution equation for the Hamiltonian (3.26) and the state  $\hat{\Psi}(\mathbf{r}', t)$ , one gets

$$\begin{aligned} i\hbar \frac{\partial \hat{\Psi}(\mathbf{r}', t)}{\partial t} &= [\hat{\Psi}(\mathbf{r}', t), \hat{H}(\mathbf{r}, t)] \\ &= \int d^3\mathbf{r} \left[ \hat{\Psi}(\mathbf{r}', t), \hat{\Psi}^\dagger(\mathbf{r}, t) \left( -\frac{\hbar^2}{2m} \nabla^2(\mathbf{r}, t) + V_{\text{trap}}(\mathbf{r}) \right) \hat{\Psi}(\mathbf{r}, t) \right] \\ &\quad + \frac{g}{2} \int d^3\mathbf{r} \left[ \hat{\Psi}(\mathbf{r}', t), \hat{\Psi}^\dagger(\mathbf{r}, t) \hat{\Psi}^\dagger(\mathbf{r}, t) \hat{\Psi}(\mathbf{r}, t) \hat{\Psi}(\mathbf{r}, t) \right]. \end{aligned} \quad (3.27)$$

Using the property of the commutation relation

$$[\hat{A}, \hat{B}\hat{C}] = [\hat{A}, \hat{B}]\hat{C} + \hat{B}[\hat{A}, \hat{C}], \quad (3.28)$$

applying relations (3.24) and (3.25), and replacing  $\mathbf{r}'$  by  $\mathbf{r}$  based on Eq. (3.22), we arrive finally at the operator form of the GPE which reads as

$$\begin{aligned} i\hbar \frac{\partial \hat{\Psi}(\mathbf{r}, t)}{\partial t} &= \left( -\frac{\hbar^2}{2m} \nabla^2(\mathbf{r}, t) + V_{\text{trap}}(\mathbf{r}) \right) \hat{\Psi}(\mathbf{r}, t) \\ &\quad + g \hat{\Psi}^\dagger(\mathbf{r}, t) \hat{\Psi}(\mathbf{r}, t) \hat{\Psi}(\mathbf{r}, t). \end{aligned} \quad (3.29)$$

This is a differential equation in the form of operators, and hence difficult to solve it even numerically without carrying further approximations. To this aim, it is common to split the Bose field operator in Eq. (3.29) into

$$\hat{\Psi}(\mathbf{r}, t) = \Phi(\mathbf{r}, t) + \delta\hat{\psi}(\mathbf{r}, t), \quad (3.30)$$

where

$$\Phi(\mathbf{r}, t) = \langle \hat{\Psi}(\mathbf{r}, t) \rangle \quad (3.31)$$

is the ground state expectation value of the Bose field that describes a non-uniform condensate, and  $\delta\hat{\psi}(\mathbf{r}, t)$  and  $\delta\hat{\psi}^\dagger(\mathbf{r}, t)$  annihilates and creates non-condensate particles respectively.

Making use of the decomposition (3.31) and setting  $\Phi(\mathbf{r}, t) = \Phi$ ,  $\Phi^*(\mathbf{r}, t) = \Phi^*$ ,  $\delta\hat{\psi}(\mathbf{r}, t) = \delta\hat{\psi}$  and  $\delta\hat{\psi}^\dagger(\mathbf{r}, t) = \delta\hat{\psi}^\dagger$  for convenience, the cubic non-linearity of the Bose operator is expressed as

$$\begin{aligned} \hat{\Psi}^\dagger \hat{\Psi} \hat{\Psi} &= (\Phi^* + \delta\hat{\psi}^\dagger)(\Phi + \delta\hat{\psi})(\Phi + \delta\hat{\psi}) \\ &= |\Phi|^2 \Phi + 2|\Phi|^2 \delta\hat{\psi} + \Phi^2 \delta\hat{\psi}^\dagger \\ &+ \Phi^* \delta\hat{\psi} \delta\hat{\psi} + 2\Phi \delta\hat{\psi}^\dagger \delta\hat{\psi} + \delta\hat{\psi}^\dagger \delta\hat{\psi} \delta\hat{\psi}. \end{aligned} \quad (3.32)$$

The last term in Eq. (3.32) can be treated using the self consistent mean-field approximation, as used in [82, 83], to obtain

$$\delta\hat{\psi}^\dagger \delta\hat{\psi} \delta\hat{\psi} \approx 2\langle \delta\hat{\psi}^\dagger \delta\hat{\psi} \rangle \delta\hat{\psi} + \langle \delta\hat{\psi} \delta\hat{\psi} \rangle \delta\hat{\psi}^\dagger. \quad (3.33)$$

In view of Eq. (3.33), Eq. (3.32) leads to

$$\begin{aligned} \hat{\Psi}^\dagger \hat{\Psi} \hat{\Psi} &= |\Phi|^2 \Phi + 2[|\Phi|^2 + \langle \delta\hat{\psi}^\dagger \delta\hat{\psi} \rangle] \delta\hat{\psi} + [\Phi^2 + \langle \delta\hat{\psi} \delta\hat{\psi} \rangle] \delta\hat{\psi}^\dagger \\ &+ 2\Phi \delta\hat{\psi}^\dagger \delta\hat{\psi} + \Phi^* \delta\hat{\psi} \delta\hat{\psi}. \end{aligned} \quad (3.34)$$

Now substituting Eqs. (3.30, 3.34) into Eq. (3.29) yields

$$\begin{aligned} i\hbar \left( \frac{\partial \Phi}{\partial t} + \frac{\partial \delta\hat{\psi}}{\partial t} \right) &= \left( -\frac{\hbar^2}{2m} \nabla^2 + V_{\text{trap}}(\mathbf{r}) \right) (\Phi + \delta\hat{\psi}) + g|\Phi|^2 \Phi \\ &+ 2g(|\Phi|^2 + \langle \delta\hat{\psi}^\dagger \delta\hat{\psi} \rangle) \delta\hat{\psi} + g(\Phi^2 + \langle \delta\hat{\psi} \delta\hat{\psi} \rangle) \delta\hat{\psi}^\dagger \\ &+ 2g\Phi \delta\hat{\psi}^\dagger \delta\hat{\psi} + g\Phi^* \delta\hat{\psi} \delta\hat{\psi}. \end{aligned} \quad (3.35)$$

Neglecting all sort of fluctuations, Eq. (3.35) reduces to

$$i\hbar \frac{\partial \Phi(\mathbf{r}, t)}{\partial t} = \left( -\frac{\hbar^2}{2m} \nabla^2 + V_{\text{trap}} \right) \Phi(\mathbf{r}, t) + g|\Phi|^2(\mathbf{r}, t) \Phi(\mathbf{r}, t) \quad (3.36)$$

which is the Gross-Pitaevskii equation [79–81] that describes the time evolution of the condensate wavefunction. This equation is very useful in the numerical study of weakly interacting condensates at low temperatures. Note also that the terms  $\langle \delta\hat{\psi}^\dagger \delta\hat{\psi} \rangle$  and  $\langle \delta\hat{\psi} \delta\hat{\psi} \rangle$  neglected above for the ground state can be used in the determination of fluctuations/excitations employing the Bogoliubov-de Gennes equations [84] described in Sec. 3.3.3.

In this Thesis we employ the GPE (3.36) to investigate the dynamics of weakly interacting 1D condensates at zero and finite temperature in the next two Chapters. The structure of the GPE in 1D is basically similar to its 3D counterpart: with  $\mathbf{r} \rightarrow x_i$ , where  $i$  stands for  $x, y$  or  $z$ ,  $n \rightarrow n_{1D}$  and  $g \rightarrow g_{1D}$ .

### 3.3.2 Ground State Energy of Condensates

Within the formalism of the mean-field theory it is not difficult to obtain the ground state energy from the stationary solution of the Gross-Pitaevskii equation (3.36). In this case, the condensate wave function can be written as

$$\Phi(\mathbf{r}, t) = \Phi_0(\mathbf{r}) \exp(-i\mu t/\hbar), \quad (3.37)$$

where  $\mu$  is the chemical potential and  $\Phi_0(\mathbf{r})$  is the time independent ground state wavefunction which is real and normalised to the total number of condensed particles

$$\int |\Phi_0(\mathbf{r})|^2 d\mathbf{r} = N. \quad (3.38)$$

Substituting Eq. (3.37) into the GPE (3.36) leads to the time independent Gross-Pitaevskii equation

$$\left[ -\frac{\hbar^2}{2m} \nabla^2 + V_{\text{trap}}(\mathbf{r}) + g |\Phi_0(\mathbf{r})|^2 \right] \Phi_0(\mathbf{r}) = \mu \Phi_0(\mathbf{r}). \quad (3.39)$$

### 3.3.3 The Bogoliubov-de Gennes Equations

As mentioned earlier, the GPE (3.36) is a useful tool to study the properties of BECs. In deriving the GPE, both quantum and thermal fluctuations are considered to be negligible. In order to incorporate effects of fluctuations, one can begin by looking for a solution of the GPE (3.36) in the form of small excitations or oscillations. For this purpose the fluctuations of the order parameter around the ground state are assumed

$$\Phi(\mathbf{r}, t) = e^{-i\mu t/\hbar} \left( \Phi_0(\mathbf{r}) + u(\mathbf{r}) e^{-i\omega t} + v^*(\mathbf{r}) e^{i\omega t} \right), \quad (3.40)$$

where  $\omega$  is the frequency of the excitations, and  $u(\mathbf{r})$  and  $v(\mathbf{r})$  being complex wave functions. This equation (3.40) describes weak perturbations of the wavefunction  $\Phi(\mathbf{r}, t)$ .

Now substituting equation (3.40) into Eq. (3.36) leads to

$$\begin{aligned} i\hbar \frac{\partial}{\partial t} \Phi(\mathbf{r}, t) &= e^{-i\mu t/\hbar} \left[ \mu \Phi_0(\mathbf{r}) + (\mu + \hbar\omega) u(\mathbf{r}) e^{-i\omega t} \right. \\ &\quad \left. + (\mu - \hbar\omega) v^*(\mathbf{r}) e^{i\omega t} \right]. \end{aligned} \quad (3.41)$$

The nonlinear term in Eq. (3.36), using Eq. (3.40), can be expressed as

$$\begin{aligned} |\Phi(\mathbf{r}, t)|^2 \Phi(\mathbf{r}, t) &= e^{-i\mu t/\hbar} \left[ \Phi_0^*(\mathbf{r}) + u^*(\mathbf{r}) e^{i\omega t} + v(\mathbf{r}) e^{-i\omega t} \right] \\ &\quad \times \left[ \Phi_0(\mathbf{r}) + u(\mathbf{r}) e^{-i\omega t} + v^*(\mathbf{r}) e^{i\omega t} \right] \\ &\quad \times \left[ \Phi_0(\mathbf{r}) + u(\mathbf{r}) e^{-i\omega t} + v^*(\mathbf{r}) e^{i\omega t} \right] \end{aligned} \quad (3.42)$$

Inserting Eqs. (3.40), (3.41) and (3.42) into Eq. (3.36), dropping all higher order terms of  $u(\mathbf{r})$  and  $v(\mathbf{r})$  (a detail derivation is available in Appendix A) one arrives finally to the following coupled equations

$$\begin{cases} \hbar\omega u(\mathbf{r}) = \left( -\frac{\hbar^2}{2m}\nabla^2 + V_{\text{trap}}(\mathbf{r}) - \mu + 2g|\Phi_0(\mathbf{r})|^2 \right) u(\mathbf{r}) + g\Phi_0^2(\mathbf{r}) v(\mathbf{r}) \\ -\hbar\omega v(\mathbf{r}) = \left( -\frac{\hbar^2}{2m}\nabla^2 + V_{\text{trap}}(\mathbf{r}) - \mu + 2g|\Phi_0(\mathbf{r})|^2 \right) v(\mathbf{r}) + g\Phi_0^{*2}(\mathbf{r}) u(\mathbf{r}). \end{cases} \quad (3.43)$$

These equations (3.43) are known as Bogoliubov-de Gennes (BdG) equations [84] and refer to weakly interacting dilute bosonic gases with excited states. By solving these coupled equations, one can determine the energy of excitations  $\hbar\omega$ . For this purpose, one needs to rewrite the above coupled equations (3.43) in matrix form, in terms  $u(\mathbf{r})$  and  $v(\mathbf{r})$  as

$$\begin{pmatrix} H_0 - \mu + 2g|\Phi_0(\mathbf{r})|^2 & g\Phi_0^2(\mathbf{r}) \\ g\Phi_0^{*2}(\mathbf{r}) & H_0 - \mu + 2g|\Phi_0(\mathbf{r})|^2 \end{pmatrix} \begin{pmatrix} u(\mathbf{r}) \\ v(\mathbf{r}) \end{pmatrix} = \hbar\omega \begin{pmatrix} u(\mathbf{r}) \\ -v(\mathbf{r}) \end{pmatrix} \quad (3.44)$$

where

$$H_0 = -\frac{\hbar^2}{2m}\nabla^2 + V_{\text{trap}}(\mathbf{r}). \quad (3.45)$$

Solutions to the matrix (3.44) can be obtained by solving the eigenvalue equation

$$\begin{vmatrix} H_0 - \mu - \hbar\omega + 2g|\Phi_0(\mathbf{r})|^2 & g\Phi_0^2(\mathbf{r}) \\ g\Phi_0^{*2}(\mathbf{r}) & H_0 - \mu + \hbar\omega + 2g|\Phi_0(\mathbf{r})|^2 \end{vmatrix} = 0. \quad (3.46)$$

Solving the determinant (3.46) yields the required expression for the excitation energy

$$(\hbar\omega)^2 = \left( -\frac{\hbar^2}{2m}\nabla^2 + V_{\text{trap}}(\mathbf{r}) - \mu + 2g|\Phi_0(\mathbf{r})|^2 \right)^2 - (g|\Phi_0(\mathbf{r})|^2)^2. \quad (3.47)$$

For spatially homogeneous Bose gas ( $V_{\text{trap}}(\mathbf{r}) = 0$ ) with background density  $n(\mathbf{r}) = |\Phi_0(\mathbf{r})|^2 = n$ , and  $\mu = ng$ , Eq. (3.47) can be expressed as

$$(\hbar\omega)^2 = \left( \frac{\hbar^2 q^2}{2m} + gn \right)^2 - (gn)^2, \quad (3.48)$$

which finally leads to the Bogoliubov dispersion law

$$(\hbar\omega)^2 = \left( \frac{\hbar^2 q^2}{2m} \right) \left( \frac{\hbar^2 q^2}{2m} + 2gn \right). \quad (3.49)$$

For increasing momentum or for oscillations having wavelengths much smaller than the size of the condensate, the spectrum coincides with that of the free particle energy  $\hbar\omega = \hbar^2 q^2 / 2m$ . These are referred to as particle-like excitations. However at the opposite limit, i.e. at low momentum, the spectrum becomes linear, i.e.,  $\omega = cq$  which is a phonon dispersion, where  $c$  is the sound velocity  $c = \sqrt{gn/m}$ .

### 3.3.4 The Thomas-Fermi Approximation

For large number of particles and when the chemical potential  $\mu$  greatly exceeds the level spacing of the trap, the quantum pressure, i.e. the kinetic energy term in Eq. (3.39), becomes much smaller than the non-linear term and can be neglected. This approach finally leads to

$$[V_{\text{trap}}(\mathbf{r}) + g|\Phi_0(\mathbf{r})|^2 - \mu] \Phi_0(\mathbf{r}) = 0, \quad (3.50)$$

which is called the Thomas-Fermi approximation. For an harmonic trap, the density profile takes the expression

$$n(\mathbf{r}) = \begin{cases} \frac{\mu - V_{\text{trap}}(\mathbf{r})}{g}, & \text{for } \mu > V_{\text{trap}}(\mathbf{r}) \\ 0 & \text{otherwise.} \end{cases} \quad (3.51)$$

When in particular the radial component is assumed to be frozen, Eq. (3.51) reduces into 1D Thomas Fermi density profile. This is a downward parabola (see Fig. 3.3).

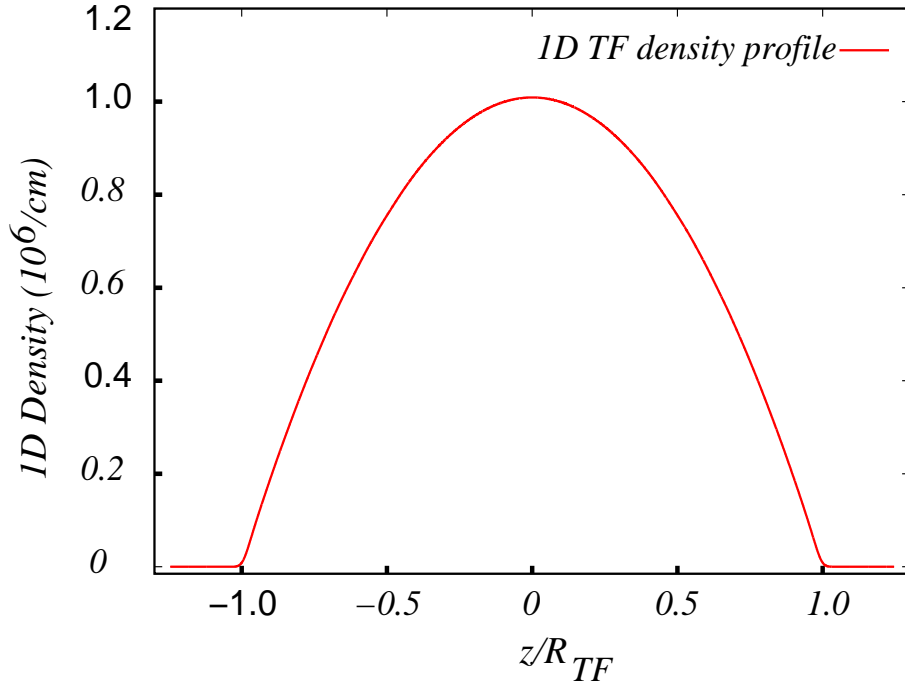


Figure 3.3: (Color online) Thomas-Fermi density distribution (atoms/cm) of 12000  $^{87}\text{Rb}$  bosonic atoms in a one-dimensional configuration as a function of axial coordinate per Thomas-Fermi radius of the condensate ( $z/R_{\text{TF}}$ ).

For a 1D harmonic trap whose radial motion is frozen due to the fact that the 1D chemical potential  $\mu$  (given in Eq. 4.2) is of the order of the radial level spacing ( $\hbar\omega_\perp$ ), the 1D Thomas-Fermi density profile,  $n(z)$ , can be found by integrating Eq. (3.51) with respect to the radial components  $x$  and  $y$ . An analytical approach to the same equation in the 1D case yields

$$n(z) = \begin{cases} n_{max} (1 - (z/R_{TF})^2), & \text{for } |z| < R_{TF}, \\ 0 & \text{otherwise.} \end{cases} \quad (3.52)$$

where  $R_{TF}$  is the Thomas-Fermi radius,  $n_{max} = \mu/g_{1D}$  is the maximum density at the centre of the trap ( $z/R_{TF} = 0$ ) and  $g_{1D} = 2\hbar\omega_\perp a_s$  is the 1D coupling constant.

### 3.4 Summary

In this Chapter we have reviewed the introductory concepts and historical developments of Bose-Einstein condensation.

We have derived the Gross-Pitaevskii and Bogoliubov-de Gennes equations for weakly interacting Bose-Einstein condensates at zero temperature. By including small depletion or fluctuations on the ground state order parameter, we have described quantum fluctuations at zero temperature via the BdG equations.

# Chapter 4

## Splitting and Merging Elongated BEC at Finite Temperature

The experimental exploration of Bose-Einstein condensates (BECs) in many different systems such as alkali metal gases [5–7], hydrogen [70], meta-stable helium [72], and molecular Bose-Einstein condensation [77, 85–88] and condensation of fermionic atoms [89] has led to a surge of interest in manipulating ultracold atomic samples under very different circumstances. One of the initial motivations for such development was and is the prospect of creating a continuous and coherent atomic beam [90–92], which is the atomic analogy of the optical laser beam [93].

Among the major challenges in achieving a continuous atom laser is how to overcome the difficulty due to the restrictive cooling conditions for continuously condensing the atomic gas. Spatial separation of the evaporative cooling from the destructive laser cooling may play a role in alleviating these challenges [94]. Recently, a continuous BEC source was achieved by periodically replenishing a reservoir with condensates [92]. There, optical tweezers were used to transport sodium condensates from where they were created to the reservoir. Such procedure allows one to continuously replenish the reservoir which contains on average more than  $10^6$  atoms. Bringing a new condensate to the reservoir each time implies the merging of condensates with different relative phases since each condensate is created with a different phase. The merging of two condensates with different phases poses a limitation on the coherence of the process.

Recently, interference effects in the merging of 30 uncorrelated Bose-Einstein condensates released from a one-dimensional optical lattice have been discussed in [95], whereas coherent splitting of BECs by deforming an

optical single-well into a double-well potential for a trapped atom interferometer have been addressed in Refs. [96, 97]. Very recently, Schumm *et al.* [98] has demonstrated a coherent beam splitter on an atom chip by splitting the condensate in a double-well potential and merging it again. They have demonstrated phase preservation in this process, even in the case when the Split BECs are far enough apart to inhibit tunnel coupling.

In this Chapter, we analyze the axial splitting of a very much elongated cigar-shaped condensate into two condensates [99, 100] and their subsequent merging along the axial direction. Our analysis includes finite temperature effects. In other words, phase fluctuations arising due to temperature are taken into account during the whole process: splitting and merging. We observe that as long as the process of splitting and merging is adiabatic enough, both the Split and the Merged condensates, even at relatively large temperatures, do survive the effects of these fluctuations.

The opposite extreme, in which the maximum heat transfer with its surroundings occurs, causing the temperature to remain constant, is known as an isothermal process. Since temperature is thermodynamically conjugate to entropy, the isothermal process is conjugate to the adiabatic process for reversible transformations.

A transformation of a thermodynamic system can be considered adiabatic when it is quick enough so that no significant heat transfer happens between the system and the outside. At the opposite, a transformation of a thermodynamic system can be considered isothermal if it is slow enough so that the system's temperature can be maintained by heat exchange with the outside.

Low-dimensional quantum gases exhibit very fascinating properties and have attracted a lot of interest, both theoretically and experimentally [101–107]. It is known that low-dimensional [one- (1D) and two- (2D) dimensional] quantum gases differ qualitatively from their 3D counterparts [103, 108–110]. From a theoretical point of view, the use of a mean-field theory to describe a low-dimensional quantum gas is severely restricted. A widely used criterion to apply a mean-field approach is to demand that the average distance between particles,  $d$ , is clearly smaller than the correlation length of the condensate  $l_c = \hbar/\sqrt{mng}$  where  $m$ ,  $g$ , and  $n$  denote the mass, the interaction coupling, and the density, respectively. In three dimensions, the above condition leads to  $l_c/d \propto n^{-1/6}$  and is well satisfied for small densities, and the description of the system at  $T = 0$  with a mean-field Gross-Pitaevskii equation is fully satisfactory. In the one-dimensional case, however, this ratio behaves as  $l_c/d \propto n^{1/2}$  and this fact changes drastically the range of applicability of a mean-field treatment.

A careful analysis of the validity of a mean-field treatment in the 1D

case [111] leads to the following condition

$$\left(\frac{Na_s a_z}{a_\perp^2}\right)^{1/3} \gg 1, \quad (4.1)$$

where  $N$  is the number of condensed atoms,  $a_z = \sqrt{\hbar/(m\omega_z)}$  and  $a_\perp = \sqrt{\hbar/(m\omega_\perp)}$  are the axial and radial oscillator lengths, respectively, and  $\omega_z$  and  $\omega_\perp$  are the angular frequencies in the corresponding directions. Thus, in 1D, contrary to the 3D case, when the density decreases the gas gradually becomes strongly correlated, acquires a fermionic character, and enters into the so-called Tonks-Girardeau regime [112–115]. Experimental demonstration of a Tonks gas has been recently achieved [101, 102].

The possibility of generating low-dimensional bosonic gases raises the question of the effects of quantum fluctuations. In an untrapped 1D Bose system these fluctuations destroy finite as well as zero temperature condensation. For trapped Bose gases, the situation is quite different: for non-interacting bosons in such a trap the finite spacing between the lowest and the next energy level allows for the occurrence of 1D Bose-Einstein condensation even at finite temperatures as stipulated in Refs. [103, 105]. In such a case the absence of gapless excitations indicates that the BEC will not be destroyed immediately as interactions between bosons are turned on.

In 1D trapping geometries, long-wavelength density and phase fluctuations lead to a new intermediate state between a condensate and a non-condensed system, which is commonly referred to as a *quasi-condensate*. In quasi-condensates, the phase of the condensate is only coherent over a finite distance that is smaller than the system size. In other words, the phase coherence length is smaller than the axial size of the sample. To understand the nature of quasi-condensates at finite temperature, one has to analyze the behaviour of the single particle correlation function by calculating the fluctuations of phase and density as has been done by Petrov *et al.* [103]. There it is shown that for temperatures below the degeneracy temperature, the phase of the condensate indeed fluctuates, but fluctuations of the density are still highly suppressed. This character of thermal fluctuations is also present in highly elongated 3D gases [24], and has been recently observed experimentally in [17, 23, 26, 116, 117].

Quasi-1D geometries can be accessible in magnetic traps with a cylindrically symmetric harmonic potential along the axial direction that have transverse frequencies  $\omega_\perp$  much larger than the axial one  $\omega_z$ . In such configurations the resulting condensate looks like a cigar aligned along the symmetry or  $z$  axis. With current technology, condensates with aspect ratio  $\lambda = \omega_\perp/\omega_z$  as large as 1000 are achievable.

In this Chapter, we study the process of splitting and subsequent merging of an elongated condensate confined in a 1D geometry both at  $T = 0$ , i.e., when the condensate has a well-defined phase, and at finite temperature ( $T > 0$ ), in the quasi-condensate regime. For finite  $T$ , we analyze the process of splitting and merging for a wide range of temperatures, i.e.,  $T_\phi < T < T_d$ , where  $T_\phi = T_d \hbar \omega_z / \mu$  ( $\mu$  being the chemical potential) corresponds to the characteristic temperature above which a true-condensate turns into a quasi-condensate in which phase fluctuations begin to play a role. On the other hand  $T_d = N \hbar \omega_z / k_B$  is the 1D degeneracy temperature [103]. The transition, or crossover, between the different regimes for the 1D degenerate interacting bosonic gas, i.e., true-condensate, quasi-condensate, and Tonks gas is smooth. Thus, in the regime of quasi-condensation density fluctuations are relatively suppressed while phase fluctuations are enhanced. By keeping all parameters fixed and reducing the number of atoms, phase fluctuations become more and more pronounced, mean-field theory fails, and the gas enters into the strongly correlated regime or Tonks gas [112–115].

In our case, the splitting of the condensate is achieved by means of a double-well potential grown adiabatically on top of a trapping harmonic potential. By adiabatically switching off the double-well potential, we merge these condensates into a single one (Merged BEC). We would like to stress that we use the mean-field Gross-Pitaevskii equation (GPE) throughout this Chapter. It is worth pointing out that although the Gross-Pitaevskii equation [118] describes properly coherent evolution of the atomic mean-field at  $T = 0$ , it can also be used to solve time evolution at finite temperature in a relatively straightforward manner. It might look like that the mean-field method of the GPE allows to make statements only about first order coherence. But, as it is well known, a closely inspection reveals that the GPE contains as such classical Bogoliubov-de Gennes (BdG) equations, i.e., equations describing small fluctuations around a given solution of the GPE. Since we are here interested in the study of relatively high temperatures  $T > T_\phi$ , classical description of fluctuations is fully appropriate. It turns out that one can simulate temperature effects by adding fluctuations to the ground state solution of the GPE at  $T = 0$  in a way which mimics thermal fluctuations. At low temperatures  $T < T_c$ , where  $T_c = N / \ln(2N) \hbar \omega_z / k_B$  [105], this can be generally done by identifying phonon (quasi-particle) modes, i.e., eigensolutions of the BdG equations. The fluctuations are expressed thus as sums over the quasi-particles with amplitudes taken from Monte Carlo sampling and corresponding to the thermal (Boltzmann) populations of the quasi-particle modes. Such a method is used in this Chapter, with the additional simplification that for quasi-1D situations only the phase fluctuations are relevant.

Note that once we add the fluctuations initially at  $t = 0$ , and as long as they remain small in the course of evolution, they will propagate in time with a very good approximation as appropriate solutions of the time dependent BdG equations. Note also, that our approach allows in principle to obtain information about all correlation functions: either in the form of an average over Monte Carlo realizations of the initial fluctuations, or in the form of time averages, due to the (expected) ergodic character of the evolution. In some cases, even averaging over the initial data is not necessary: the results for different realizations are so similar that looking for few single cases allows one to draw conclusions about “coherence”. By coherence we mean here, that the splitting process of an initial 1D BEC into two spatially separated 1D BECs occurs with a well-defined relative phase between them. Their subsequent merging into a single merged BEC, when the process is fully coherent, should result in a single condensate with a well-defined relative phase with respect to the initial one. If this is the case, there is a perfect overlap between the densities of the initial and merged condensates.

It is worth stressing that our approach is a simplified version of the classical field methods used by several groups [119–127]. In their approach some emphasis was put on the explanation of the temperature concept, and a certain model of finite temperature effects has been studied. Particularly interesting is here the possibility of extracting higher order correlations from a single shot measurements [128–130], which in our case corresponds to a single realizations of the initial fluctuations.

## 4.1 Description of the Model

Here we consider  $^{87}\text{Rb}$  condensate with  $N = 1.2 \times 10^4$  atoms confined in an harmonic trap with frequencies  $\omega_{\perp}/2\pi = 715$  Hz and  $\omega_z/2\pi = 5$  Hz. For such parameters, the system is in the 1D Thomas-Fermi regime ( $\mu \gg \hbar\omega_z$ ) along the axial direction. The 1D chemical potential is given by

$$\mu = \hbar\omega_z \left( \frac{3}{4\sqrt{2}} \frac{N m g_{1D} \sqrt{\hbar/m\omega_z}}{\hbar^2} \right)^{2/3} \quad (4.2)$$

where  $g_{1D} = 2\hbar\omega_{\perp}a_s$  is the effective 1D coupling strength [131]. For our parameters, transverse excitations are suppressed ( $\mu \simeq \hbar\omega_{\perp}$ ), and the dynamics of such a Bose gas can be described by the usual mean-field GPE in 1D

$$i\hbar \frac{\partial \Psi(z, t)}{\partial t} = \left( -\frac{\hbar^2}{2m} \frac{\partial^2}{\partial z^2} + V_T(z, t) + g_{1D} N |\Psi(z, t)|^2 \right) \Psi(z, t), \quad (4.3)$$

where  $\Psi(z, t)$  is the mean-field order parameter, or in other words the condensate wavefunction. The potential term  $V_T(z, t)$  includes both the magnetic trap and the double-well potential as described below

$$\begin{aligned} V_T(z, t) &= V_{\text{trap}}(z) + V_{\text{op}}(z, t) \\ &= \frac{1}{2}m\omega_z^2 z^2 + S(t)V_0 \cos^2(k_l z). \end{aligned} \quad (4.4)$$

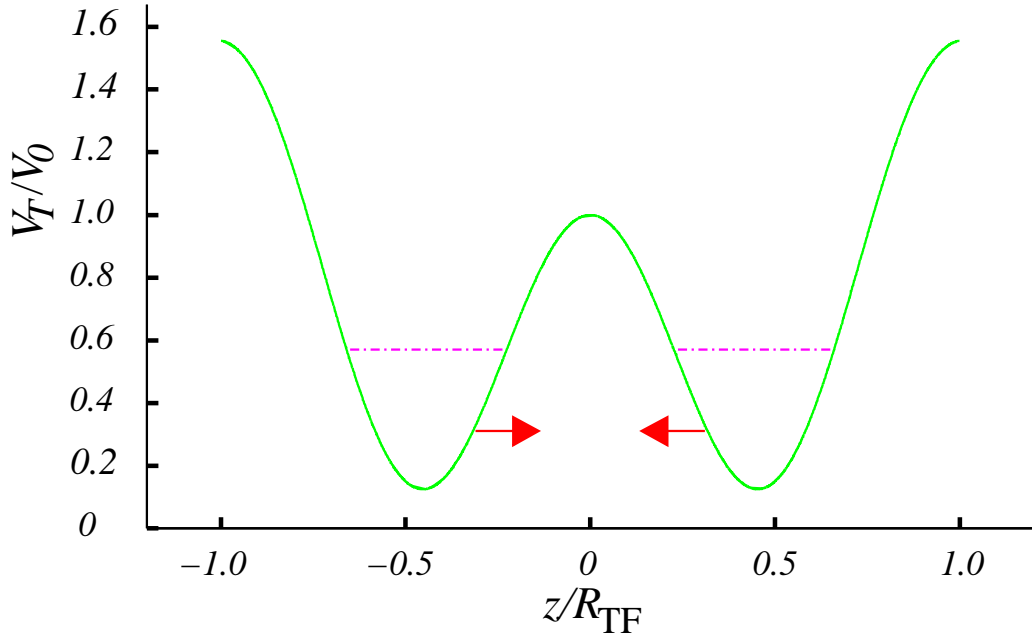


Figure 4.1: (Color online) Illustration of a double-well potential for splitting and merging of an elongated 1D BEC: a strong optical potential and an axial trapping potential are combined for creating a double-well potential which is used for splitting a 1D condensate, when switched on adiabatically, into two spatially separated symmetrical 1D condensates at the center of each well, and then merge them into one when switched off adiabatically again.

The potential used to split the condensate into two spatially separated condensates,  $V_{\text{op}}(z, t)$ , is switched on and off adiabatically by means of a time-dependent function  $S(t)$ . The maximum depth of this potential is  $V_0 = 2.2 \times 10^4 E_r$  in terms of the recoil energy  $E_r = \hbar^2 k_l^2 / 2m$  and  $k_l = 2\pi / \lambda_l$ . To achieve spatial separation of the Split condensates one has to require that the distance between the two wells is, at least, of the order of the Thomas-Fermi radius ( $R_{\text{TF}}$ ). It is given by

$$R_{\text{TF}} = \sqrt{2\mu / (m\omega_z^2)}, \quad (4.5)$$

so that  $k_l = \pi/R_{TF}$ . For  $N \simeq 10^4$  atoms, the Thomas-Fermi radius is  $R_{TF} \simeq 88\mu\text{m}$ . This is in agreement with the experimental results in Refs. [96, 98].

The time dependent function  $S(t)$  controls the switching on and off of the double-well potential and hence the overall splitting and merging process of the condensates. We define this function as

$$S(t) = \begin{cases} 0, & \text{for } t \leq t_{evo} \text{ and } t \geq t_{mer}, \\ \sin^2\left(\frac{\pi}{2} \frac{t-t_{evo}}{t_{spl}-t_{evo}}\right), & \text{for } t_{evo} < t < t_{spl}, \\ 1, & \text{for } t_{spl} \leq t \leq t_{con}, \\ \cos^2\left(\frac{\pi}{2} \frac{t-t_{con}}{t_{mer}-t_{con}}\right), & \text{for } t_{con} < t < t_{mer}. \end{cases} \quad (4.6)$$

In this equation (4.6),  $t_{evo}$  is the time duration required for evolving the 1D BEC in real time before the splitting process begins. It extends for 10ms. Just immediately after, the splitting process begins and continues for a time interval  $t_{spl}$ . At the end of  $t_{spl}$ , the function  $S(t)$  attains a maximum value of unity and remains constant for a time interval  $t_{con}$ . During this time interval, two spatially separated 1D BECs are created. At the beginning of the time span  $t_{mer}$ , merging of the condensates starts by switching off the double-well potential. This process continues until the two 1D BECs merge together. A complete merging is only possible when  $S(t)$  becomes finally zero, i.e., when the optical potential is completely switched off. In this case the atoms remain only under the influence of the trapping potential.

To ensure coherence during the process of the switching on and off of the optical potential, the raising of the double-well has to be slow enough to avoid excitations and to allow for quantum tunnelling between the two wells. Notice that the relevant time scale of excitations is given by the inverse of the frequency of the trap, in our case  $t_{sys} = 2\pi/\omega_z = 200$  ms. If  $t_{spl}, t_{mer} \gg t_{sys}$  we expect coherent splitting and merging. On the other hand, for  $t_{spl}, t_{mer}$  of the order of  $t_{sys}$  or less, the process creates more and more excitations that cause incoherence. The faster the double-well potential switches on and off the stronger the excitations are. To check our claims we have carried out further numerical simulations for several values of  $t_{spl}$  and  $t_{mer}$  around  $t_{sys}$ . In general, we have observed that a coherent process, at  $T = 0$ , is achieved for switching times of 400 ms (or larger).

The full time dependency of  $S(t)$  necessary for the coherent splitting and merging of the condensates based on Eq. (4.6) is illustrated in Fig. 4.2.

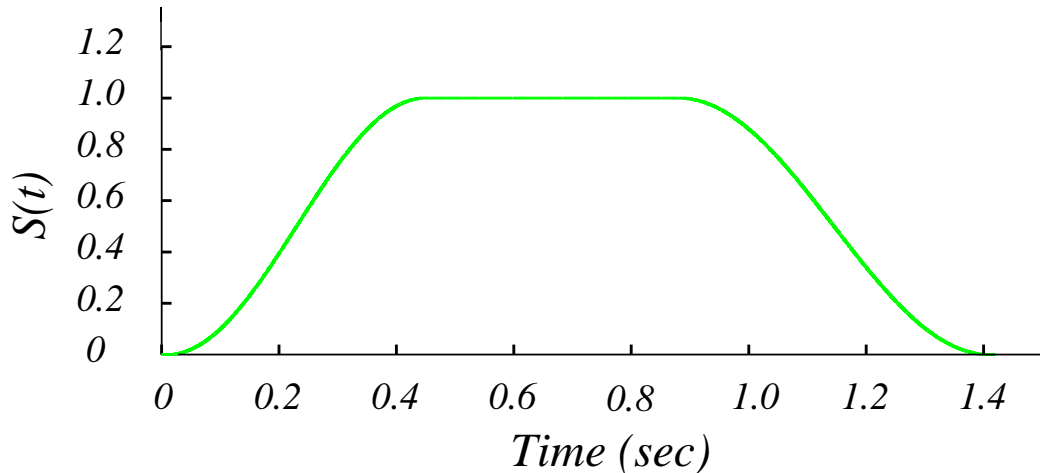


Figure 4.2: (Color online) Time dependence of the function  $S(t)$ . For the whole process, we fixed a time evolution of  $t_{\text{evo}} = 10$  ms, a splitting time of  $t_{\text{spl}} = 440$  ms, a time  $t_{\text{con}} = 430$  ms in which  $S(t)$  remains constant (unity), and a time of merging  $t_{\text{mer}} = 530$  ms and an additional time of 10 ms for allowing the Merged condensate to make its final evolution into a single condensate.

## 4.2 Splitting and Merging at Zero Temperature

We calculate first the ground state of the system by evolving the GPE (4.3) with  $S(t) = 0$  in imaginary time. After the ground state has been found, we numerically solve Eq. (4.3) with the pulse profile given by the time dependent-function  $S(t)$ .

The results of our simulations at temperature  $T = 0$ , are summarized in Fig. 4.3. There we display the condensates' density at three different times. First at  $t = 0$ , the Initial condensate (Initial 1D BEC) has a characteristic Thomas-Fermi profile with  $R_{\text{TF}} = 88\mu\text{m}$ . Then at  $t = 800$  ms (corresponding to the ramping up of the double-well potential in 400 ms and keeping it constant during additional 400 ms), two spatially well separated identical condensates (Split BECs) appeared, centered at  $z/R_{\text{TF}} = \pm 0.5$ , each of them with a number of atoms  $N_s = N/2$ . Finally, we display the density of the condensate at  $t = 1400$  ms. The Merged condensate (Merged 1D BEC) has exactly the same profile as the Initial one (Initial 1D BEC) and thus they cannot be distinguished in the figure, asserting that the process of splitting and merging is fully coherent.

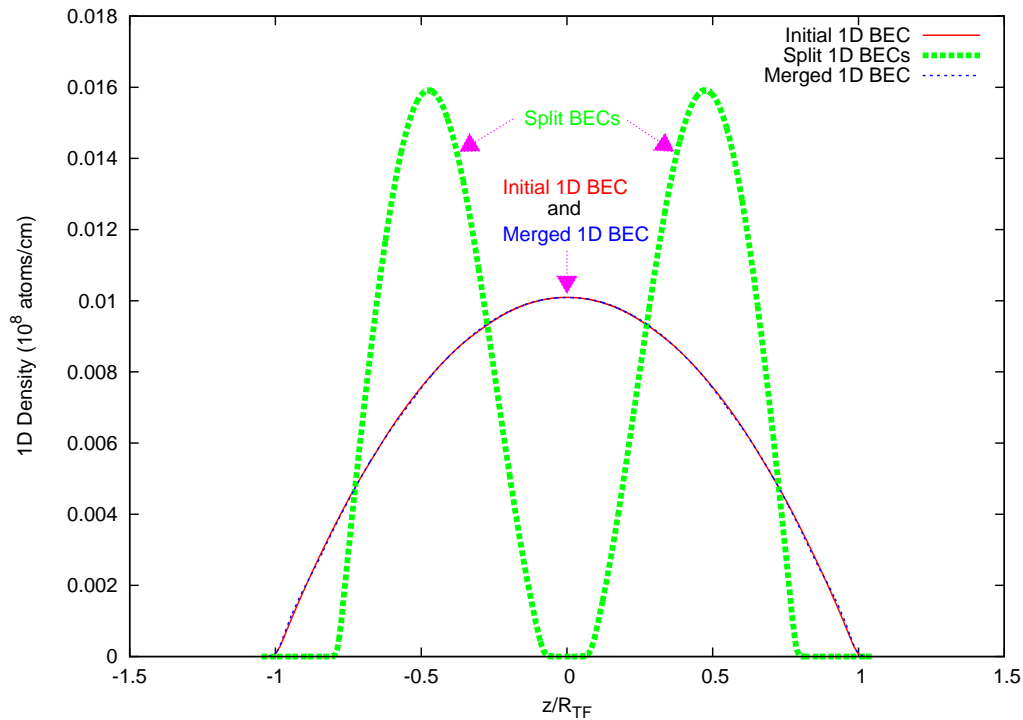


Figure 4.3: (Color online) Adiabatic splitting and merging of an elongated condensate at  $T = 0$ . After coherently splitting an initial 1D condensate (Initial BEC (red solid line)) into two spatially separated ones (Split BECs (green dashed line)), by adiabatically switching on the double-well potential given in Fig. 4.1, centered at  $z/R_{\text{TF}} = -0.5$  and  $z/R_{\text{TF}} = 0.5$ , the optical potential is again switched off adiabatically. This leads to a coherent merging of the Split condensates into a single one (Merged 1D BEC (blue dotted)). The Merged 1D BEC overlaps on top of the Initial 1D BEC which is an indication of a completely coherent merging process.

Coherence may be a prerequisite for further applications such as in atom interferometry and quantum-information processing [132].

Before we proceed to the case of finite temperature, it may be relevant to address the case of a non-adiabatic splitting and merging process, i.e., when the double-well potential switches on and off too fast. We have carried out simulations for switching times as short as 20 ms. In such cases the splitting of the condensate (even at  $T = 0$ ) becomes completely incoherent, there is no trace of phase preservation, and the condensate is destroyed, as is shown in Fig. 4.4. For shorter splitting times,  $t_{\text{spl}} < 20$  ms, it is not even possible to split the Initial BEC into two well spatially separated condensates. When

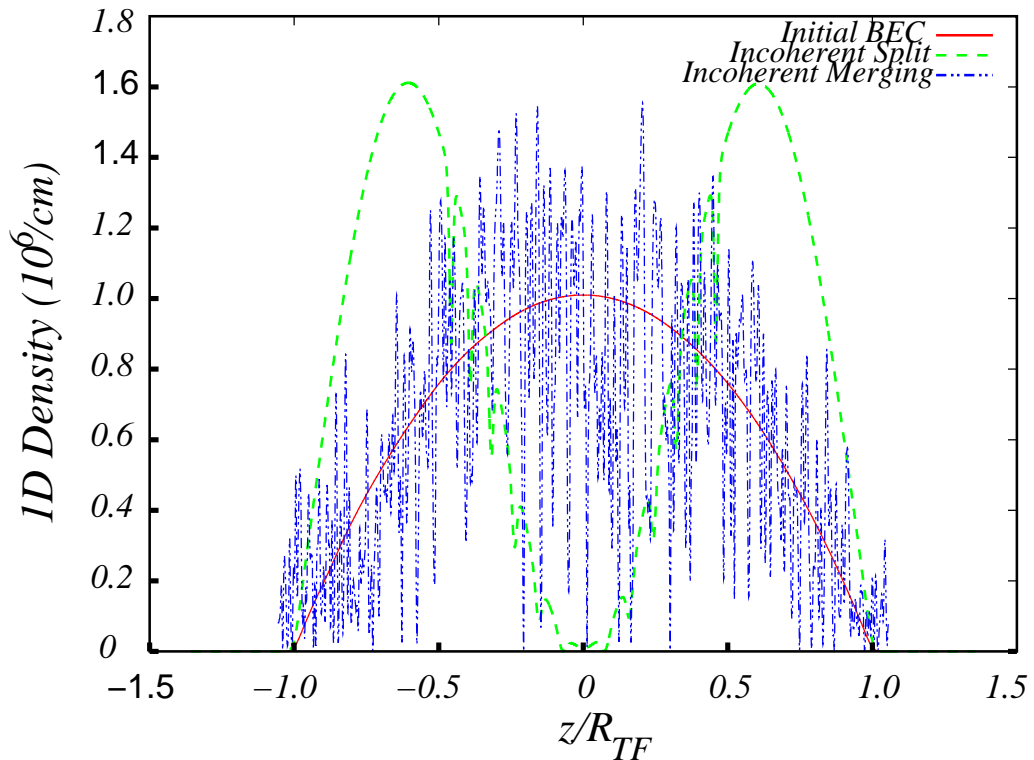


Figure 4.4: (Color online) Non-adiabatic splitting and merging of an elongated condensate at  $T = 0$ . The Initial BEC (red solid line) is split incoherently by considering a very small splitting time ( $t_{\text{spl}}$ ) into two picked spatially separated ones (Incoherent Split (green dashed line)) by non-adiabatically switching on the double-well potential (Fig. 4.1). The optical potential is again switched off non-adiabatically which leads to a completely incoherent pattern (Incoherent Merging (blue dotted line)) due to larger excitations.

it comes to the time of merging ( $t_{\text{mer}}$ ), a similar behaviour is observed if  $t_{\text{mer}} \leq t_{\text{sys}}$ .

### 4.3 Splitting and Merging at Finite Temperature

So far we have considered only the case of  $T = 0$  where the Initial condensate has a well-defined phase. In this section, following exactly the same approach as in the previous section, we investigate the effects that finite temperature might have on the overall coherence during the splitting and merging process.

Fluctuations of phase and density of a BEC are the result of thermal excitations, and appear usually at finite temperature [23, 24]. In such a case the system includes some non-condensed or thermal particles and hence the total Bose field operator in 1D can be expressed as

$$\hat{\Psi}(z, t) = \Psi(z, t) + \delta\hat{\Psi}(z, t), \quad (4.7)$$

where  $\delta\hat{\Psi}(z, t)$  describes the thermal depletion part. For a BEC in 3D trapping geometries, fluctuations of density and phase are only important in a narrow temperature range near the BEC transition temperature  $T_c$  [24]. For 1D systems, however, phase fluctuations are present at temperatures far below the degeneracy temperature. Phase fluctuations can be studied by solving the Bogoliubov-de Gennes equations (3.43) describing elementary excitations in 1D. Writing the quantum field operator as

$$\hat{\Psi}(z) = \sqrt{n_{1D}(z)} \exp[i\hat{\phi}(z)] \quad (4.8)$$

where  $n_{1D}(z) = |\Psi(z, t)|^2$  denotes the condensate density at  $T = 0$  [ $n_{1D}(z = 0) = \mu/g_{1D}$ ] the phase and density operators take, respectively, the following forms [133]

$$\hat{\phi}(z) = \frac{1}{\sqrt{4n_{1D}(z)}} \sum_{j=1}^{\infty} \left[ f_j^+(z) \hat{a}_j + f_j^-(z) \hat{a}_j^\dagger \right] \quad (4.9)$$

and

$$\hat{n}_{1D}(z) = \sqrt{n_{1D}(z)} \sum_{j=1}^{\infty} i \left( f_j^- \hat{a}_j - f_j^+ \hat{a}_j^\dagger \right), \quad (4.10)$$

where  $\hat{a}_j$  ( $\hat{a}_j^\dagger$ ) is the annihilation (creation) operator of the excitations with quantum number  $j$  and energy  $\epsilon_j = \hbar\omega_z \sqrt{j(j+1)/2}$ , and  $f_j^\pm = u_j \pm v_j$ , where  $u_j$  and  $v_j$  denote the excitation functions determined by the BdG equations. More explicitly, the functions  $f_j^\pm$  in a 1D Thomas-Fermi regime and at finite temperature take the form

$$f_j^\pm(z) = \sqrt{\frac{(j+1/2)}{R_{TF}}} \left( \frac{2\mu}{\epsilon_j} [1 - (z/R_{TF})^2] \right)^{\pm 1/2} P_j(z/R_{TF}) \quad (4.11)$$

where  $P_j(z/R_{TF})$  are Legendre polynomials. The phase coherence length, in terms of the Thomas-Fermi radius  $R_{TF}$ , is expressed as  $L_\phi = R_{TF} T_d \mu / T \hbar \omega_z$  and characterizes the maximal distance between two phase-correlated points in the condensate. Phase fluctuations increase for large trap aspect ratios and small  $N$  [17].

Temperature is included at the level of the 1D GPE (4.3) by calculating first the density at  $T = 0$  in the presence of the magnetic trap only, and then mimicking finite temperature effects via the phase operator of Eq. (4.9). In other words a phase is imprinted on the condensate wavefunction at this stage. To this aim, we calculate the Bose occupation  $N_j = (e^{\epsilon_j/(k_B T)} - 1)^{-1}$  modes in the Bogoliubov approximation for fixed temperatures replacing the operators  $\hat{a}_j$  and  $\hat{a}_j^\dagger$  by random complex variables  $\alpha_j$  and  $\alpha_j^*$ , respectively such that  $\langle |\alpha_j|^2 \rangle = N_j$  [17].

Although the GPE (4.3) in this limit remains valid, the BdG equations become modified by the integration over the transverse profile of the condensate [113]. In effect the mode functions  $f_j^\pm$  are given by Jacobi polynomials, whereas  $\epsilon_j$  are given by a slightly different expression than in the pure 1D case. We stress, however, that for the regimes of temperatures we consider, there will be no qualitative and practically no quantitative difference between the pure- and quasi-1D results.

The dependence of the magnitude of the phase fluctuations of the condensate on the temperature is shown in Fig. 4.5. Even though we present here results calculated for a fixed number of condensate atoms ( $N$ ), it is numerically verifiable that the magnitude of the phase fluctuations is inversely proportional to the square root of the number of atoms and hence to the peak density of the condensate as described by Eq. (4.9). As can be seen by inspecting the different plots (a)-(d) in Fig. 4.5, the phase fluctuations get more and more enhanced with the increase of temperature.

Having seen the enhancement of phase fluctuations with temperature, we proceed now to analyze the coherence properties of splitting and merging of a 1D BEC in the presence of these phase fluctuations for temperatures in the range of  $T_\phi < T < T_c$ . Our results for finite temperature are summarized in Fig. 4.6.

Using exactly the same approach that we employed for the adiabatic case at  $T = 0$  but now including temperature we study again the splitting and merging process for the same parameters. In this case, the density fluctuations, which are highly suppressed in elongated 3D condensates, are very pronounced in the 1D density after time evolution, when the temperature increases from a very small value ( $T/T_c = 0.01$ ) to a value near the critical point for condensation ( $T/T_c = 0.8$ ). At high temperatures, the density fluctuations get more and more enhanced. However, notice that the effect of fluctuations is very similar on the single and on the Merged condensates. On the other hand, fluctuations on the Split condensates remain relatively small due to fact that the densities in the double-well are higher as shown in all plots of Fig. 4.6. This is in confirmation of the prediction of Eq. (4.9). The presence of fluctuations on the density profile is a consequence of the

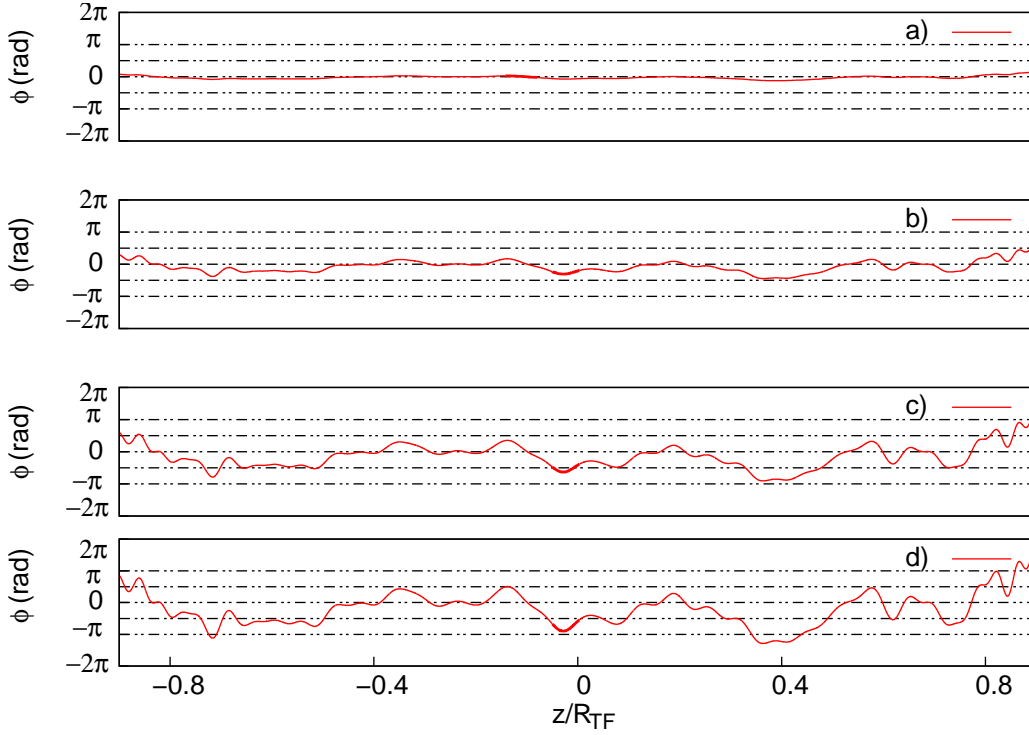


Figure 4.5: (Color online) Enhancement of phase fluctuations with the increase in temperature. (a) At the top, we have very weak phase fluctuations at very low temperature ( $T/T_c = 0.01$ ). (b) With the rise in temperature ( $T/T_c = 0.1$ ), the phase fluctuations begin to be enhanced. (c) Still at an intermediate but relatively high temperature ( $T/T_c = 0.4$ ), the magnitude of phase fluctuations increases. (d) Finally at  $T/T_c = 0.8$ , which is near the critical point, stronger phase fluctuations are displayed.

BdG equations present in the GPE equation. In spite of such fluctuations, the Split and Merged condensates present almost the same Thomas-Fermi density profiles for any temperature  $T < T_c$ .

From these observations, we conclude that in spite of the Initial phase fluctuations in the quasi-condensate regime at finite temperature, there is a preservation of “phase coherence length” during the splitting and merging process, if adiabaticity is satisfied.

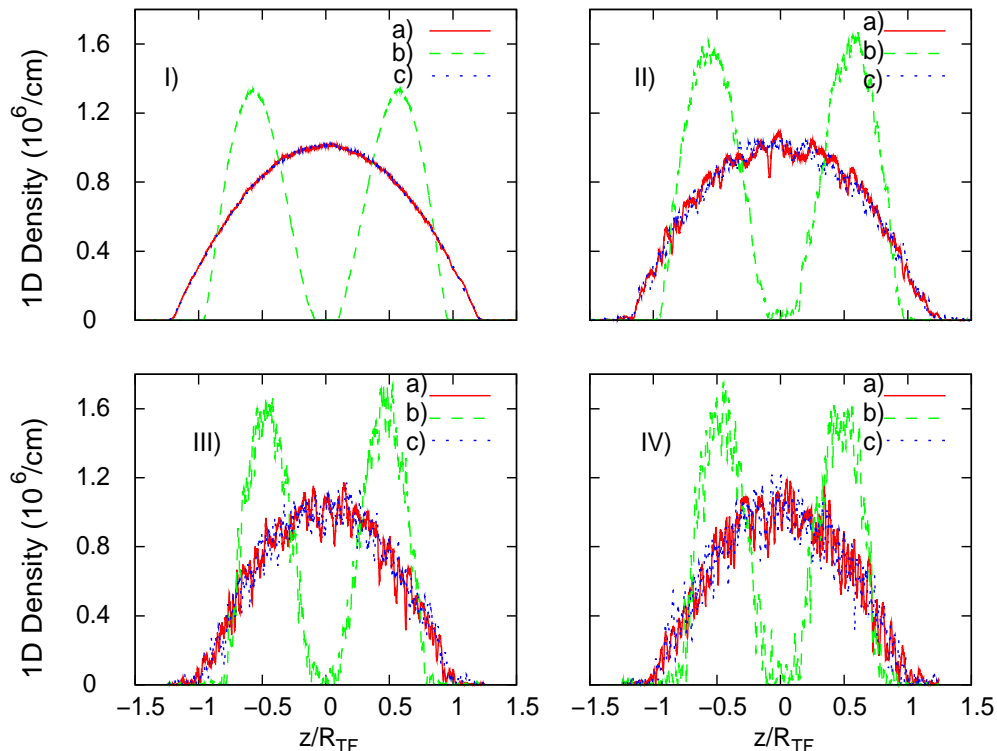


Figure 4.6: (Color online) Splitting and merging of 1D BECs at finite temperature, i.e., in the presence of phase and density fluctuations. The four plots are the fluctuating densities at  $T/T_c =$  (I) 0.01, (II) 0.1, (III) 0.4 and (IV) 0.8. Each one in turn consists three plots with in it: curve a, the Initial 1D BEC (red solid line); curve b the Split 1D BECs (green dashed line); and curve c, the Merged 1D BEC (blue dotted line).

## 4.4 Summary

Summarizing, we have discussed coherence effects in the splitting and merging of a 1D  $^{87}\text{Rb}$  BEC. This is done by creating two spatially separated condensates from an initial 1D condensate by deforming the trapping potential into a double-well potential. We have analysed the case of zero temperature as well as finite temperature in the so-called quasi-condensate regime, where the phase coherence length is smaller than the size of the system. At zero temperature and for a process adiabatic enough where the splitting and merging times are much larger than the characteristic time of the system given by the inverse of the trap frequency  $t_{\text{sys}} = 2\pi/\omega_z$ , a coherent splitting followed by a coherent merging is achieved and there is a constant relative

---

phase between the Initial and the final Merged condensates. On the contrary if the splitting and merging times are not larger than the relevant time scale, the Split condensates acquire a random relative phases and merging is no longer possible. In this case, the system acquires large density and phase fluctuations on a length scale comparable with the coherence length  $l_c$ , and a description based on the GPE becomes invalid. In the case of finite temperature our results show that even in the presence of strong phase fluctuations, if the process of splitting and merging is carried out fully adiabatically, the condensate preserves the Thomas-Fermi density profile and there is phase coherence length preservation. In such cases, the Merged condensate is a quasi-condensate with the same initial density profile as the Initial condensate and with the same phase coherence length, although the “overall” phase of the quasi-condensate is not preserved. This situation occurs even at temperatures very near the critical value for condensation as long as the trapping potential remains in place. Our results may have a useful implication for manipulating 1D BECs at zero as well as finite temperatures such as in atom lasers, interferometry, and solitons. In particular, our results agree qualitatively well with the recent measurements in Ref. [98].



# Chapter 5

## Quantum Switches and Memories for Matter Wave Lattice Solitons

Bose Einstein condensates in optical lattices have attracted a lot of attention both in the mean field regime [134] as well as in the strongly correlated regime [135]. The main reason for the burst of activities is the unprecedented level of control such systems offer, making them unique candidates for the exploration of a broad range of fundamental phenomena.

In the mean field regime, a huge interest has been devoted to non-linear dynamics of matter waves in periodic media and specifically in matter wave solitons. Matter wave solitons are self-stabilised coherent atomic structures that appear in non-linear systems due to the balance between the non-linearity and the dispersive effects. The nature of the solitons supported by BECs is determined by the character of the interactions: attractive (repulsive) non-linearity supports bright [136, 137] (dark [138–140]) solitons. In the presence of an optical lattice, this scenario changes completely due to the appearance of a band structure in the spectrum and the possibility of having either bright or dark lattice solitons with either repulsive or attractive interactions arise. Very recently, the first experimental demonstration of bright lattice solitons in repulsive condensates [141] was reported.

Since the first proposals of BEC lattice solitons in [142, 143], there has been an explosion of contributions regarding generation, mobility and interactions of this novel type of matter wave solitons both in one-dimensional systems [144–149] and in higher dimensions [150–154]. The interest is mainly centred in bright matter-wave lattice solitons due to their potential applications in energy and information transport in non-linear systems. Proposals for controlling the dynamics of bright gap solitons are mainly devoted to the

manipulation of the optical lattice [155–159] and to the modification of the non-linearity [160, 161]. Nevertheless, a complete control on the dynamics of bright matter wave gap solitons also requires a profound knowledge of their interactions with defects.

The interaction of solitons with defects is a subject that appears in the literature in different contexts. The interaction of solitons with a point like impurity has been studied in the framework of different non-linear equations [162]. One of the most studied case is the non-linear Schrödinger equation, where there have been contributions either in the continuum regime [163–167] or in discrete systems [168–170]. More extended defects have also been addressed [171–173] and very recently interactions of matter wave solitons with defects have also been addressed [174–177].

In this Chapter, we propose different possibilities of control of the dynamics of bright lattice matter wave solitons by using their interaction with defects of arbitrary amplitude and width.

## 5.1 The Physical System

We consider a zero temperature  $^{87}\text{Rb}$  condensate confined in a one-dimensional geometry and in the presence of an optical lattice. The description of the system is performed within the one dimensional Gross-Pitaevskii equation (GPE)

$$i\hbar\frac{\partial\Psi(z,t)}{\partial t} = \left( -\frac{\hbar^2}{2m}\frac{\partial^2}{\partial z^2} + V_T(z) + gN|\Psi(z,t)|^2 \right)\Psi(z,t) \quad (5.1)$$

where, as expressed in the previous Chapter,  $g = 2\hbar a_s \omega_\perp$ , being  $a_s$  the  $s$ -wave scattering length and  $\omega_\perp$  the radial angular magnetic frequency, is the averaged one-dimensional coupling constant; and  $V_T(z)$  is the total external potential which is given by

$$V_T(z) = V_{\text{trap}}(z) + V_L(z) = \frac{1}{2}m\omega_z^2 z^2 + V_0 \sin^2\left(\frac{\pi z}{d}\right). \quad (5.2)$$

This potential (5.2) describes both the axial magnetic trap potential,  $V_{\text{trap}}(z)$ , with angular frequency  $\omega_z$ , and the optical lattice potential,  $V_L(z)$ , with spatial period  $d = \lambda/2 \sin(\theta/2)$ , being  $\lambda$  the wavelength of the lasers forming the optical lattice and  $\theta$  is the angle between them. The depth of the optical lattice,  $V_0$ , is given in units of the recoil energy  $E_r = \hbar^2 k^2 / 2m$  where  $k = \pi/d$  is the lattice recoil momentum.

The generation of the bright lattice soliton is performed as it is reported in [144]. The procedure is briefly summarised in what follows. The starting

point is an  $^{87}\text{Rb}$  condensate ( $a_s = 5.8\text{nm}$ ) of  $N = 500$  atoms in the presence of a magnetic trap with frequencies  $\omega_{\perp}/2\pi = 715\text{ Hz}$  and  $\omega_z/2\pi = 14\text{ Hz}$ , and an optical lattice, with potential depth  $V_0 = 1E_r$  and period  $d = 397.5\text{nm}$ . The axial magnetic trap is suddenly turned off and the appropriate phase imprinting, corresponding to jumps of  $\pi$  in adjacent sites, is performed [144]. After the phase imprinting, the system evolves towards a negative mass, self-maintained staggered soliton at rest, which contains approximately 35% of the initial atoms ( $N = 187$ ) and occupies around 11 sites. The exceeding atoms are lost by radiation.

The total energy of the generated bright soliton can be calculated using the energy functional of the GPE (5.1) that contains the total kinetic, interaction and potential energies

$$E = \int \left[ \frac{\hbar^2}{2m} |\nabla \Psi(z)|^2 + \frac{g}{2} |\Psi(z)|^4 + V_T(z) |\Psi(z)|^2 \right]. \quad (5.3)$$

By calculating the linear band spectrum of the system, the energy of the band edge is obtained to be  $1.25E_r$ , which is in good agreement with the total energy obtained from Eq. (5.3) ( $E = 1.31E_r$ ). The linear band spectrum predicts an effective mass at the edge of the first Brillouin zone corresponding to  $m_{\text{eff}} = 0.15m$ .

Once the lattice soliton is created, it is set into motion by applying an instantaneous transfer of momentum at  $t = 0$ . This momentum has to be large enough to overcome the Peierls-Nabarro (PN) barrier [144] but sufficiently small to assure that the soliton remains in the region of the negative effective mass, i.e.,  $0.009k\hbar < p < 0.2k\hbar$ . The soliton starts to move opposite to the direction of the kick ( $\kappa k\hbar$ , where  $\kappa$  is the coefficient of the kick) manifesting thus its negative effective mass. The concept of effective mass is used through out the chapter in order to give an intuitive explanation of the observed dynamics. Nevertheless, all the results presented in what follows have been obtained by a direction integration of Eq. (5.1), without any approximation.

At a certain distance  $z_m$  of the initial position of the soliton ( $z = 0$ ), the lattice potential  $V_L(z)$  is modified as

$$V_L(z) = \begin{cases} V_0 \sin^2\left(\frac{\pi z}{d}\right) + V_m \left(1 - \frac{(z-z_m)^2}{2\sigma^2}\right) & \text{if } z_+ \leq z \leq z_-; \\ V_0 \sin^2\left(\frac{\pi z}{d}\right) & \text{otherwise,} \end{cases} \quad (5.4)$$

where we have used  $\sigma = 3\lambda$  and,  $z_+ = z_m + l/2$  and  $z_- = z_m - l/2$ ; and  $V_m$  is the barrier height or well depth which can be either positive or negative. For  $|V_m| < 0$ , the local decrease of the lattice potential corresponds to an "effective" potential barrier for the soliton due to its negative effective mass

while if  $|V_m| > 0$ , i.e. a local increase of the potential acts as an "effective" well for the soliton. For the case of an effective barrier,  $z_m$  is fixed to match exactly with a minimum of the optical lattice while in the effective well case,  $z_m$  corresponds to a maximum of the optical lattice. We have checked the results reported here do not strongly depend on the specific shape of the potential by reproducing them with a Gaussian and square potentials.

To analyse the interaction of the bright lattice soliton with the defect (barrier/well), it is crucial to know the total energy of the soliton while it moves. To study the dynamical behaviour of the soliton, we have numerically calculated the contributions to the total energy as a function of time. Immediately after the kick, the soliton expels atoms and its energy abruptly decreases becoming much smaller than the energy that it would need to remain at rest at the edge of the first Brillouin zone. In the framework of the linear band theory this would correspond to displace the particle from the edge the first Brillouin zone by changing its quasimomentum. To illustrate the dynamics of the system, we consider the case in which we give a kick of  $p = 0.1k\hbar$  to the soliton generated at rest. At  $t = 0$ , just after the kick, the total energy of the soliton is its energy at rest plus the contribution of the transfer of momentum, i.e.  $E = 1.35E_r + (0.1)E_r = 1.36E_r$ . At  $t = 1\text{ms}$ , the soliton energy has already decreased to  $0.96E_r$ , the rest of the energy has been taken away by the repelled atoms. A steady state is reached for a soliton energy of  $E = 0.92E_r$ . While moving, some energy is devoted to cross the PN barrier (the soliton configuration changes its shape from a configuration centered in one well of the optical lattice to a configuration centered in one maximum and viceversa). This change of the shape of the soliton is reflected in the out of phase oscillations of the kinetic energy with respect to the potential plus nonlinear energy in such a way that the mean value of the energy remains constant.

## 5.2 "Effective" Potential Barrier

We discuss first the interaction of a bright lattice soliton with an "effective" potential barrier. Scattering depends on the width of the defect ( $l$ ) and the relevant energy scale, settled by the ratio  $|V_m|/E_k$ , where  $E_k = \langle p \rangle / 2m$  is the fraction of the total kinetic energy devoted to move the soliton, and  $\langle \rangle$  denotes the time average (before reaching the defect). The momentum  $p$  is defined as

$$p(t) = -i\hbar \int \Psi^*(z, t) \nabla \Psi(z, t) dz. \quad (5.5)$$

The rest of the kinetic energy is needed to keep the structure and cannot

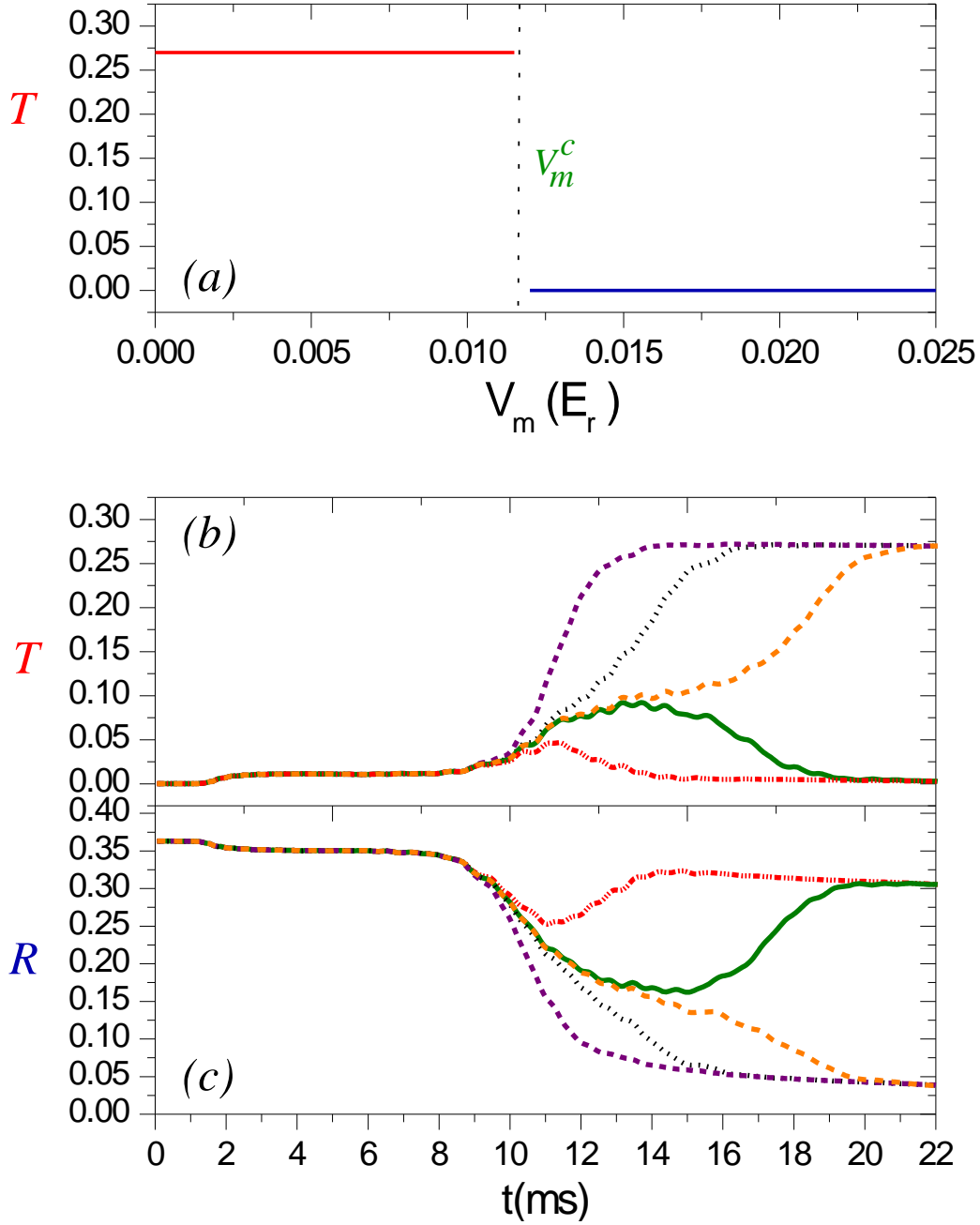


Figure 5.1: (Color online) (a) Transmission coefficient,  $T$ , as a function of the amplitude of the "effective" potential barrier,  $|V_m|$ ; (b) Transmission coefficient,  $T$  and (c) reflection coefficient  $R$  as a function of time for different amplitude defects:  $|V_m| = 0$  (magenta dashed line),  $|V_m| = 0.01E_r$  (black dotted line),  $|V_m| = 0.0115E_r$  (golden dashed-dotted line),  $V_m = 0.0117E_r$  (green solid line) and  $|V_m| = 0.018E_r$  (red dashed dotted-dotted line). In all the plots the soliton kinetic energy is  $E_k = 0.01E_r$  and the width of the defect  $l = 2d$ .

be used to overcome the “effective” potential barrier. We have checked that, apart from the necessary change to overcome the NP barrier, the soliton keeps its shape when it reaches the defect. This corroborates that there is no transfer between nonlinear and kinetic energies apart from the one corresponding to the already discussed PN barrier. We distinguish two regimes of parameters: (i) when the amplitude of the “effective” potential barrier is of the order of the kinetic energy of the soliton ( $|V_m| \sim E_k$ ) and (ii) when the amplitude of the potential barrier is much larger than the kinetic energy of the soliton. In the former case, the potential barrier acts as a quantum switch, i.e., either the entire soliton is transmitted or it is completely reflected depending on the amplitude of the barrier ( Fig. 5.1 (a)). The transmission ( $T$ ) and reflection ( $R$ ) coefficients are calculated by integrating over space (and time) the density of the wavefunction in the region before and after the defect. Note that since only approximately 35% of the atoms survive the initial kick and form a soliton, the merit figure for perfect transmission is well below 1 and corresponds approximately to  $T \sim 0.27$  ( $N = 187$ ).

For a fixed width of the defect a drastic change of behaviour occurs for a given height of the barrier  $|V_m^c|$ . The wider the defect is the lower the critical value of the potential amplitude  $|V_m^c|$ . The critical values, indicating the transition between complete transmission and complete reflection for different potential widths are shown in Fig. 5.2 (a) by black solid squares. Below these values, depicted by a gray region in Fig. 5.2 (a), the soliton experiences complete transmission but as one approaches the critical value from below the soliton experiences a time delay with respect to free propagation (i.e., in the absence of the defect). This delay increases as one gets closer to the critical point and eventually the time needed by the soliton to cross the barrier diverges as shown in Fig. 5.3. Fig. 5.3 shows the delay time in transmission with respect to the absence of defect,  $t_d$ , for  $l = d$  as a function of the amplitude of the barrier,  $|V_m|$ , including the cases where tunnelling occurs ( $|V_m| > 0.01E_r$ ).

Above the transition line in Fig. 5.2 (a), reflection of the entire soliton occurs after a storage time inside the region of the barrier that increases as one approaches the critical value. To illustrate this behaviour, Fig. 5.1 (b,c) show the transmission and reflection coefficients as a function of time for a barrier of fixed width of  $l = 2d$  and different values of the amplitude.

In the situation shown in Fig. 5.1, the critical value is nearly equal to the kinetic energy of the soliton but if the width of the barrier is reduced, this critical value can exceed the kinetic energy of the soliton. In this case, for instance when  $l = d$ , the soliton tunnels through the barrier, i.e., transmission is obtained for values of the amplitude of the barrier higher than the kinetic energy of the soliton as shown in Fig. 5.2 (a). On the other hand, for wider

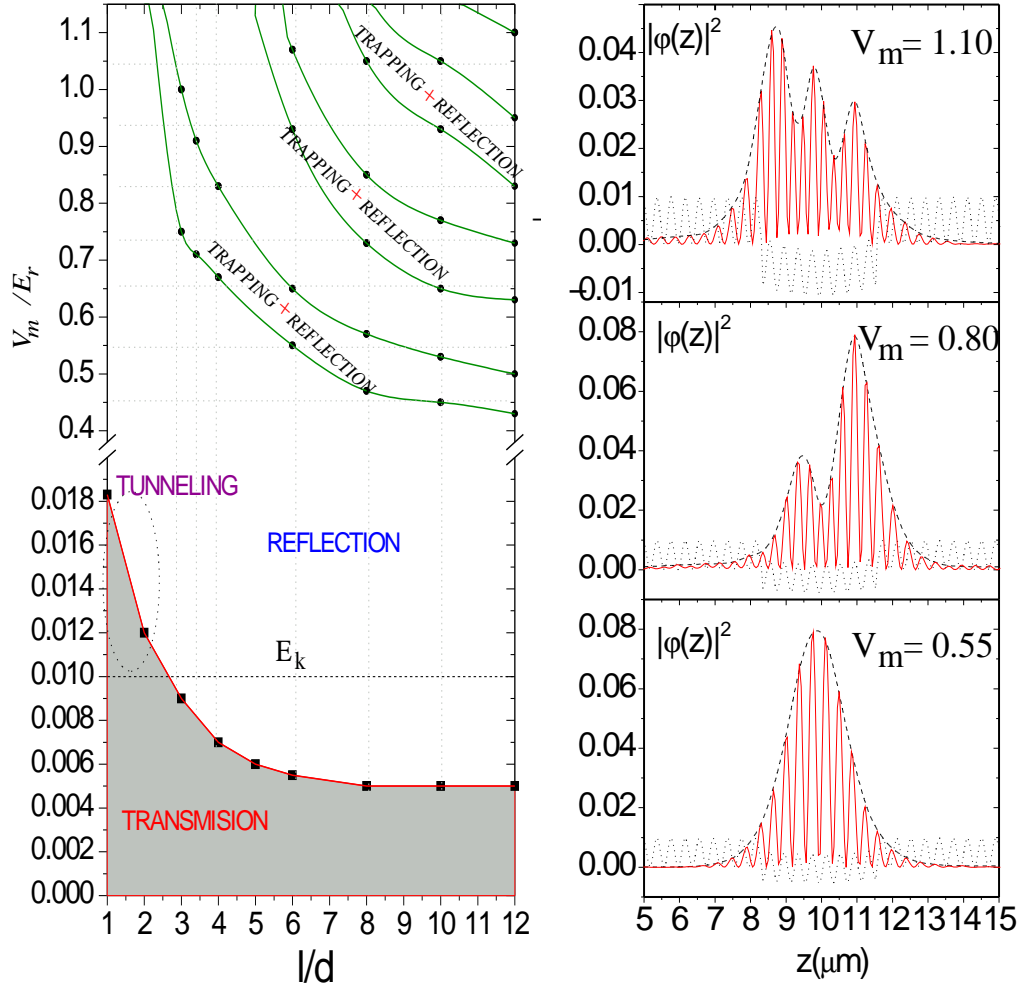


Figure 5.2: (Color online) (a) Reflection and transmission behaviour of a soliton interacting with an effective potential barrier as a function of the potential width  $l$  (in  $d$  units) and potential amplitude  $|V_m|$  (in  $E_r$  units): the region of total transmission in gray, and the region of total reflection in white. Inside the reflection region, bands in which trapping and reflection occurs appear. In the region of transmission the parameters for which tunnelling occurs are also shown. The dotted gray horizontal line shows the value of the kinetic energy of the soliton. (b) Density profiles of the trapped structure that appears for  $|V_m| = 0.55E_r$  (lower plot),  $|V_m| = 0.8E_r$  (middle plot) and  $|V_m| = 1.1E_r$  (upper plot). In the three cases  $l = 8d$ .

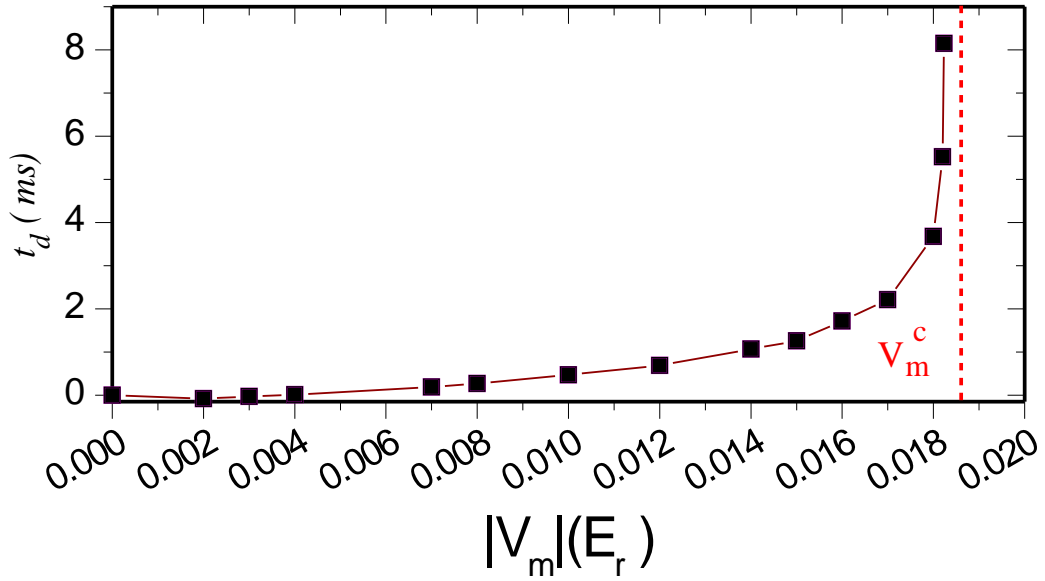


Figure 5.3: (Color online) Transmission delay time as a function of  $|V_m|$  for a soliton with kinetic energy  $E_k = 0.01E_r$  crossing a defect of width  $l = d$ .

defects, a region of overbarrier reflection appears (Fig. 5.2 (a)). There, the lattice soliton is completely reflected although it has a kinetic energy larger than the height of the potential barrier. This region extends for wide range of widths of the defect. We have checked that overbarrier reflection occurs even in the limit when the the width of the defect is much larger than the size of the soliton.

Up to now we have described the transition from complete transmission to complete reflection by fixing the width of the defect and varying the amplitude. It is worth noticing that a similar switching behaviour can be obtained by fixing the amplitude of the effective potential and changing its width. This would correspond to horizontal lines in the diagram of Fig. 5.2 (a) crossing the transition line (solid black squares) in the region where  $|V_m|$  is on the order of the kinetic energy of the soliton. This observed abrupt transition from complete reflection to complete transmission opens the possibility to use the system as a quantum switch.

Let us now focus on the regime where the amplitude of the barrier is much larger than the kinetic energy of the soliton  $|V_m| \gg E_k$ , where the expected behaviour is complete reflection of the soliton. Complete reflection occurs but there are specific values of the ratio  $l/|V_m|$  for which the soliton splits into two parts: a fraction of the initial soliton becomes trapped inside the region of the barrier while the other part is reflected back keeping a solitonic structure. Fig 5.2 (a), for  $|V_m| \gg E_k$ , shows the regions where

the soliton splits into two parts (trapping and reflection) embedded in the complete reflection regions.

The fraction of atoms trapped inside the defect region has its origin on the atoms lost by radiation due to the repulsive force experienced by the soliton when it reaches the potential barrier. These radiated atoms enter the region of the barrier and for some specific ratios of the width and the height of the defect the fraction of trapped atoms increases. These trapping regions appear as bands as shown in Fig. 5.2 (a). In each band, the trapped fraction exhibits different spatial distributions: for the lowest height region, the structure is a single hump; in the second region a double hump structure appears, and so on (see 5.2 (b)). A noticeable feature of this trapped fraction is that the density maxima of the structure are located at the positions of the maxima of the optical potential.

Increasing the amplitude of the barrier, the structure becomes more independent of the lattice periodicity. The extension of the trapped structure is also independent of the features of the barrier but the number of trapped atoms differs for different widths of the barrier. This number spatial size of the trapped structure is the same independently of the features of the barrier. The narrower defect is the larger the number of trapped atoms. This number changes also with  $|V_m|$  inside each band, being maximum at the center of the band. For all cases the number of atoms forming the reflected soliton is always larger than the trapped fraction. We have checked that these "resonance" band-like structures do not correspond to the bound states of the linear case. We have observed that this behaviour occurs for all the accessible initial transfers that allow motion of the soliton.

### 5.3 "Effective" Potential Well

Let us now turn to the interaction of a lattice soliton with an "effective" potential well with a depth of the order of its kinetic energy. For a fixed depth of the well, the soliton exhibits different behaviours depending on its kinetic energy. For low kinetic energies, the soliton gets bound with the defect and exhibits oscillations while for kinetic energies overcoming a certain threshold, the soliton crosses the defect region. In the latter case, the only detectable effect of the potential well is the speed up of the soliton with respect to free propagation. It is important to note that as the width of the defect increases, the range of velocities for which transmission occurs decreases. To illustrate the described behaviour, Fig. 5.4 (a) shows the time evolution of the trapped fraction density,  $D = |\Psi(z, t)|^2$ , for different initial transfer of momentum: momentum  $p = 0.05k\hbar$  (black line),  $p = 0.1k\hbar$

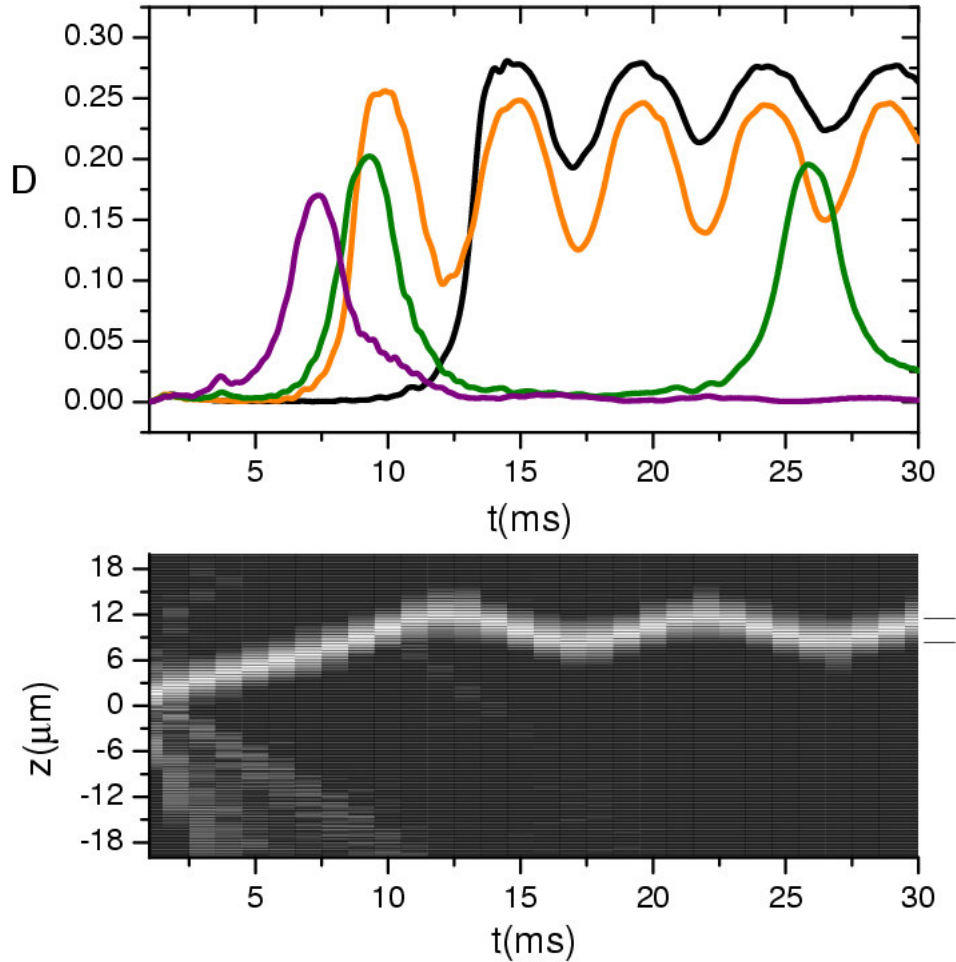


Figure 5.4: (Color online) (a) Temporal evolution of the trapped fraction of the soliton interacting with an “effective” well of depth  $|V_m| = 0.018E_r$  and width the soliton with  $l = 8d$  after an instantaneous transfer of momentum  $p = 0.05k\hbar$  (black line),  $p = 0.1k\hbar$  (golden line),  $p = 0.17k\hbar$  (green line) and  $p = 0.2k\hbar$  (magenta line). (b) Contour plot of the evolution in space and time of the lattice soliton with conditions corresponding to the golden line case in (a).

(golden line),  $p = 0.17k\hbar$  (green line) and  $p = 0.2k\hbar$  (magenta line) keeping the depth ( $|V_m| = 0.018E_r$ ) and the width ( $l = 8d$ ) of the well fixed. The positions in time of the minima of the trapped fraction correspond to the turning points of the oscillating movement of the soliton around the "effective" well. The maxima indicates the times for which the soliton is completely inside the well. As expected, the amplitude of the oscillations increase with an increasing momentum transfer. If the amplitude of oscillation is larger than the width of the defect, the turning points are located outside the potential well. This is reflected by a lower value of  $D$ .

Fig. 5.4 (b) shows a contour plot of the evolution in space and time of a lattice soliton with  $E_k = 0.01E_r$  (golden line case in (a)). The width of the "effective" well is shown at the right hand side of the plot to illustrate that indeed the turning points are outside the defect.

Let us now explore the dependence of the oscillations on the depth ( $l$ ) and width of the "effective" potential well ( $|V_m|$ ) by fixing  $E_k = 0.01E_r$ . Fig 5.5 (a) displays the temporal evolution of the trapped fraction density  $D$ , for a potential well with  $|V_m| = 0.018E_r$  and different values of the width of the defect:  $l = 4d$  (green solid line),  $l = 8d$  (golden dashed line) and  $l = 12d$  (red dotted line). The frequency of the oscillations indicates the width of the defect while the amplitude remains approximately the same for all widths. In Fig. 5.5 (b) we fix  $l = 4d$  and display the trapped fraction,  $D$ , as a function of time for  $|V_m| = 0.018E_r$  (green solid line),  $|V_m| = 0.03E_r$  (golden dashed line) and  $|V_m| = 0.08E_r$  (red dotted line). By inspection of Fig. 5.5 (b), one can confirm that the frequency of the oscillations increases with the depth of the potential while the amplitude of the oscillations decreases. This is due to the fact that the soliton experiences a much larger attractive force as the depth of the defect increases limiting the displacements around the central position of the well.

The trapping of the entire lattice soliton around the position of the defect opens possibilities to use the system as a quantum memory because it provides the capacity of storage. Nevertheless, in order to perform a memory, one should also be able to release the trapped structure after a desirable time and with the minimum losses. We have checked that a soliton trapped in an "effective" potential well can be released with a certain velocity keeping the totality of its initial atoms if the defect amplitude is instantaneously set to zero. In fact the velocity of the lattice soliton after releasing it will depend on the amplitude of the oscillations it was performing while it was trapped. Specifically, the velocity structure, after releasing it, grows with the amplitude of the oscillations. Moreover, choosing appropriately the time at which the release takes place, one can vary the direction of movement.

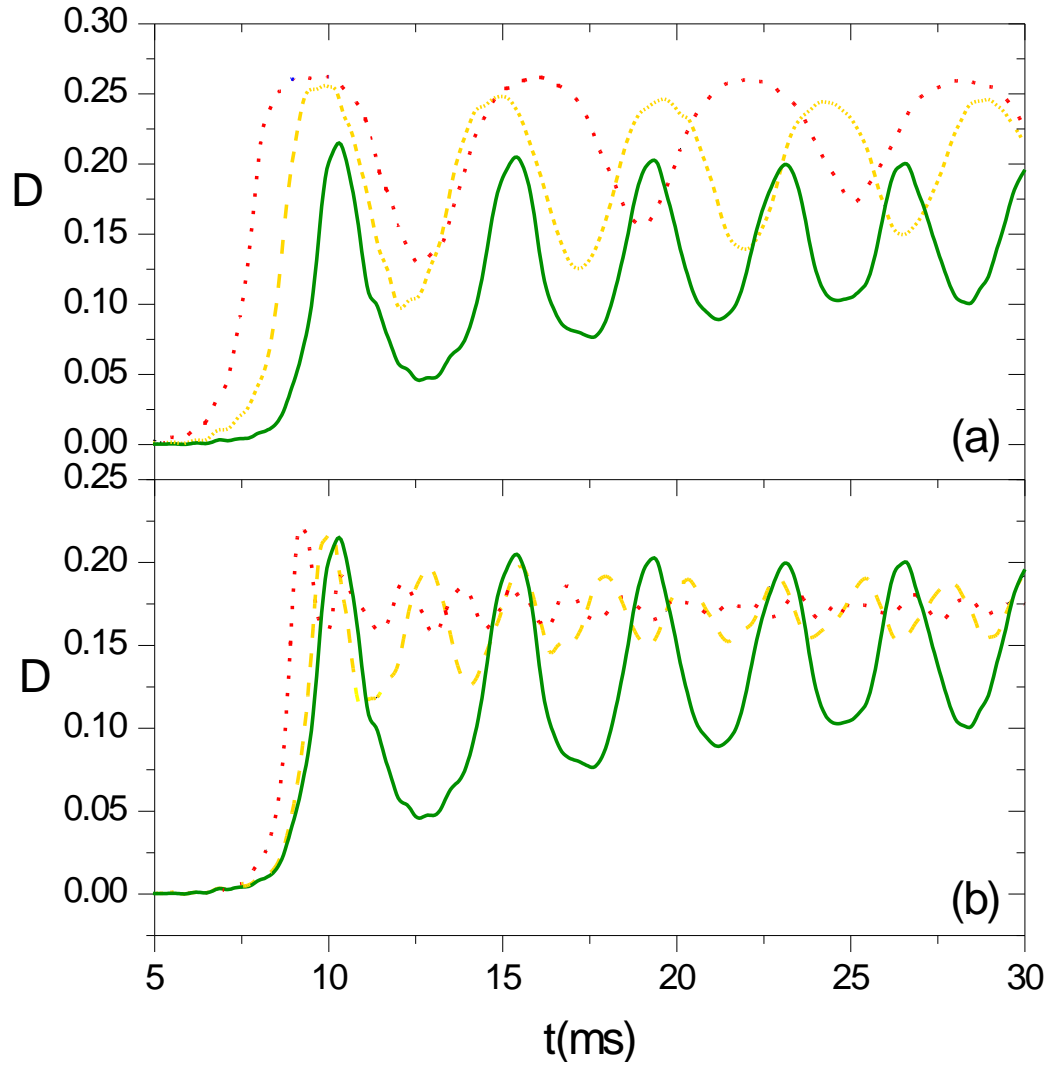


Figure 5.5: (Color online) Temporal evolution of the trapped fraction density of a lattice soliton with  $E_k = 0.01E_r$  interacting with an "effective" well with (a)  $|V_m| = 0.018E_r$  and different width:  $l = 4d$  (green solid line),  $l = 8d$  (golden dashed line) and  $l = 12d$  (red dotted line); (b)  $l = 4d$  and different defect depth:  $|V_m| = 0.018E_r$  (solid green line),  $|V_m| = 0.03E_r$  (golden dashed line) and  $|V_m| = 0.08E_r$  (red dotted line).

## 5.4 Control of the Collisions

Now we investigate if the inclusion of a defect in the lattice helps to control the interactions between two lattice solitons. It has been shown that

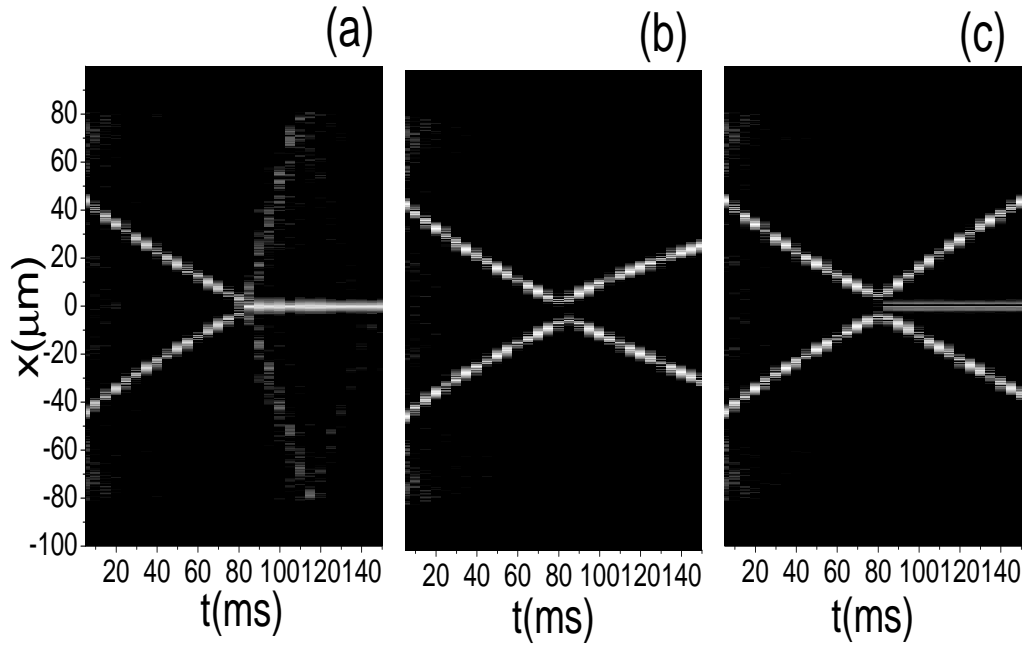


Figure 5.6: (Color online) Contour plot of the evolution in space and time of a collision between two identical solitons initially placed at symmetrical positions with respect  $z = 0$  and moving in opposite directions when an "effective" potential barrier with  $l = 2d$  and (a)  $|V_m| = 0.012E_r$ , (b)  $|V_m| = 0.2E_r$  and (c)  $|V_m| = 0.5E_r$  is placed at  $z = 0$ .

collision between two identical lattice solitons (moving in opposite directions with the same speed and with the same average phase) merge into a soliton with the same number of atoms as the initial ones [145]. The exceeding atoms are lost by radiation. If an "effective" potential barrier of width much narrower than the solitons dimensions placed at the crossing point, we find the following behaviours: (i) for  $|V_m| \leq E_k$  the merging behaviour is maintained (Fig. 5.6 (a)); (ii) for  $|V_m| \gg E_k$ , each soliton reflects back (Fig. 5.6 (b)). Moreover, for the same values of  $|V_m|$ , in

addition to the reflection, a fraction of atoms trapped in the defect appears (Fig. 5.6 (c)). The trapped fraction shows the same features as in the single soliton case (Sec. 5.2). Modifying the features of the defect, different outcomes can be engineered. For instance, when the width of the barrier is of the order of the dimensions of the initial solitons, effects like the trapping of both solitons at the edge of the barrier can occur.

## 5.5 Summary

Summarising, we have found that bright matter-wave lattice solitons behave as “quantum” particles when colliding with an “effective” potential barrier/well, corresponding to a defect in the optical lattice. Among the rich dynamics exhibited by the system, we would like to remark on two effects. The first one corresponds to the interaction of a soliton with an “effective” potential barrier which permits the implementation of a quantum switch. In this case, a sharp transition from complete reflection to a complete transmission is present at specific value of the height of the barrier. Although this resembles a behaviour of a classical particle, the quantum nature of the solitons is explicitly manifested in the appearance of the overbarrier reflection and tunneling. The second effect we would like to stress appears when the defect acts as an “effective” potential well. We have shown that trapping of the entire soliton around the position of the defect and its release on demand with a given velocity and direction of motion is possible. This fact indicates the suitability of the system as a quantum memory. Finally, it has been also reported that the presence of a defect in the lattice can help to control the interactions of two lattice solitons.

# Chapter 6

## Parametric Oscillation with Squeezed Vacuum Reservoirs

Non-classical effects of light such as squeezing, antibunching and sub-Poissonian statistics have been attracting the attention of several authors in quantum optics over the last decades [8, 12, 178–184]. A review article on non-classical states of the first 75 years is found in Ref. [179].

Non-classical states of the electromagnetic field are produced by interaction between light and matter. One can identify two fundamental mechanisms: the emission of atom radiation by resonant interaction, and the interaction of light with a non-linear medium in a non-resonant process. For resonant interactions a system can be active or passive, depending on the population of the resonant atomic levels. Active systems, such as the lasers, operate with population inversion of the atomic levels.

Squeezed states are non-classical states characterised by a reduction of quantum fluctuations (noise) in one quadrature component below the vacuum level (standard quantum limit), or below that achievable in a coherent state [8, 12] at the expense of increased fluctuations in the other component such that the product of these fluctuations still obeys the uncertainty relation [8, 181]. By the choice to observe only the quadrature of the lowest noise, limitation on the measurement of quantum fields that were previously thought to be fundamental can be removed [185].

It was Takahashi [186] who, in 1965, first pointed out that a degenerate parametric amplifier enhances the noise in one quadrature component and attenuates it in the other quadrature. This prediction has been confirmed by several authors for degenerate and non-degenerate parametric amplifiers and oscillators. Operating below threshold, the parametric amplifier is a source of squeezed states. In the initial experiments carried out to observe squeezing, a noise reduction of 4-17% relative to the standard quantum limit has been

obtained [9]. In order to increase the gain, the parametric medium may be placed inside an optical cavity where it is coherently pumped and becomes a parametric oscillator [10, 11, 15, 187–191].

An optical parametric oscillator is a quantum device with a definite threshold for self sustained oscillations. It is one of the most interesting and well characterised optical devices in quantum optics. This simple dissipative quantum system plays an important role in the study of squeezed states. In a parametric oscillator a strong pump photon interacts with a non-linear-medium (crystal) inside a cavity and is down-converted into two photons of smaller frequencies. In the non-degenerate parametric oscillator (NDPO), we assume that the strong pump photon is down converted into two modes and these modes are referred to as signal and idler modes.

A quantum-mechanical treatment of different optical systems such as the NDPO is essential as they may generate squeezed states with non-classical properties which have potential applications in quantum optical communications [8] and computation [192], gravitational wave detection [193–196], interferometry [196–198], spectroscopical measurements [199] and for the study of fundamental concepts.

For systems with non-classical features such as the NDPO, for which the Glauber-Sudarshan P-function is highly singular [183, 200, 201], one may use the Q-function. The Q-function is expressible in terms of the Q-function propagator and the initial Q-function. It is possible to determine the Q-function propagator by directly solving the Fokker-Planck equation. In this Chapter, we find it convenient to evaluate the Q-function propagator applying the method developed in [202].

## 6.1 The Master Equation

The description of system-reservoir interactions via the master equation is a standard technique in quantum optics [12, 182]. In this section, however, we found it useful to include a non-detailed a derivation of the master equation describing the interaction of the signal-idler modes generated by a NDPO coupled to two USVR and the detailed derivation is given in Appendix B.

Denoting the density operator of the optical system and the squeezed reservoir modes by  $\hat{\chi}(t)$ , the density operator for the system alone is defined by

$$\hat{\rho}(t) = \text{Tr}_R \hat{\chi}(t),$$

where  $\text{Tr}_R$  indicates that the trace is taken over the reservoir variables only.

The density operator  $\hat{\chi}(t)$  evolves in time according to

$$\frac{d\hat{\chi}(t)}{dt} = \frac{1}{i\hbar} \left[ \hat{H}_{SR}(t), \hat{\chi}(t) \right], \quad (6.1)$$

where  $\hat{H}_{SR}(t)$  is the Hamiltonian describing the interaction between the system and the reservoirs. Note that the Hamiltonian describing only the reservoir modes ( $\hat{H}_R(t)$ ) is not involved in the derivation as it cancels out when we apply the cyclic property of the trace. Furthermore, in order to simplify our calculations, the Hamiltonian that describes the interaction of the system with the pump mode ( $\hat{H}_S(t)$ ) will be added at the end of the derivation.

Since initially the system and the reservoirs are uncorrelated, one can write, for the density operator of the system and the reservoirs at the initial time ( $t = 0$ ), that  $\hat{\chi}(0) = \hat{\rho}(0) \otimes \hat{R}$  [12], where  $\hat{\rho}(0)$  and  $\hat{R}$  are the density operators of the system and the reservoirs at the initial time, respectively. Then in view of this relation, Eq. (6.1) results in

$$\frac{d\hat{\chi}(t)}{dt} = \frac{1}{i\hbar} \left[ \hat{H}_{SR}(t), \hat{\rho}(0) \otimes \hat{R} \right] - \frac{1}{\hbar^2} \int_0^t dt' \left[ \hat{H}_{SR}(t), \left[ \hat{H}_{SR}(t'), \hat{\chi}(t') \right] \right]. \quad (6.2)$$

Applying the weak coupling approximation which implies that  $\hat{\chi}(t') = \hat{\rho}(t') \otimes \hat{R}$  [12], it follows that

$$\begin{aligned} \frac{d\hat{\rho}(t)}{dt} &= \frac{1}{i\hbar} \text{Tr}_R \left\{ \left[ \hat{H}_{SR}(t), \hat{\rho}(0) \otimes \hat{R} \right] \right\} \\ &- \frac{1}{\hbar^2} \int_0^t dt' \text{Tr}_R \left\{ \left[ \hat{H}_{SR}(t), \left[ \hat{H}_{SR}(t'), \hat{\rho}(t') \otimes \hat{R} \right] \right] \right\}. \end{aligned} \quad (6.3)$$

We consider the system to be a two-mode light with frequencies  $\omega_a$  and  $\omega_b$  in a cavity coupled to two USVR. The interaction between the two-mode light and the squeezed vacuum reservoirs can be described, in the interaction picture, by the Hamiltonian

$$\begin{aligned} \hat{H}_{SR}(t) &= i\hbar \left[ \sum_j \lambda_j \left( \hat{a}^\dagger \hat{A}_j e^{i(\omega_a - \omega_j)t} - \hat{a} \hat{A}_j^\dagger e^{-i(\omega_a - \omega_j)t} \right) \right. \\ &\quad \left. + \sum_k \lambda_k \left( \hat{b}^\dagger \hat{B}_k e^{i(\omega_b - \omega_k)t} - \hat{b} \hat{B}_k^\dagger e^{-i(\omega_b - \omega_k)t} \right) \right], \end{aligned} \quad (6.4)$$

in which  $\hat{a}$  ( $\hat{a}^\dagger$ ) and  $\hat{b}$  ( $\hat{b}^\dagger$ ) are the annihilation (creation) operators for the intracavity modes and  $\hat{A}_j$  ( $\hat{A}_j^\dagger$ ) and  $\hat{B}_k$  ( $\hat{B}_k^\dagger$ ) are the annihilation (creation)

operators for the reservoir modes with frequencies  $\omega_j$  and  $\omega_k$ , respectively. The coefficients  $\lambda_j$  and  $\lambda_k$  are coupling constants describing the interaction between the intracavity modes and the reservoir modes. Applying the cyclic property of trace and the relation  $\text{Tr}_R(\hat{R} \otimes \hat{H}_{SR}(t)) = \langle \hat{H}_{SR}(t) \rangle_R$ , and taking into account that, for squeezed vacuum reservoirs [12],

$$\langle \hat{A}_j \rangle_R = \langle \hat{A}_j^\dagger \rangle_R = \langle \hat{B}_k \rangle_R = \langle \hat{B}_k^\dagger \rangle_R = 0,$$

one can show

$$\frac{1}{i\hbar} \text{Tr}_R \left\{ \left[ \hat{H}_{SR}(t), \hat{\rho}(0) \otimes \hat{R} \right] \right\} = 0,$$

and as a result, expression (6.4) reduces to

$$\frac{d\hat{\rho}(t)}{dt} = -\frac{1}{\hbar^2} \int_0^t dt' \text{Tr}_R \left\{ \left[ \hat{H}_{SR}(t), \left[ \hat{H}_{SR}(t'), \hat{\rho}(t') \otimes \hat{R} \right] \right] \right\}. \quad (6.5)$$

Applying the Markov approximation, in which  $\hat{\rho}(t')$  is replaced by  $\hat{\rho}(t)$ , and using the cyclic property of the trace, the above equation can be expressed as

$$\begin{aligned} \frac{d\hat{\rho}(t)}{dt} = & -\frac{1}{\hbar^2} \int_0^t dt' \left[ \langle \hat{H}_{SR}(t) \hat{H}_{SR}(t') \rangle_R \hat{\rho}(t) - \langle \hat{H}_{SR}(t') \hat{H}_{SR}(t) \rangle_R \hat{\rho}(t) \right. \\ & \left. - \hat{\rho}(t) \langle \hat{H}_{SR}(t) \hat{H}_{SR}(t') \rangle_R + \hat{\rho}(t) \langle \hat{H}_{SR}(t') \hat{H}_{SR}(t) \rangle_R \right]. \end{aligned} \quad (6.6)$$

We note again that for squeezed vacuum reservoirs [12]

$$\langle \hat{A}_j \hat{A}_l \rangle_R = -M_A \delta_{l, 2j_a - j}, \quad (6.7a)$$

$$\langle \hat{A}_j^\dagger \hat{A}_l \rangle_R = N_A \delta_{j,l}, \quad (6.7b)$$

$$\langle \hat{A}_j \hat{A}_l^\dagger \rangle_R = (N_A + 1) \delta_{j,l}, \quad (6.7c)$$

where  $\delta_{j,l}$  is the Kronecker delta symbol and

$$\langle \hat{A}_j \hat{B}_m \rangle_R = \langle \hat{A}_j \hat{B}_m^\dagger \rangle_R = \langle \hat{A}_j^\dagger \hat{B}_m^\dagger \rangle_R = 0. \quad (6.8)$$

This equation is a consequence of the fact that the two squeezed vacuum reservoirs are uncorrelated. The parameters  $N_A, N_B, M_A$  and  $M_B$  describe the effects of squeezing of the reservoir modes. Actually, the parameters  $N$  and  $M$  represent the mean photon number and the phase property of the reservoirs, respectively, and are related as  $|M|^2 = N(N+1)$ . For the explicit

expressions of  $N$  and  $M$  see (C.21) and (C.25) in Appendix C. Furthermore, introducing the density of states  $g(\omega)$ , where

$$\sum_j \lambda_j \lambda_{2j_a-j} \rightarrow \int_0^\infty d\omega g(\omega) \lambda(\omega) \lambda(2\omega_a - \omega),$$

and setting  $t - t' = \tau$ , one can easily show that

$$\int_0^t dt' e^{\pm i(\omega_a - \omega)(t-t')} = \int_0^t d\tau e^{\pm i(\omega_a - \omega)\tau}. \quad (6.9)$$

Since the exponential is a rapidly decaying function of time, the upper limit of integration can be extended to infinity. Making use of the approximate relation

$$\int_0^\infty e^{\pm i(\omega_a - \omega)\tau} = \pi \delta(\omega_a - \omega), \quad (6.10)$$

and applying the property of the Dirac delta function to the integrals of Eq. (6.6), we get

$$\pi g(\omega_a) \lambda^2(\omega_a) = \frac{\gamma_A}{2}, \quad (6.11)$$

where  $\gamma_A = 2\pi g(\omega_a) \lambda^2(\omega_a)$  is the cavity damping constant for mode  $A$ . Similarly one can also show that the cavity damping constant for mode  $B$  is given by  $\gamma_B = 2\pi g(\omega_b) \lambda^2(\omega_b)$ .

In view of Eqs. (6.7,6.8,6.9,6.10,6.11), after evaluating lengthy but straightforward consecutive integrations as presented in detail in Ap-

pendix B, Eq. (6.6) takes the form

$$\begin{aligned}
\frac{d\hat{\rho}(t)}{dt} &= \frac{\gamma_A}{2}(N_A + 1) [2\hat{a}\hat{\rho}(t)\hat{a}^\dagger - \hat{a}^\dagger\hat{a}\hat{\rho}(t) - \hat{\rho}(t)\hat{a}^\dagger\hat{a}] \\
&+ \frac{\gamma_A N_A}{2} [2\hat{a}^\dagger\hat{\rho}(t)\hat{a} - \hat{a}\hat{a}^\dagger\hat{\rho}(t) - \hat{\rho}(t)\hat{a}\hat{a}^\dagger] \\
&+ \frac{\gamma_A M_A}{2} [2\hat{a}^\dagger\hat{\rho}(t)\hat{a}^\dagger + 2\hat{a}\hat{\rho}(t)\hat{a} - \hat{a}^{\dagger 2}\hat{\rho}(t) \\
&- \hat{\rho}(t)\hat{a}^{\dagger 2} - \hat{a}^2\hat{\rho}(t) - \hat{\rho}(t)\hat{a}^2] \\
&+ \frac{\gamma_B}{2}(N_B + 1) [2\hat{b}\hat{\rho}(t)\hat{b}^\dagger - \hat{b}^\dagger\hat{b}\hat{\rho}(t) - \hat{\rho}(t)\hat{b}^\dagger\hat{b}] \\
&+ \frac{\gamma_B N_B}{2} [2\hat{b}^\dagger\hat{\rho}(t)\hat{b} - \hat{b}\hat{b}^\dagger\hat{\rho}(t) - \hat{\rho}(t)\hat{b}\hat{b}^\dagger] \\
&+ \frac{\gamma_B M_B}{2} [2\hat{b}^\dagger\hat{\rho}(t)\hat{b}^\dagger + 2\hat{b}\hat{\rho}(t)\hat{b} - \hat{b}^{\dagger 2}\hat{\rho}(t) \\
&- \hat{\rho}(t)\hat{b}^{\dagger 2} - \hat{b}^2\hat{\rho}(t) - \hat{\rho}(t)\hat{b}^2]. \tag{6.12}
\end{aligned}$$

In the cavity we consider two-modes of light known as the signal and idler modes produced by the NDPO as shown in Fig. 6.1. The cavity has one single-port mirror in which light can enter or leave through while its other side is a mirror through which light may enter but cannot leave. In this

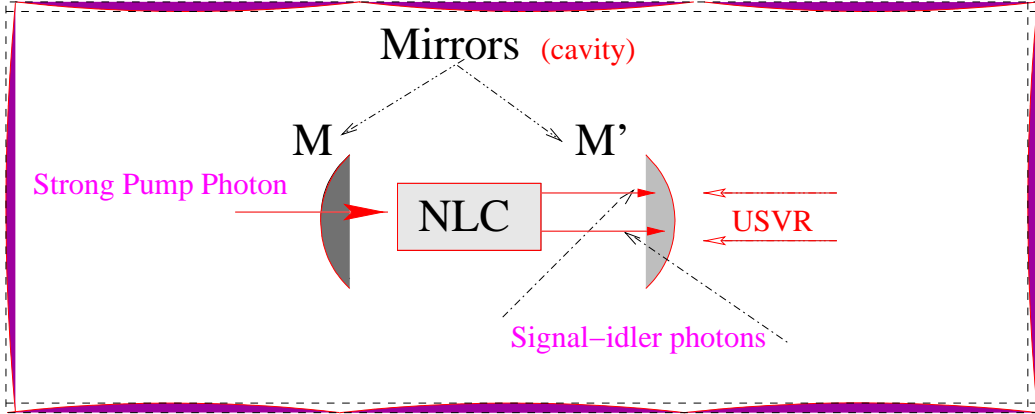


Figure 6.1: (Color online) Schematic illustration for the generation of squeezed states from a non-degenerate parametric oscillator (NDPO) coupled to squeezed vacuum reservoir. A strong pump photon interacts with a non-linear-crystal in side a cavity and is down converted into two photons usually called signal and idler photons. These photons are coupled with two uncorrelated squeezed vacuum reservoirs (USVR).

system, we assume that a strong pump light of frequency  $\omega_0$  interacts with a non-linear-medium (crystal) inside the cavity and gives rise to a two-mode squeezed light (the signal-idler modes) with frequencies  $\omega_a$  and  $\omega_b$  such that  $\omega_0 = \omega_a + \omega_b$ . This is actually a requirement of the energy conservation.

In terms of the annihilation/creation operators corresponding to the signal ( $\hat{a}$ ), idler ( $\hat{b}$ ) and pump ( $\hat{c}$ ) photons or modes, the Hamiltonian of the system, in the interaction picture, can be described as

$$\hat{H}_S = \hbar\kappa \left( \hat{a}\hat{b}\hat{c}^\dagger - \hat{a}^\dagger\hat{b}^\dagger\hat{c} \right), \quad (6.13)$$

where  $\kappa$  is the coupling constant containing the non-linearity  $\chi^{(2)}$ . In this description  $\chi^{(2)}$  is a scalar but actually it is a tensor whose components depend on the combination of frequencies. The signal (a) and idler (b) photons start in the vacuum while the pump photon begins with a coherent state with a large amplitude such that  $\hat{c} \approx \hat{c}^\dagger \approx \gamma_0$ , i.e., the annihilation and creation operators are approximated not only to be equal but also to be a c-number amplitude. In this case, when the pump photon is so strong, the Hamiltonian (6.13) takes the form

$$\hat{H}_S = \hbar\kappa\gamma_0 \left( \hat{a}\hat{b} - \hat{a}^\dagger\hat{b}^\dagger \right). \quad (6.14)$$

Upon substituting Eq. (6.14) into Eq. (6.12) one obtains

$$\begin{aligned} \frac{d\hat{\rho}(t)}{dt} &= -\kappa\gamma_0 \left[ \hat{a}\hat{b}\hat{\rho}(t) - \hat{\rho}(t)\hat{a}\hat{b} + \hat{\rho}(t)\hat{a}^\dagger\hat{b}^\dagger - \hat{a}^\dagger\hat{b}^\dagger\hat{\rho}(t) \right] \\ &+ \frac{\gamma_A}{2}(N_A + 1) \left[ 2\hat{a}\hat{\rho}(t)\hat{a}^\dagger - \hat{a}^\dagger\hat{a}\hat{\rho}(t) - \hat{\rho}(t)\hat{a}^\dagger\hat{a} \right] \\ &+ \frac{\gamma_A N_A}{2} \left[ 2\hat{a}^\dagger\hat{\rho}(t)\hat{a} - \hat{a}\hat{a}^\dagger\hat{\rho}(t) - \hat{\rho}(t)\hat{a}\hat{a}^\dagger \right] \\ &+ \frac{\gamma_A M_A}{2} \left[ 2\hat{a}^\dagger\hat{\rho}(t)\hat{a}^\dagger + 2\hat{a}\hat{\rho}(t)\hat{a} - \hat{a}^{\dagger 2}\hat{\rho}(t) \right. \\ &\quad \left. - \hat{\rho}(t)\hat{a}^{\dagger 2} - \hat{a}^2\hat{\rho}(t) - \hat{\rho}(t)\hat{a}^2 \right] \\ &+ \frac{\gamma_B}{2}(N_B + 1) \left[ 2\hat{b}\hat{\rho}(t)\hat{b}^\dagger - \hat{b}^\dagger\hat{b}\hat{\rho}(t) - \hat{\rho}(t)\hat{b}^\dagger\hat{b} \right] \\ &+ \frac{\gamma_B N_B}{2} \left[ 2\hat{b}^\dagger\hat{\rho}(t)\hat{b} - \hat{b}\hat{b}^\dagger\hat{\rho}(t) - \hat{\rho}(t)\hat{b}\hat{b}^\dagger \right] \\ &+ \frac{\gamma_B M_B}{2} \left[ 2\hat{b}^\dagger\hat{\rho}(t)\hat{b}^\dagger + 2\hat{b}\hat{\rho}(t)\hat{b} - \hat{b}^{\dagger 2}\hat{\rho}(t) \right. \\ &\quad \left. - \hat{\rho}(t)\hat{b}^{\dagger 2} - \hat{b}^2\hat{\rho}(t) - \hat{\rho}(t)\hat{b}^2 \right]. \end{aligned} \quad (6.15)$$

This is called the master equation for the NDPO coupled to the two USVR. Equation (6.15) is the basis of our analysis and describes the interactions

inside the cavity as well as the interaction of the signal-idler modes produced by the NDPO and the squeezed vacuum reservoirs via the partially transmitting mirror. This master equation is consistent with that given in Ref. [12] except that the expression there is for a single mode in a cavity coupled to a single mode vacuum reservoir.

## 6.2 The Fokker-Planck Equation

In this section we derive the Fokker-Planck equation for the Q-function. In order to obtain the Fokker-Planck equation for the Q-function corresponding to the master equation (6.15), one has first to put all terms in normal order. Applying the commutation relations

$$[\hat{a}, f(\hat{a}, \hat{a}^\dagger)] = \frac{\partial f(\hat{a}, \hat{a}^\dagger)}{\partial \hat{a}^\dagger}, \quad (6.16a)$$

$$[\hat{a}^\dagger, f(\hat{a}, \hat{a}^\dagger)] = -\frac{\partial f(\hat{a}, \hat{a}^\dagger)}{\partial \hat{a}}, \quad (6.16b)$$

one can verify that  $\hat{a}\hat{\rho} = \hat{\rho}\hat{a} + \frac{\partial \hat{\rho}}{\partial \hat{a}^\dagger}$ ,  $\hat{\rho}\hat{a}^\dagger = \hat{a}^\dagger\hat{\rho} + \frac{\partial \hat{\rho}}{\partial \hat{a}}$ , where the density operator  $\hat{\rho} = \hat{\rho}(\hat{a}, \hat{a}^\dagger, t)$  is considered to be in normal order. Making use of Eqs. (6.16), the relation  $[\hat{a}, \hat{b}\hat{c}] = \hat{b}[\hat{a}, \hat{c}] + [\hat{a}, \hat{b}]\hat{c}$  and the photonic commutation relation  $\hat{a}\hat{a}^\dagger = \hat{a}^\dagger\hat{a} + 1$ , the master equation (6.15) can be written as

$$\begin{aligned} \frac{d\hat{\rho}(t)}{dt} = & -\kappa\gamma_0 \left[ \frac{\partial \hat{\rho}}{\partial \hat{b}^\dagger} \hat{a} + \hat{a}^\dagger \frac{\partial \hat{\rho}}{\partial \hat{b}} + \hat{b}^\dagger \frac{\partial \hat{\rho}}{\partial \hat{a}} + \frac{\partial \hat{\rho}}{\partial \hat{a}^\dagger} \hat{b} + \frac{\partial^2 \hat{\rho}}{\partial \hat{a} \partial \hat{b}} + \frac{\partial^2 \hat{\rho}}{\partial \hat{a}^\dagger \partial \hat{b}^\dagger} \right] \\ & + \frac{\gamma_A}{2} (N_A + 1) \left[ \frac{\partial}{\partial \hat{a}} (\hat{\rho} \hat{a}) + \frac{\partial}{\partial \hat{a}^\dagger} (\hat{a}^\dagger \hat{\rho}) + 2 \frac{\partial^2 \hat{\rho}}{\partial \hat{a} \partial \hat{a}^\dagger} \right] \\ & - \frac{\gamma_A N_A}{2} \left[ \frac{\partial}{\partial \hat{a}^\dagger} (\hat{a}^\dagger \hat{\rho}) + \frac{\partial}{\partial \hat{a}} (\hat{\rho} \hat{a}) \right] \\ & - \frac{\gamma_A}{2} M_A \left[ \frac{\partial^2 \hat{\rho}}{\partial \hat{a}^2} + \frac{\partial^2 \hat{\rho}}{\partial \hat{a}^{\dagger 2}} \right] \\ & + \frac{\gamma_B}{2} (N_B + 1) \left[ \frac{\partial}{\partial \hat{b}} (\hat{\rho} \hat{b}) + \frac{\partial}{\partial \hat{b}^\dagger} (\hat{b}^\dagger \hat{\rho}) + 2 \frac{\partial^2 \hat{\rho}}{\partial \hat{b} \partial \hat{b}^\dagger} \right] \\ & - \frac{\gamma_B N_B}{2} \left[ \frac{\partial}{\partial \hat{b}^\dagger} (\hat{b}^\dagger \hat{\rho}) + \frac{\partial}{\partial \hat{b}} (\hat{\rho} \hat{b}) \right] \\ & - \frac{\gamma_B}{2} M_B \left[ \frac{\partial^2 \hat{\rho}}{\partial \hat{b}^2} + \frac{\partial^2 \hat{\rho}}{\partial \hat{b}^{\dagger 2}} \right]. \end{aligned} \quad (6.17)$$

In order to transform this equation into a c-number Fokker-Planck equation for the Q-function, one needs to multiply it on the left by  $\langle \alpha, \beta |$  and on the

right by  $|\alpha, \beta\rangle$ , so that

$$\begin{aligned}
\frac{\partial Q}{\partial t} = & \left[ \kappa\gamma_0 \left( \frac{\partial^2}{\partial\alpha\partial\beta} + \frac{\partial^2}{\partial\alpha^*\partial\beta^*} + \frac{\partial}{\partial\beta^*}\alpha + \frac{\partial}{\partial\beta}\alpha^* + \frac{\partial}{\partial\alpha^*}\beta + \frac{\partial}{\partial\alpha}\beta^* \right) \right. \\
& + \gamma_A(N_A + 1) \frac{\partial^2}{\partial\alpha\partial\alpha^*} + \frac{\gamma_A}{2} \left( \frac{\partial}{\partial\alpha}\alpha + \frac{\partial}{\partial\alpha^*}\alpha^* \right) \\
& - \frac{\gamma_A M_A}{2} \left( \frac{\partial^2}{\partial\alpha^2} + \frac{\partial^2}{\partial\alpha^{*2}} \right) \\
& + \gamma_B(N_B + 1) \frac{\partial^2}{\partial\beta\partial\beta^*} + \frac{\gamma_B}{2} \left( \frac{\partial}{\partial\beta}\beta + \frac{\partial}{\partial\beta^*}\beta^* \right) \\
& \left. - \frac{\gamma_B M_B}{2} \left( \frac{\partial^2}{\partial\beta^2} + \frac{\partial^2}{\partial\beta^{*2}} \right) \right] Q, \tag{6.18}
\end{aligned}$$

where

$$Q = Q(\alpha^*, \alpha, \beta^*, \beta, t) = \frac{1}{\pi^2} \langle \alpha, \beta | \hat{\rho}(\hat{a}^\dagger, \hat{a}, \hat{b}^\dagger, \hat{b}, t) | \alpha, \beta \rangle.$$

Expression (6.18) is the Fokker-Planck equation for the Q-function for the signal-idler modes produced by the NDPO coupled to two USVR. To obtain the solution of this equation, we introduce the Cartesian coordinates defined by

$$\alpha = x_1 + iy_1, \alpha^* = x_1 - iy_1, \beta = x_2 + iy_2, \beta^* = x_2 - iy_2,$$

and note that

$$x_1 = \frac{1}{2}(\alpha + \alpha^*), y_1 = -i\frac{1}{2}(\alpha - \alpha^*), x_2 = \frac{1}{2}(\beta + \beta^*), y_2 = -i\frac{1}{2}(\beta - \beta^*) \tag{6.19}$$

One can show that

$$\frac{\partial}{\partial\alpha} = \frac{1}{2} \left( \frac{\partial}{\partial x_1} - i \frac{\partial}{\partial y_1} \right), \tag{6.20a}$$

$$\frac{\partial}{\partial\beta} = \frac{1}{2} \left( \frac{\partial}{\partial x_2} - i \frac{\partial}{\partial y_2} \right). \tag{6.20b}$$

Thus combining these results and their complex conjugates, one readily obtains

$$\begin{aligned}
\frac{\partial Q}{\partial t} = & \left[ \frac{\kappa\gamma_0}{2} \left( \frac{\partial^2}{\partial x_1 \partial x_2} - \frac{\partial^2}{\partial y_1 \partial y_2} \right) + \kappa\gamma_0 \left( \frac{\partial}{\partial x_1} x_2 + \frac{\partial}{\partial x_2} x_1 - \frac{\partial}{\partial y_1} y_2 - \frac{\partial}{\partial y_2} y_1 \right) \right. \\
& + \frac{\gamma_A(N_A + 1)}{4} \left( \frac{\partial^2}{\partial x_1^2} - \frac{\partial^2}{\partial y_1^2} \right) - \frac{\gamma_A M_A}{4} \left( \frac{\partial^2}{\partial x_1^2} - \frac{\partial^2}{\partial y_1^2} \right) \\
& \left. + \frac{\gamma_B(N_B + 1)}{4} \left( \frac{\partial^2}{\partial x_2^2} - \frac{\partial^2}{\partial y_2^2} \right) - \frac{\gamma_B M_B}{4} \left( \frac{\partial^2}{\partial x_2^2} - \frac{\partial^2}{\partial y_2^2} \right) \right] Q, \tag{6.21}
\end{aligned}$$

where  $Q = Q(x_1, x_2, y_1, y_2, t)$ .

Next, introducing the transformation defined by  $x_1 = x + u$ ,  $x_2 = x - u$ ,  $y_1 = y + v$ ,  $y_2 = v - y$ , one can verify that

$$x = \frac{1}{2}(x_1 + x_2), \quad u = \frac{1}{2}(x_1 - x_2), \quad (6.22a)$$

$$y = \frac{1}{2}(y_1 - y_2), \quad v = \frac{1}{2}(y_1 + y_2). \quad (6.22b)$$

In view of these relations, it follows that

$$\frac{\partial}{\partial x_1} = \frac{1}{2} \left[ \frac{\partial}{\partial x} + \frac{\partial}{\partial u} \right], \quad \frac{\partial}{\partial x_2} = \frac{1}{2} \left[ \frac{\partial}{\partial x} - \frac{\partial}{\partial u} \right] \quad (6.23a)$$

$$\frac{\partial}{\partial y_1} = \frac{1}{2} \left[ \frac{\partial}{\partial y} + \frac{\partial}{\partial v} \right], \quad \frac{\partial}{\partial y_2} = \frac{1}{2} \left[ \frac{\partial}{\partial y} - \frac{\partial}{\partial v} \right]. \quad (6.23b)$$

Making use of Eqs. (6.22) and (6.23) in Eq. (6.21) and setting  $\gamma_A = \gamma_B = \gamma$ ,  $N_A = N_B = N$  and  $M_A = M_B = M$ , for convenience, one arrives at

$$\begin{aligned} \frac{\partial Q}{\partial t} = & \left[ \frac{\kappa\gamma_0 + \gamma(N - M + 1)}{8} \frac{\partial^2}{\partial x^2} + \frac{\kappa\gamma_0 + \gamma(N + M + 1)}{8} \frac{\partial^2}{\partial y^2} \right. \\ & - \frac{\kappa\gamma_0\gamma(N - M + 1)}{8} \frac{\partial^2}{\partial u^2} - \frac{\kappa\gamma_0 - \gamma(N + M + 1)}{8} \frac{\partial^2}{\partial v^2} \\ & \left. + \frac{2\kappa\gamma_0 + \gamma}{2} \left( \frac{\partial}{\partial x} x + \frac{\partial}{\partial y} y \right) - \frac{2\kappa\gamma_0 - \gamma}{2} \left( \frac{\partial}{\partial u} u + \frac{\partial}{\partial v} v \right) \right] Q, \quad (6.24) \end{aligned}$$

which is the Fokker-Planck equation for the Q-function where  $Q = Q(x, y, u, v, t)$ .

### 6.3 Solution of the Fokker-Planck Equation

In this section the explicit expression for the Q-function that describes the optical system is derived. In order to solve the differential equation (6.24) using the propagator method discussed in Ref. [202], one needs to transform the above equation into a Schrödinger-type equation. This can be achieved upon replacing  $(\frac{\partial}{\partial x}, \frac{\partial}{\partial y}, \frac{\partial}{\partial u}, \frac{\partial}{\partial v}, x, y, u, v)$  and  $Q(x, y, u, v, t)$  by  $(i\hat{p}_x, i\hat{p}_y, i\hat{p}_u, i\hat{p}_v, \hat{x}, \hat{y}, \hat{u}, \hat{v})$  and  $|Q(t)\rangle$  respectively. Hence Eq. (6.24) can be expressed as

$$\begin{aligned} i \frac{d |Q(t)\rangle}{dt} = & i \left[ -\frac{\lambda_1}{8} \hat{p}_x^2 - \frac{\lambda_2}{8} \hat{p}_y^2 + \frac{\lambda_3}{8} \hat{p}_u^2 + \frac{\lambda_4}{8} \hat{p}_v^2 + i \frac{\lambda_5}{2} (\hat{p}_x \hat{x} + \hat{p}_y \hat{y}) \right. \\ & \left. - i \frac{\lambda_6}{2} (\hat{p}_u \hat{u} + \hat{p}_v \hat{v}) \right] |Q(t)\rangle = \hat{H} |Q(t)\rangle, \quad (6.25) \end{aligned}$$

where

$$\lambda_{1,2} = \kappa\gamma_0 + \gamma(N \mp M + 1), \quad (6.26a)$$

$$\lambda_{3,4} = \kappa\gamma_0 - \gamma(N \mp M + 1), \quad (6.26b)$$

$$\lambda_{5,6} = 2\kappa\gamma_0 \pm \gamma. \quad (6.26c)$$

A formal solution of Eq. (6.25) can be put in the form

$$|Q(t)\rangle = \hat{u}(t) |Q(0)\rangle, \quad (6.27)$$

where  $\hat{u}(t) = \exp(-i\hat{H}t/\hbar)$  is a unitary operator and

$$\begin{aligned} \hat{H} = & - i\frac{\lambda_1}{8}\hat{p}_x^2 - i\frac{\lambda_2}{8}\hat{p}_y^2 + i\frac{\lambda_3}{8}\hat{p}_u^2 + i\frac{\lambda_4}{8}\hat{p}_v^2 \\ & - \frac{\lambda_5}{2}(\hat{p}_x\hat{x} + \hat{p}_y\hat{y}) + \frac{\lambda_6}{2}(\hat{p}_u\hat{u} + \hat{p}_v\hat{v}) \end{aligned} \quad (6.28)$$

is a quadratic quantum Hamiltonian. Multiplying (6.27) by  $\langle x, y, u, v |$  on the left yields

$$Q(x, y, u, v, t) = \langle x, y, u, v | \hat{u}(t) | Q(0)\rangle, \quad (6.29)$$

where

$$Q(x, y, u, v, t) = \langle x, y, u, v | Q(t)\rangle.$$

Introducing a four-dimensional completeness relation for the position eigenstates

$$\hat{I} = \int dx' dy' du' dv' |x', y', u', v'\rangle \langle x', y', u', v'|$$

in expression (6.29), one can see that

$$\begin{aligned} Q(x, y, u, v, t) &= \int dx' dy' du' dv' Q(x, y, u, v, t|x', y', u', v', 0) \\ &\times Q_o(x', y', u', v'), \end{aligned} \quad (6.30)$$

where

$$Q_o(x', y', u', v') = \langle x', y', u', v' | Q(o)\rangle$$

is the initial Q-function and

$$Q(x, y, u, v, t|x', y', u', v', 0) = \langle x, y, u, v | \hat{u}(t) | x', y', u', v'\rangle$$

is the Q-function propagator.

Following Fesseha [202], the propagator associated with a quadratic Hamiltonian of the form

$$\hat{H}(\hat{x}_1, \dots, \hat{x}_n, \hat{p}_1, \dots, \hat{p}_n, t) = \sum_{i=1}^n \left[ a_i \hat{p}_i^2 + b_i(t) \hat{p}_i \hat{x}_i + c_i(t) \hat{x}_i^2 \right] \quad (6.31)$$

is expressible as

$$Q(x_1, \dots, x_n, t | x'_1, \dots, x'_n, 0) = \left[ \frac{i}{2\pi} \right]^{\frac{n}{2}} \prod_{j=1}^n \sqrt{\frac{\partial^2 S_c}{\partial x_j \partial x'_j}} \exp \left[ -\xi \int_0^t b_j(t') dt' + i S_c \right],$$

where  $S_c$  is the classical action,  $\xi$  is a parameter related with operator ordering and  $a_i$  is constant different from zero for the Hamiltonian to remain quadratic. Comparing Eqs. (6.31) and (6.28), it follows that  $a_i = a_{x,y,u,v} = -\frac{i}{8} \lambda_{1,2,3,4}$ ,  $(x_1, x_2, x_3, x_4) = (x, y, u, v)$ ,  $c_x = c_y = c_u = c_v = 0$ ,  $b_x = b_y = -\frac{\lambda_5}{2}$ ,  $b_u = b_v = \frac{\lambda_6}{2}$  and the anti-standard operator ordering  $\xi = \frac{1}{2}$ . Thus the Q-function propagator associated with the Hamiltonian (6.28) is expressible as

$$Q(x, y, u, v, t | x', y', u', v', 0) = \frac{1}{4\pi^2} \left[ \frac{\partial^2 S_c}{\partial x' \partial x} \frac{\partial^2 S_c}{\partial y' \partial y} \frac{\partial^2 S_c}{\partial u' \partial u} \frac{\partial^2 S_c}{\partial v' \partial v} \right]^{\frac{1}{2}} \times \exp \left( i S_c + \frac{(\lambda_5 - \lambda_6)}{2} t \right). \quad (6.32)$$

In order to obtain the explicit form of this expression, one has first to determine the classical action. To this end, the Hamiltonian function corresponding to the quantum Hamiltonian (6.28) is given by

$$H = -i \frac{\lambda_1}{8} p_x^2 - i \frac{\lambda_2}{8} p_y^2 + i \frac{\lambda_3}{8} p_u^2 + i \frac{\lambda_4}{8} p_v^2 - \frac{\lambda_5}{2} (p_x x + p_y y) + \frac{\lambda_6}{2} (p_u u + p_v v).$$

With the help of the Lagrangian  $L = \sum_i \dot{x}_i p_i - H$  and the Hamilton equations  $\dot{x}_i = \frac{\partial H}{\partial p_i}$  ( $i = x, y, u, v$ ) one can readily show that

$$L = \frac{2i}{\lambda_1} \left( \dot{x} + \frac{\lambda_5}{2} x \right)^2 + \frac{2i}{\lambda_2} \left( \dot{y} + \frac{\lambda_5}{2} y \right)^2 - \frac{2i}{\lambda_3} \left( \dot{u} - \frac{\lambda_6}{2} u \right)^2 - \frac{2i}{\lambda_4} \left( \dot{v} - \frac{\lambda_6}{2} v \right)^2. \quad (6.33)$$

Applying the Euler-Lagrange equations

$$\frac{d}{dt} \left( \frac{\partial L}{\partial \dot{x}_i} \right) - \frac{\partial L}{\partial x_i} = 0,$$

along with Eq. (6.33), leads to

$$\begin{aligned}\ddot{x} - \left(\frac{\lambda_5}{2}\right)^2 x &= 0, & \ddot{y} - \left(\frac{\lambda_5}{2}\right)^2 y &= 0, \\ \ddot{u} - \left(\frac{\lambda_6}{2}\right)^2 u &= 0, & \ddot{v} - \left(\frac{\lambda_6}{2}\right)^2 v &= 0.\end{aligned}$$

The solutions of these differential equations can be written as

$$x(t) = a_1 e^{\frac{\lambda_5}{2}t} + a_2 e^{-\frac{\lambda_5}{2}t}, \quad y(t) = b_1 e^{\frac{\lambda_5}{2}t} + b_2 e^{-\frac{\lambda_5}{2}t}, \quad (6.34a)$$

$$u(t) = c_1 e^{\frac{\lambda_6}{2}t} + c_2 e^{-\frac{\lambda_6}{2}t}, \quad v(t) = d_1 e^{\frac{\lambda_6}{2}t} + d_2 e^{-\frac{\lambda_6}{2}t}. \quad (6.34b)$$

Now substituting these expressions and their corresponding first order time derivatives into Eq. (6.33), the Lagrangian takes the form

$$L = 2i\lambda_5^2 \left( \frac{a_1^2}{\lambda_1} + \frac{b_1^2}{\lambda_2} \right) e^{\lambda_5 t} - 2i\lambda_6^2 \left( \frac{c_2^2}{\lambda_3} + \frac{d_2^2}{\lambda_4} \right) e^{-\lambda_6 t}.$$

On account of the above result, the classical action defined by  $S_c = \int_0^T L(t)dt$  takes the form

$$S_c = 2i\lambda_5^2 \left( \frac{a_1^2}{\lambda_1} + \frac{b_1^2}{\lambda_2} \right) (e^{\lambda_5 T} - 1) + 2i\lambda_6^2 \left( \frac{c_2^2}{\lambda_3} + \frac{d_2^2}{\lambda_4} \right) (e^{-\lambda_6 T} - 1). \quad (6.35)$$

Applying the boundary conditions  $x_i(0) = x'_i$  and  $x_i(T) = x''_i$  in Eq. (6.34), one can obtain that

$$\begin{aligned}a_1 &= \frac{x'' e^{\frac{\lambda_5}{2}T} - x'}{e^{\lambda_5 T} - 1}, & b_1 &= \frac{y'' e^{\frac{\lambda_5}{2}T} - y'}{e^{\lambda_5 T} - 1}, \\ c_2 &= \frac{u'' e^{-\frac{\lambda_6}{2}T} - u'}{e^{-\lambda_6 T} - 1}, & d_2 &= \frac{v'' e^{-\frac{\lambda_6}{2}T} - v'}{e^{-\lambda_6 T} - 1}.\end{aligned}$$

Inserting the above expressions into Eq. (6.35) and replacing  $(x'', y'', u'', v'', T)$  by  $(x, y, u, v, t)$  yields

$$\begin{aligned}S_c &= 2i\lambda_5 \left[ \frac{(x' - e^{\frac{\lambda_5}{2}t})^2}{\lambda_1 (e^{\lambda_5 t} - 1)} + \frac{(y' - e^{\frac{\lambda_5}{2}t})^2}{\lambda_2 (e^{\lambda_5 t} - 1)} \right] \\ &+ 2i\lambda_6 \left[ \frac{(u' - e^{-\frac{\lambda_6}{2}t})^2}{\lambda_3 (e^{-\lambda_6 t} - 1)} + \frac{(v' - e^{-\frac{\lambda_6}{2}t})^2}{\lambda_4 (e^{-\lambda_6 t} - 1)} \right]\end{aligned}$$

and employing this relation the following results are obtained:

$$\frac{\partial^2 S_c}{\partial x \partial x'} = -\frac{4i\lambda_5 e^{\frac{\lambda_5}{2}t}}{\lambda_1 (e^{\lambda_5 t} - 1)}, \quad \frac{\partial^2 S_c}{\partial y \partial y'} = -\frac{4i\lambda_5 e^{\frac{\lambda_5}{2}t}}{\lambda_2 (e^{\lambda_5 t} - 1)}, \quad (6.36a)$$

$$\frac{\partial^2 S_c}{\partial u \partial u'} = -\frac{4i\lambda_6 e^{-\frac{\lambda_6}{2}t}}{\lambda_3 (e^{-\lambda_6 t} - 1)}, \quad \frac{\partial^2 S_c}{\partial v \partial v'} = -\frac{4i\lambda_6 e^{-\frac{\lambda_6}{2}t}}{\lambda_4 (e^{-\lambda_6 t} - 1)}. \quad (6.36b)$$

Thus, in view of Eq. (6.36), the Q-function propagator (6.32) can be expressed as

$$\begin{aligned}
Q(x, y, u, v, t | x', y', u', v', 0) &= \frac{4\lambda_5\lambda_6}{\pi^2\sqrt{\lambda_1\lambda_2\lambda_3\lambda_4}} \frac{e^{(\lambda_5-\lambda_6)t}}{(e^{\lambda_5 t} - 1)(e^{-\lambda_6 t} - 1)} \\
&\times \exp \left[ -\frac{2\lambda_5}{(e^{\lambda_5 t} - 1)} \left( \frac{x'^2 - 2xx' e^{\frac{\lambda_5}{2}t} + x^2 e^{\lambda_5 t}}{\lambda_1} \right. \right. \\
&+ \left. \frac{y'^2 - 2yy' e^{\frac{\lambda_5}{2}t} + y^2 e^{\lambda_5 t}}{\lambda_2} \right) \\
&- \frac{2\lambda_6}{(e^{-\lambda_6 t} - 1)} \left( \frac{u'^2 - 2uu' e^{-\frac{\lambda_6}{2}t} + u^2 e^{-\lambda_6 t}}{\lambda_3} \right. \\
&+ \left. \left. \frac{v'^2 - 2vv' + v^2 e^{-\lambda_6 t}}{e^{-\frac{\lambda_6}{2}t} \lambda_4} \right) \right].
\end{aligned}$$

Considering the signal-idler modes produced by the NDPO to be initially in a two-mode vacuum state, the initial Q-function is expressible as

$$Q_0(\alpha', \beta') = \frac{1}{\pi^2} \langle \alpha', \beta' | 0, 0 \rangle \langle 0, 0 | \alpha', \beta' \rangle = \exp(-\alpha'^* \alpha' - \beta'^* \beta'),$$

and in terms of the Cartesian variables of expression (6.19), this equation becomes

$$Q_0(x'_1, x'_2, y'_1, y'_2) = \frac{1}{\pi^2} \exp \left[ - (x'^2_1 + x'^2_2 + y'^2_1 + y'^2_2) \right].$$

Furthermore, in terms of  $x', y', u'$  and  $v'$ , one can write

$$\int dx'_1 dx'_2 dy'_1 dy'_2 Q_0(x'_1, x'_2, y'_1, y'_2) = \int dx' dy' du' dv' Q_0(x', y', u', v'),$$

where

$$Q_0(x', y', u', v') = \frac{|J|}{\pi^2} \exp \left[ - 2(x'^2 + y'^2 + u'^2 + v'^2) \right]$$

and  $J$  is the Jacobian of the transformation of  $x_1, x_2, y_1$  and  $y_2$  with respect to  $x, y, u$  and  $v$ . Making use of Eq. (6.19) in the Jacobian, one can show that  $|J| = 4$ . Hence

$$Q_0(x', y', u', v') = \frac{4}{\pi^2} \exp \left[ - 2(x'^2 + y'^2 + u'^2 + v'^2) \right]. \quad (6.37)$$

Substituting expression (6.36) into Eq. (6.32) and then combining the result with Eq. (6.37) and finally carrying out the integration in Eq. (6.30) applying the relation

$$\int_{-\infty}^{\infty} dx' \exp \left[ -kx'^2 + dx' \right] = \sqrt{\frac{\pi}{k}} \exp \left[ \frac{d^2}{4k} \right], \quad k > 0,$$

the Q-function takes the compact form

$$Q(x, y, u, v, t) = \frac{4}{\pi^2 \sqrt{a_1 a_2 a_3 a_4}} \exp \left[ -\frac{2}{a_1} x^2 - \frac{2}{a_2} y^2 - \frac{2}{a_3} u^2 - \frac{2}{a_4} v^2 \right], \quad (6.38)$$

where

$$a_{1,2} = \frac{\lambda_{1,2}(e^{\lambda_5 t} - 1) + \lambda_5}{\lambda_5 e^{\lambda_5 t}}, \quad (6.39a)$$

$$a_{3,4} = \frac{\lambda_{3,4}(e^{-\lambda_6 t} - 1) + \lambda_6}{\lambda_6 e^{-\lambda_6 t}}. \quad (6.39b)$$

It can be easily verified that the Jacobian of the inverse transformation is  $|J'| = \frac{1}{4}$ . One can then write

$$\int dx dy du dv Q(x, y, u, v, t) = \int dx_1 dx_2 dy_1 dy_2 Q'(x_1, x_2, y_1, y_2, t),$$

in which the final expression for  $Q'(x_1, x_2, y_1, y_2, t)$  is obtained from Eq. (6.38) employing the inverse transformations (6.22). Upon carrying out further inverse transformations (6.19), the required final form the Q-function for the signal-idler modes produced by the NDPO coupled to two uncorrelated squeezed vacuum reservoirs takes the form

$$\begin{aligned} Q(\alpha, \alpha^*, \beta, \beta^*, t) &= \frac{D}{\pi^2} \exp \left[ -b_1(|\alpha|^2 + |\beta|^2) + b_2(\alpha\beta + \alpha^*\beta^*) \right. \\ &\quad \left. + b_3(\alpha\beta^* + \alpha^*\beta) + \frac{b_4}{2}(\alpha^2 + \alpha^{*2} + \beta^2 + \beta^{*2}) \right], \quad (6.40) \end{aligned}$$

where

$$D = \frac{1}{\sqrt{a_1 a_2 a_3 a_4}}, \quad (6.41a)$$

$$b_{1,2} = \frac{1}{4} \left[ \frac{1}{\pm a_1} \pm \frac{1}{a_2} + \frac{1}{a_3} + \frac{1}{a_4} \right], \quad (6.41b)$$

$$b_{3,4} = \frac{1}{4} \left[ -\frac{1}{a_1} + \frac{1}{a_2} \pm \frac{1}{a_3} \mp \frac{1}{a_4} \right]. \quad (6.41c)$$

This Q-function is useful to calculate the expectation values of anti-normally ordered operators and consequently the quadrature variances. It can also be used to calculate the photon number distribution of different optical systems. In this Chapter, this function is used to calculate the quadrature fluctuations of the NDPO coupled to two USVR. It can be readily verified that the Q-function (6.40) is positive and normalised.

Now we proceed to obtain the expressions for the Q-function for some special cases of interest: For the case when there are no squeezed vacuum reservoirs ( $r = 0$ ), that is, when the external environment is an ordinary vacuum, the Q-function (6.40) takes the form

$$Q(\alpha, \alpha^*, \beta, \beta^*, t) = \frac{1}{\pi^2 a_1 a_3} \exp \left[ -\frac{1}{2} \left( \frac{a_1 + a_3}{a_1 a_3} \right) (|\alpha|^2 + |\beta|^2) + \frac{1}{2} \left( \frac{a_1 - a_3}{a_1 a_3} \right) (\alpha\beta + \alpha^*\beta^*) \right]. \quad (6.42)$$

This is the Q-function for the non-degenerate parametric oscillator coupled to ordinary vacuum. On the other hand, in the absence of damping ( $\gamma = 0$ ), Eq. (6.40) reduces to

$$Q(\alpha, \alpha^*, \beta, \beta^*, t) = \frac{\operatorname{sech} \kappa \gamma_0 t}{\pi^2} \exp \left[ -|\alpha|^2 - |\beta|^2 - (\tanh \kappa \gamma_0 t) (\alpha\beta + \alpha^*\beta^*) \right], \quad (6.43)$$

which is the Q-function for the non-degenerate parametric amplifier.

Next we obtain the Q-function for the single-mode generated by a degenerate parametric oscillator (DPO) coupled to a single-mode squeezed vacuum reservoir from the Q-function for the NDPO (6.40). The Q-function for the single-mode can be expressed as

$$Q(\alpha, \alpha^*, t) = \int d^2\beta Q(\alpha, \alpha^*, \beta, \beta^*, t),$$

so that using Eq. (6.40) and the relation

$$\begin{aligned} & \int d^2\alpha \exp \left[ -a'|\alpha|^2 + b'\alpha + c'\alpha^* + A'\alpha^2 + B'\alpha^{*2} \right] \\ &= \frac{1}{\sqrt{(a'^2 - 4A'B')}} \exp \left[ \frac{a'b'c' + A'c'^2 + B'b'^2}{a'^2 - 4A'B'} \right], a' > 0 \end{aligned} \quad (6.44)$$

the Q-function for the DPO coupled to a single-mode squeezed vacuum reservoir takes the form

$$Q(\alpha, \alpha^*, t) = \frac{D}{\pi\sqrt{y}} \exp \left[ -a|\alpha|^2 + \frac{A}{2} (\alpha^2 + \alpha^{*2}) \right], \quad (6.45)$$

where

$$y = b_1^2 - b_4^2, \quad (6.46a)$$

$$a = \frac{1}{y} \left[ (b_1 + b_4)(b_1(b_1 - b_4) + 2b_2b_3) - b_1(b_2 + b_3)^2 \right], \quad (6.46b)$$

$$A = \frac{1}{y} \left[ (b_1 + b_4)(b_4(b_1 - b_4) + 2b_2b_3) + b_4(b_2 + b_3)^2 \right]. \quad (6.46c)$$

Upon integrating Eqs. (6.42) and (6.43) with respect to  $\beta$  by employing relation (6.44), one can also find the Q-function for the DPO in the absence of squeezed vacuum reservoir ( $r = 0$ ) and in the absence of damping ( $\gamma = 0$ ) to be

$$Q(\alpha, \alpha^*, t) = \frac{2}{\pi(a_1 + a_3)} \exp \left[ -\frac{2}{a_1 + a_3} |\alpha|^2 \right]$$

and

$$Q(\alpha, \alpha^*, t) = \frac{\text{sech}^2 \kappa \gamma_0 t}{\pi} \exp \left[ -(\text{sech}^2 \kappa \gamma_0 t) (|\alpha|^2) \right], \quad (6.47)$$

respectively.

## 6.4 Quadrature Squeezing

In this section the intracavity quadrature fluctuations for the single-mode generated by the DPO as well as the signal-idler modes produced by the NDPO coupled to the two squeezed vacuum reservoirs using the pertinent Q-functions derived in the previous section are analysed. Before we proceed into the mathematical details we begin first by giving a general pictorial demonstration regarding quadrature squeezing in the diagram shown below (Fig. 6.2).

### 6.4.1 Quadrature Squeezing in a DPO

Here the first focus is the squeezing properties of the single-mode light. These properties can be described by two Hermitian operators defined as  $\hat{a}_1 = \hat{a}^\dagger + \hat{a}$  and  $\hat{a}_2 = i(\hat{a}^\dagger - \hat{a})$ . These quadrature operators obey the commutation relation

$$[\hat{a}_1, \hat{a}_2] = 2i. \quad (6.48)$$

The variance of these quadrature operators can be put in the form

$$(\Delta \hat{a}_{1,2})^2 = \langle \hat{a}_{1,2}^2 \rangle - \langle \hat{a}_{1,2} \rangle^2 \quad (6.49)$$

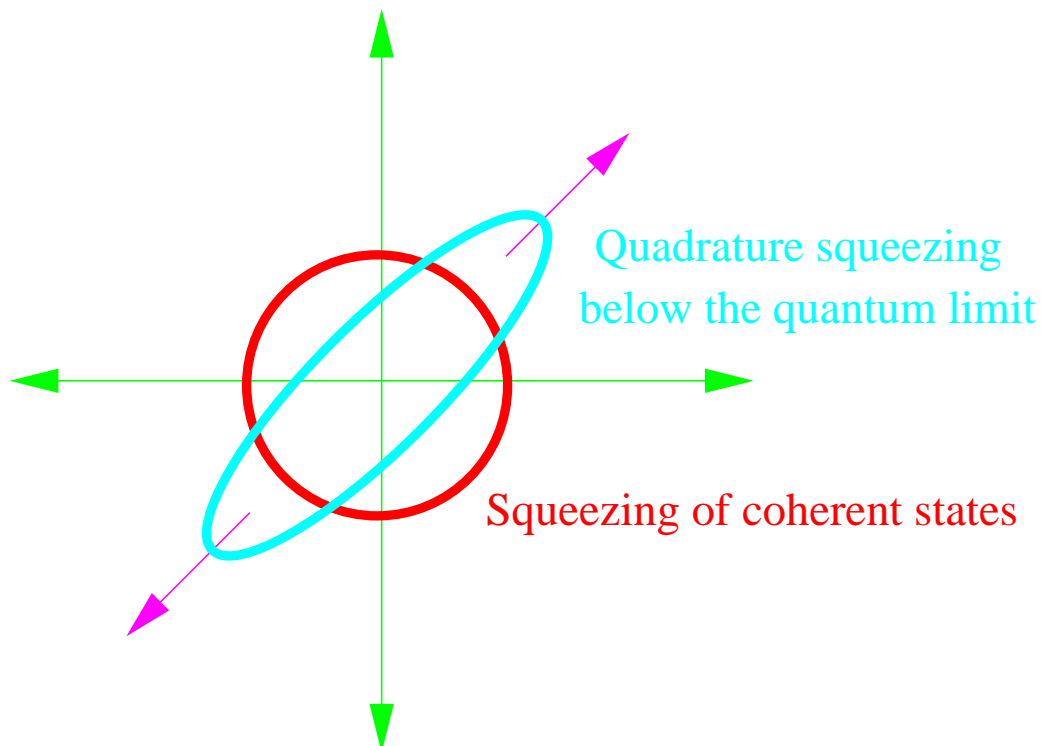


Figure 6.2: (Color online) Demonstration of squeezing quadrature operators below the vacuum level or below that is achievable by coherent states. In the case of coherent states both quadrature components have the same value as shown by the red circle on the centre. The elliptical figure on the other hand illustrates how fluctuations are squeezed below the vacuum level on one quadrature component and enhances above the vacuum level on the other so that the uncertainty principle remains valid.

We now proceed to calculate the expectation values involved in expression (6.49). Applying the relation

$$\langle \hat{A}(\hat{a}, \hat{a}^\dagger) \rangle = \int_{-\infty}^{\infty} d^2\alpha Q(\alpha, \alpha^*, t) A_a(\alpha, \alpha^*), \quad (6.50)$$

in which  $A_a(\alpha, \alpha^*)$  is the c-number equivalent of the operator  $\hat{A}(\hat{a}, \hat{a}^\dagger)$  for the anti-normal ordering, one arrives at

$$\langle \hat{a} \rangle = \int_{-\infty}^{\infty} d^2\alpha Q(\alpha, \alpha^*, t) \alpha.$$

Upon using the Q-function (6.45) for the single mode, the above equation can be expressed as

$$\langle \hat{a} \rangle = \frac{D}{\sqrt{y}} \frac{\partial}{\partial b} \int_{-\infty}^{\infty} \frac{d^2\alpha}{\pi} \exp \left[ -a\alpha^* \alpha + \frac{A}{2} (\alpha^2 + \alpha^{*2}) + b\alpha \right] \Bigg|_{b=0},$$

and on the basis of (6.44) for which  $c' = 0$  and  $A' = B'$ , one can verify that

$$\langle \hat{a} \rangle = \frac{D}{\sqrt{y}} \frac{\partial}{\partial b} \left[ \frac{\exp \left( \frac{Ab^2}{2(a^2 - A^2)} \right)}{\sqrt{a^2 - A^2}} \right] \Bigg|_{b=0} = 0. \quad (6.51)$$

Similarly we can easily see that

$$\langle \hat{a}^2 \rangle = \langle \hat{a}^{\dagger 2} \rangle = 0. \quad (6.52)$$

In view of this result expression (6.50) reduces to

$$(\Delta \hat{a}_{1,2})^2 = 1 + 2\langle \hat{a}^\dagger \hat{a} \rangle \pm \langle \hat{a}^{\dagger 2} \rangle \pm \langle \hat{a}^2 \rangle. \quad (6.53)$$

Making use of the fact that the c-number equivalent of  $\hat{a}^\dagger \hat{a}$  for the anti-normal ordering is  $\alpha^* \alpha - 1$  and applying relation (6.50) in evaluating all the expectation values in Eq. (6.53), we arrive at

$$(\Delta \hat{a}_{1,2})^2 = \frac{2}{a \mp A} - 1. \quad (6.54)$$

Finally the quadrature fluctuations of the single-mode at any time  $t$ , in view of Eqs. (6.46, 6.40 and 6.39), take the form

$$(\Delta \hat{a}_{1,2})^2 = \frac{\lambda_{1,2}(e^{\lambda_5 t} - 1) + \lambda_5}{\lambda_5 e^{\lambda_5 t}} + \frac{\lambda_{3,4}(e^{-\lambda_6 t} - 1) + \lambda_6}{\lambda_6 e^{-\lambda_6 t}} - 1.$$

At steady-state ( $t \rightarrow \infty$ ), the variances given above reduce to

$$(\Delta \hat{a}_{1,2})^2 = \frac{\lambda_{1,2}}{\lambda_5} + \frac{\lambda_{3,4}}{\lambda_6} - 1,$$

and with the aid of Eq. (6.26) one can rewrite these expressions as

$$(\Delta \hat{a}_{1,2})^2 = \frac{2(N \mp M) + 1}{1 - \left( \frac{2\kappa\gamma_0}{\gamma} \right)^2}.$$

Since for squeezed vacuum reservoirs, as shown in (C.21) and (C.25),

$$N = \sinh^2 r, \quad (6.55a)$$

$$M = \sinh r \cosh r, \quad (6.55b)$$

where  $r$  is the squeezing parameter taken to be real and positive for convenience, expression (6.55) takes the form

$$(\Delta \hat{a}_{1,2})^2 = \frac{e^{\mp 2r}}{1 - \left(\frac{2\kappa\gamma_0}{\gamma}\right)^2}. \quad (6.56)$$

Using Eq. (6.56) one can show that  $(\Delta \hat{a}_1)^2 < 1$ , for

$$r > -\frac{1}{2} \ln \left[ 1 - \left(\frac{2\kappa\gamma_0}{\gamma}\right)^2 \right] \quad (6.57)$$

and  $(\Delta \hat{a}_2)^2 > 1$  for all  $r$ . This shows that the degenerate parametric oscillator coupled to a squeezed vacuum reservoir is in a squeezed state for the value of  $r$  specified by Eq. (6.57).

In the absence of squeezing, i.e.,  $r = 0$ , substitution of Eq. (6.26) into Eq. (6.54) leads to

$$(\Delta \hat{a}_1)^2 = (\Delta \hat{a}_2)^2 = \frac{1 - \frac{\kappa\gamma_0}{\gamma} e^{-(\gamma - 2\kappa\gamma_0)t}}{\left[1 - \left(\frac{2\kappa\gamma_0}{\gamma}\right)^2\right]} \left[ (1 - e^{-4\kappa\gamma_0 t}) + \frac{2\kappa\gamma_0}{\gamma} (1 + e^{-4\kappa\gamma_0 t}) \right].$$

At steady-state and when the parametric oscillator is operating below threshold ( $\gamma > 2\kappa\gamma_0$ ), this equation reduces to

$$(\Delta \hat{a}_1)^2 = (\Delta \hat{a}_2)^2 = \frac{1}{\left[1 - \left(\frac{2\kappa\gamma_0}{\gamma}\right)^2\right]}$$

in which both variances become greater than unity. Hence the single-mode in this case is not in a squeezed state.

In the absence of damping ( $\gamma = 0$ ), Eq. (6.54) becomes

$$(\Delta \hat{a}_1)^2 = (\Delta \hat{a}_2)^2 = 2\langle \hat{\mathcal{N}} \rangle + 1,$$

where  $\langle \hat{\mathcal{N}} \rangle = \sinh^2 \kappa\gamma_0 t$  is the mean photon number for the single-mode. From these variances one can infer that the single-mode in this case is in a chaotic state as expected. Furthermore, in the absence of parametric interaction ( $\kappa = 0$ ), Eq. (6.54) can be expressed as

$$(\Delta \hat{a}_{1,2})^2 = 2a_{1,2} - 1 = 1 - \left[1 - e^{-\gamma t}\right] \left[1 \mp e^{\mp 2r}\right] \leq 1,$$

and at steady-state these relations reduce to

$$(\Delta \hat{a}_{1,2})^2 = e^{\mp 2r}, \quad (6.58)$$

which are the quadrature fluctuations of the squeezed vacuum reservoir  $A$ .

### 6.4.2 Quadrature Squeezing in a NDPO

Now we proceed to investigate the squeezing properties of the signal-idler modes produced by the NDPO coupled to the two squeezed vacuum reservoirs applying the Q-function (6.40). The squeezing properties of two-mode light can be described by two quadrature operators defined as

$$\hat{c}_{1,2} = \frac{1}{\sqrt{2}}(\hat{a}_{1,2} + \hat{b}_{1,2}),$$

where

$$\hat{a}_1 = (\hat{a}^\dagger + \hat{a}), \quad \hat{b}_1 = (\hat{b}^\dagger + \hat{b}), \quad (6.59a)$$

$$\hat{a}_2 = i(\hat{a}^\dagger - \hat{a}), \quad \hat{b}_2 = i(\hat{b}^\dagger - \hat{b}), \quad (6.59b)$$

and  $\hat{a}$  ( $\hat{b}$ ) denotes the annihilation operator for the intra-cavity mode  $a$  ( $b$ ). The quadrature operators  $\hat{c}_1$  and  $\hat{c}_2$  satisfy the commutation relation

$$[\hat{c}_1, \hat{c}_2] = 2i. \quad (6.60)$$

On account of these expressions, the variances can be expressed as

$$\begin{aligned} (\Delta\hat{c}_{1,2})^2 &= \langle \hat{c}_{1,2}^2 \rangle - \langle \hat{c}_{1,2} \rangle^2 \\ &= \frac{1}{2}\langle \hat{a}_{1,2}^2 \rangle + \frac{1}{2}\langle \hat{b}_{1,2}^2 \rangle + \langle \hat{a}_{1,2}, \hat{b}_{1,2} \rangle, \end{aligned}$$

in which

$$\langle \hat{a}_i, \hat{b}_i \rangle = \langle \hat{a}_i \hat{b}_i \rangle - \langle \hat{a}_i \rangle \langle \hat{b}_i \rangle,$$

and  $i = 1, 2$ . In particular, when  $a$  and  $b$  represent the signal and idler modes, respectively, it can be shown that

$$\begin{aligned} (\Delta\hat{c}_{1,2})^2 &= \frac{1}{2}(\Delta\hat{a}_{1,2})^2 + \frac{1}{2}(\Delta\hat{b}_{1,2})^2 + \langle \hat{a}_{1,2}, \hat{b}_{1,2} \rangle \\ &= (\Delta\hat{a}_{1,2})^2 + \langle \hat{a}_{1,2}, \hat{b}_{1,2} \rangle \end{aligned} \quad (6.61)$$

as  $(\Delta\hat{a}_{1,2})^2 = (\Delta\hat{b}_{1,2})^2$  and  $\langle \hat{a}_{1,2} \rangle = \langle \hat{b}_{1,2} \rangle = \langle \hat{c}_{1,2} \rangle = 0$ . In order to obtain the explicit form of Eq. (6.61), we proceed as follows. In view of expression (6.59) and (6.50), one can express that

$$\langle \hat{a}_1 \hat{b}_1 \rangle = \int_{-\infty}^{\infty} d^2\alpha d^2\beta (\alpha^* + \alpha)(\beta^* + \beta) Q(\alpha, \alpha^*, \beta^*, \beta, t).$$

Then employing the Q-function (6.40) the above equation can be further expressed as

$$\begin{aligned} \langle \hat{a}_1 \hat{b}_1 \rangle &= D \int_{-\infty}^{\infty} \frac{d^2\alpha}{\pi} (\alpha^* + \alpha) \exp \left[ -b_1 \alpha^* \alpha + \frac{b_4}{2} (\alpha^2 + \alpha^{*2}) \right] \\ &\times \int_{-\infty}^{\infty} \frac{d^2\beta}{\pi} (\beta^* + \beta) \exp \left[ -b_1 \beta^* \beta + (b_2 \alpha + b_3 \alpha^*) \beta \right. \\ &\left. + (b_2 \alpha^* + b_3 \alpha) \beta^* + \frac{1}{2} b_4 (\beta^2 + \beta^{*2}) \right]. \end{aligned}$$

Upon setting  $K = b_2 \alpha + b_3 \alpha^*$ ,

$$\begin{aligned} \langle \hat{a}_1 \hat{b}_1 \rangle &= D \int_{-\infty}^{\infty} \frac{d^2\alpha}{\pi} (\alpha^* + \alpha) \exp \left[ -b_1 \alpha^* \alpha + \frac{b_4}{2} (\alpha^2 + \alpha^{*2}) \right] \\ &\times \left( \frac{\partial}{\partial K} + \frac{\partial}{\partial K^*} \right) \int_{-\infty}^{\infty} \frac{d^2\beta}{\pi} \exp \left[ -b_1 \beta^* \beta \right. \\ &\left. + (b_2 \alpha + b_3 \alpha^*) \beta + (b_2 \alpha^* + b_3 \alpha) \beta^* + \frac{1}{2} b_4 (\beta^2 + \beta^{*2}) \right], \end{aligned}$$

so that performing the integration with respect to  $\beta$  on the basis of relation (6.44) and carrying out the differentiation we obtain

$$\begin{aligned} \langle \hat{a}_1 \hat{b}_1 \rangle &= \frac{D}{y^{\frac{3}{2}}} (b_1 + b_4) (b_2 + b_3) \int_{-\infty}^{\infty} \frac{d^2\alpha}{\pi} (\alpha^2 + \alpha^{*2} + 2\alpha^* \alpha) \\ &\times \exp \left[ -a \alpha^* \alpha + \frac{A}{2} (\alpha^2 + \alpha^{*2}) \right], \end{aligned}$$

from which it follows that

$$\begin{aligned} \langle \hat{a}_1 \hat{b}_1 \rangle &= \frac{D}{y^{\frac{3}{2}}} (b_1 + b_4) (b_2 + b_3) \left( 2 \frac{\partial}{\partial A} - 2 \frac{\partial}{\partial a} \right) \\ &\times \int_{-\infty}^{\infty} \frac{d^2\alpha}{\pi} \exp \left[ -a \alpha^* \alpha + \frac{A}{2} (\alpha^2 + \alpha^{*2}) \right]. \end{aligned}$$

Next, integrating over  $\alpha$  and carrying out the differentiation, we get

$$\langle \hat{a}_1 \hat{b}_1 \rangle = \frac{D}{y^{\frac{3}{2}} (b_1 + b_4) (b_2 + b_3)} \left( \frac{2A + 2a}{a^2 - A^2} \right) \frac{1}{\sqrt{a^2 - A^2}}.$$

Making use of expression (6.41) along with Eq. (6.46) the above equation reduces to

$$\langle \hat{a}_1 \hat{b}_1 \rangle = a_1 - a_3.$$

A similar approach leads to

$$\langle \hat{a}_2, \hat{b}_2 \rangle = -(a_2 - a_4).$$

Now Eq. (6.61) can be put as

$$(\Delta \hat{c}_{1,2})^2 = 2a_{1,4} - 1,$$

and at this stage the variances are given by

$$(\Delta \hat{c}_{1,2})^2 = 2 \left[ \frac{\kappa\gamma_0 \pm \gamma(N \mp M + 1)}{2\kappa\gamma_0 \pm \gamma} \left( 1 - e^{\mp(2\kappa\gamma_0 \pm \gamma)t} \right) + e^{\mp(2\kappa\gamma_0 \pm \gamma)t} \right] - 1.$$

Finally the quadrature fluctuations of the signal-idler modes at any time  $t$ , in view of Eq. (6.55), take the form

$$(\Delta \hat{c}_1)^2 = 1 - \left[ 1 - e^{-(\gamma+2\kappa\gamma_0)t} \right] \left[ 1 - \frac{\gamma e^{-2r}}{\gamma + 2\kappa\gamma_0} \right] < 1, \quad (6.62a)$$

$$(\Delta \hat{c}_2)^2 = 1 - \left[ 1 - e^{-(\gamma-2\kappa\gamma_0)t} \right] \left[ 1 - \frac{\gamma e^{+2r}}{\gamma - 2\kappa\gamma_0} \right] > 1. \quad (6.62b)$$

Hence the signal-idler modes generated by the NDPO coupled to the USVR, when operating below threshold ( $\gamma - 2\kappa\gamma_0 > 0$ ), are in squeezed states for all values of  $r$ .

At steady-state ( $t \rightarrow \infty$ ), Eq. (6.62) can be put in the form

$$(\Delta \hat{c}_1)^2 = \left( \frac{\gamma}{\gamma + 2\kappa\gamma_0} \right) e^{-2r} < 1, \quad (6.63a)$$

$$(\Delta \hat{c}_2)^2 = \left( \frac{\gamma}{\gamma - 2\kappa\gamma_0} \right) e^{+2r} > 1. \quad (6.63b)$$

This equation clearly shows the possibility of a very large amount of squeezing (approaching 100%) below the standard quantum limit in the one quadrature at the expense of enhanced fluctuations in the other quadrature, where in this case the standard quantum limit is taken to be

$$\sqrt{(\Delta \hat{c}_1)^2} \sqrt{(\Delta \hat{c}_2)^2} = 1.$$

In addition, at threshold ( $\gamma = 2\kappa\gamma_0$ ), one obtains

$$(\Delta \hat{c}_1)^2 = \frac{1}{2} e^{-2r}, \quad (6.64a)$$

$$(\Delta \hat{c}_2)^2 \rightarrow \infty. \quad (6.64b)$$

In the absence of squeezed vacuum reservoirs ( $r = 0$ ), expression (68) becomes

$$(\Delta\hat{c}_{1,2})^2 = \frac{\gamma \pm \left(2\kappa\gamma_0 e^{-(\gamma \pm 2\kappa\gamma_0)t}\right)}{\gamma \pm 2\kappa\gamma_0} \leq 1.$$

This shows that the signal-idler modes produced by the non-degenerate parametric oscillator in the absence of squeezed vacuum reservoirs are also in squeezed states. At steady-state and at threshold, these relations reduce to

$$\begin{aligned} (\Delta\hat{c}_1)^2 &= \frac{1}{2}, \\ (\Delta\hat{c}_2)^2 &\rightarrow \infty. \end{aligned} \tag{6.65}$$

In this case one can easily see that there is only a 50% reduction of noise below the vacuum level. By comparing Eqs. (6.64) and (6.65) we can conclude that coupling of the NDPO to the squeezed vacuum reservoirs is essential for the generation of a larger amount of squeezing.

In the absence of damping ( $\gamma = 0$ ), expression (6.62) reduces to

$$(\Delta\hat{c}_{1,2})^2 = e^{\mp 2\kappa\gamma_0 t} \leq 1,$$

which are the quadrature fluctuations of the signal-idler modes produced by a non-degenerate parametric amplifier. This indicates that a non-degenerate parametric amplifier coupled to ordinary vacuum reservoirs also generates squeezed states.

Finally, when there is no parametric interaction inside the cavity ( $\kappa = 0$ ), Eq. (6.62) takes the form

$$(\Delta\hat{c}_{1,2})^2 = 1 - (1 - e^{-\gamma t}) \left[1 \mp e^{\mp 2r}\right] \leq 1,$$

which, at steady-state, leads to

$$(\Delta\hat{c}_{1,2})^2 = e^{\pm 2r}, \tag{6.66}$$

which are the quadrature fluctuations of the reservoir modes  $A$  and  $B$ . Upon comparing the relations (6.65) and (6.66) with (6.64), one can see that the quadrature variances at steady-state and at threshold are the product of the variances of the NDPO coupled to ordinary vacuum and the variances pertaining to the squeezed vacuum reservoirs. Furthermore upon comparing expressions (6.58) and (6.66) one can observe that at steady-state the variances of a signal mode squeezed vacuum reservoir as well as those of two independent squeezed vacuum reservoirs are the same.

## 6.5 Summary

We have derived the master equation for the signal-idler modes produced by the non-degenerate parametric oscillator coupled to two uncorrelated squeezed vacuum reservoirs and consequently the Fokker-Planck equation. We have solved the pertinent Fokker-Planck equation which is a second order differential equation applying the propagator method [202] and obtained a compact form of the Q-function of the optical system coupled to two independent squeezed vacuum reservoirs. We have also deduced the Q-functions for a NDPO coupled to ordinary vacuum reservoirs, degenerate parametric oscillators coupled to a squeezed vacuum reservoir and an ordinary vacuum reservoir, and for the non-degenerate and degenerate parametric amplifiers from the Q-function for the NDPO coupled to the two USVR.

In general the Q-function can be used to evaluate the expectation values of anti-normally ordered operators as well as photon number distributions for the NDPO and other similar optical systems.

We have calculated the non-linear quantum quadrature fluctuations of the signal-idler modes generated by a non-degenerate parametric oscillator below threshold coupled to two uncorrelated squeezed vacuum reservoirs, using the Q-function. Although it is a well known fact that quantum noise cannot be eliminated, we have shown that the signal-idler modes produced by the optical system are in a two-mode squeezed state at any time  $t$ . More interestingly, we have shown that at steady-state and below threshold it is possible to generate an optimal squeezing in one of the quadratures below the standard quantum limit at the expense of enhanced fluctuations in the other quadrature so that the Heisenberg uncertainty principle remains valid. Furthermore calculation of the quadrature fluctuations at threshold clearly shows that it is possible to produce an arbitrarily large squeezing (approaching 100%) in one of the quadratures with an infinitely large noise in the other quadrature. We have also shown that the degenerate parametric oscillator can be in a squeezed state for a squeezing parameter above a certain value when it is coupled to a squeezed vacuum reservoir.

We have shown that the coupling of the optical system to the squeezed vacuum reservoirs is essential in order to get a more suppressed noise in one of the quadratures.

Finally we have calculated the quadrature fluctuations for the non-degenerate parametric amplifier coupled to ordinary vacuum reservoirs and verified that it also generates squeezed states.



# Chapter 7

## Conclusion

In this Thesis we have investigated theoretically fluctuations in quantum optical systems that comprise ultracold atomic gases and squeezed states of light.

In the second Chapter we have studied the dynamics of evaporative cooling of gaseous  $^{87}\text{Rb}$  atoms towards high phase space density. In this case thermal fluctuations are addressed via classical molecular dynamics. Applying molecular dynamics simulation to atoms trapped in an anisotropic trap from a continuously incoming atomic beam, we have shown that it is possible to trap more than  $10^8$  atoms with phase space density of 0.011 at temperature of  $20\ \mu\text{K}$  in a continuous way for very long time. We have also determined the time evolution of truncation parameters along the radial and axial directions of the trap leads to be 12.3 and 6.4 respectively.

After reviewing in Chapter 3 the basics of Bose-Einstein condensation, in Chapter 4 we have studied fluctuations in an elongated 1D quasi-condensate during a splitting and merging process at zero and finite temperature. In this case fluctuations are described by quantum quasi-particle modes which are approximated via classical simulation. Based on this simulation the existence of enhanced phase fluctuations during the splitting and merging process with the increase in temperature is observed.

Another kind of fluctuations that exist in nature are those induced by non-linear dynamics. BEC is characterised by the cubic non-linearity in the GPE. We have studied non-linearity in matter wave solitons in 1D BEC in Chapter 5. We have shown that for repulsive BEC in an optical lattice bright solitons with negative mass can experience “effective” barrier and well potentials created using defects that can be used as quantum switches and quantum memories respectively.

In Chapter 6 we have studied quantum fluctuations with no classical analogy. We have explored a non-degenerate parametric oscillator coupled with

squeezed vacuum reservoirs that generates squeezed states of light referred as signal-idler modes. We have described the optical system by deriving a master equation and solving the corresponding Fokker-Planck equation for the quantum Q-function representation. Based on the solution we have calculated the quantum fluctuations. Our analytical results show that it is possible to suppress fluctuations in one quadrature component to a very small level below the standard quantum limit at the expense of extremely enhanced fluctuations on the other without violating the uncertainty principle.

# Appendix A

## The Bogoliubov-de Gennes Equations

In this Appendix we shall derive in detail the Bogoliubov-de Gennes equations (3.43) based on the Gross-Pitaevskii equation (3.36):

$$i\hbar\frac{\partial\Phi(\mathbf{r},t)}{\partial t} = \left(-\frac{\hbar^2}{2m}\nabla^2 + V_{\text{trap}}(\mathbf{r})\right)\Phi(\mathbf{r},t) + g|\Phi(\mathbf{r},t)|^2\Phi(\mathbf{r},t). \quad (\text{A.1})$$

We begin by substituting the relation (3.40) into the left hand side of equation (A.1)

$$\begin{aligned} i\hbar\frac{\partial}{\partial t}\Phi(\mathbf{r},t) &= i\hbar\frac{\partial}{\partial t}\left\{e^{-i\mu t/\hbar}[\Phi_0(\mathbf{r}) + u(\mathbf{r})e^{-i\omega t} + v^*(\mathbf{r})e^{i\omega t}]\right\} \\ &= i\hbar e^{-i\mu t/\hbar}\left\{-i\mu/\hbar[\Phi_0(\mathbf{r}) + u(\mathbf{r})e^{-i\omega t} + v^*(\mathbf{r})e^{i\omega t}] \right. \\ &\quad \left. - i\omega u(\mathbf{r})e^{-i\omega t} + i\omega v^*(\mathbf{r})e^{i\omega t}\right\} \end{aligned} \quad (\text{A.2})$$

which leads to Eq. (3.41). We now proceed with the first term of the right hand side of (A.1) which leads to

$$\begin{aligned} \left(-\frac{\hbar^2}{2m}\nabla^2 + V_{\text{trap}}(\mathbf{r})\right)\Phi(\mathbf{r},t) &= e^{-i\mu t/\hbar}\left\{\left(-\frac{\hbar^2}{2m}\nabla^2 + V_{\text{trap}}(\mathbf{r})\right)\Phi_0(\mathbf{r}) \right. \\ &\quad + \left(-\frac{\hbar^2}{2m}\nabla^2 u(\mathbf{r}) + V_{\text{trap}}(\mathbf{r})u(\mathbf{r})\right)e^{-i\omega t} \\ &\quad \left. + \left(-\frac{\hbar^2}{2m}\nabla^2 v^*(\mathbf{r}) + V_{\text{trap}}(\mathbf{r})v^*(\mathbf{r})\right)e^{i\omega t}\right\}. \end{aligned} \quad (\text{A.3})$$

The last term of (A.1), as expressed in Eq. (3.42), could be rewritten as

$$\begin{aligned}
\Phi^*(\mathbf{r}, t) \Phi(\mathbf{r}, t) \Phi(\mathbf{r}, t) &= e^{-i\mu t/\hbar} \left\{ \left[ \Phi_0^*(\mathbf{r}) + u^*(\mathbf{r}) e^{i\omega t} + v(\mathbf{r}) e^{-i\omega t} \right] \right. \\
&\times \left[ \Phi_0(\mathbf{r}) + u(\mathbf{r}) e^{-i\omega t} + v^*(\mathbf{r}) e^{i\omega t} \right] \left[ \Phi_0(\mathbf{r}) + u(\mathbf{r}) e^{-i\omega t} + v^*(\mathbf{r}) e^{i\omega t} \right] \\
&= \Phi_0^*(\mathbf{r}) \Phi_0(\mathbf{r}) \Phi_0(\mathbf{r}) + 2\Phi_0(\mathbf{r}) \left[ u^*(\mathbf{r}) u(\mathbf{r}) + v^*(\mathbf{r}) v(\mathbf{r}) \right] \\
&+ \Phi^*(\mathbf{r}) \left[ v^*(\mathbf{r}) u(\mathbf{r}) + v(\mathbf{r}) u^*(\mathbf{r}) \right] \\
&+ \left[ 2\Phi_0^*(\mathbf{r}) \Phi_0(\mathbf{r}) u(\mathbf{r}) + \Phi_0^2(\mathbf{r}) v(\mathbf{r}) + u^*(\mathbf{r}) u^2(\mathbf{r}) \right. \\
&+ \left. v^*(\mathbf{r}) v^2(\mathbf{r}) + u(\mathbf{r}) v(\mathbf{r}) v^*(\mathbf{r}) \right] e^{-i\omega t} \\
&+ \left[ 2\Phi_0^*(\mathbf{r}) \Phi_0(\mathbf{r}) v^*(\mathbf{r}) + \Phi_0^2(\mathbf{r}) u^*(\mathbf{r}) + v^*(\mathbf{r}) v(\mathbf{r}) u^*(\mathbf{r}) \right. \\
&+ \left. u^*(\mathbf{r}) u(\mathbf{r}) v^*(\mathbf{r}) + v^*(\mathbf{r}) v(\mathbf{r}) u(\mathbf{r}) \right] e^{i\omega t} \\
&+ \left[ 2\Phi_0(\mathbf{r}) u(\mathbf{r}) v(\mathbf{r}) + \Phi_0^*(\mathbf{r}) u^2(\mathbf{r}) \right] e^{-2i\omega t} \\
&+ \left[ 2\Phi_0(\mathbf{r}) u^*(\mathbf{r}) v^*(\mathbf{r}) + \Phi_0^*(\mathbf{r}) v^{*2}(\mathbf{r}) \right] e^{2i\omega t} \\
&+ \left. u^2(\mathbf{r}) v(\mathbf{r}) e^{-3i\omega t} + u^*(\mathbf{r}) v^{*2}(\mathbf{r}) e^{3i\omega t} \right\}. \tag{A.4}
\end{aligned}$$

Keeping only the terms linear (neglecting higher order terms) of  $u(\mathbf{r})$  and  $v(\mathbf{r})$ , and their complex conjugates (A.4) reduces to

$$\begin{aligned}
\Phi^*(\mathbf{r}, t) \Phi(\mathbf{r}, t) \Phi(\mathbf{r}, t) &= e^{-i\mu t/\hbar} \left\{ |\Phi_0(\mathbf{r})|^2 \Phi_0(\mathbf{r}) \right. \\
&+ \left[ 2|\Phi_0(\mathbf{r})|^2 u(\mathbf{r}) + \Phi_0^2(\mathbf{r}) v(\mathbf{r}) \right] e^{-i\omega t} \\
&+ \left. \left[ 2|\Phi_0(\mathbf{r})|^2 v^*(\mathbf{r}) + \Phi_0^2(\mathbf{r}) u^*(\mathbf{r}) \right] e^{i\omega t} \right\}. \tag{A.5}
\end{aligned}$$

Now upon equating the right hand side of (A.2) with those of (A.4) and (A.5), the common factor  $e^{-i\mu t/\hbar}$  cancels out. Then collecting terms without  $e^{-i\omega t}$  and  $e^{i\omega t}$ , we obtain the GPE for the ground state as given in Eq. (3.39). Finally equating the remaining terms by putting those having  $e^{-i\omega t}$  as a factor in one, and those with  $e^{i\omega t}$  on the other (and taking of course the complex conjugate of the later) results in the required Bogoliubov-de Gennes equations as shown in Eq. (3.43).

# Appendix B

## Derivation of Master Equation for the NDPO

Here we show in detail the derivation of the master equation of a non-degenerate parametric oscillator coupled with two uncorrelated squeezed vacuum reservoirs.

A system coupled to two uncorrelated reservoirs (any interactions between them are neglected) could be in general described by the total Hamiltonian, in the interaction picture, as

$$\hat{H} = \hat{H}_S + \hat{H}_{SR} \quad (\text{B.1})$$

where  $\hat{H}_S$  describes the interaction within the system and its interaction with some other systems, and  $\hat{H}_{SR}$  describes the interaction between the system and the reservoirs. The equation of evolution of the density operator of the system and the reservoirs is given by

$$\frac{d\hat{\chi}(t)}{dt} = \frac{1}{i\hbar} \left[ \hat{H}_S(t) + \hat{H}_{SR}(t), \hat{\chi}(t) \right]. \quad (\text{B.2})$$

Since we are interested in the quantum dynamics of the system alone, we trace the total density to get the density operator of the system as

$$\hat{\rho}(t) = \text{Tr}_R \hat{\chi}(t) = \text{Tr}_R \hat{R}(t) \otimes \hat{\rho}(t), \quad (\text{B.3})$$

where  $\text{Tr}_R$  is the trace with respect to the reservoir mode density operator  $\hat{R}$ . The system density (B.3) operator in view of (B.2) involves as

$$\frac{d\hat{\rho}(t)}{dt} = \frac{1}{i\hbar} \left( \text{Tr}_R \left[ \hat{H}_S(t), \hat{\chi}(t) \right] + \text{Tr}_R \left[ \hat{H}_{SR}(t), \hat{\chi}(t) \right] \right) \quad (\text{B.4})$$

Here (B.2) is a first order equation and its formal solution is expressible as

$$\begin{aligned}\hat{\chi}(t) &= \hat{\chi}(0) + \frac{1}{i\hbar} \int_0^t dt' \left[ \hat{H}_S(t') + \hat{H}_{SR}(t'), \hat{\chi}(t') \right]. \\ &= \hat{\chi}(0) + \frac{1}{i\hbar} \int_0^t dt' \left( \left[ \hat{H}_S(t'), \hat{\chi}(t') \right] + \left[ \hat{H}_{SR}(t'), \hat{\chi}(t') \right] \right). \quad (\text{B.5})\end{aligned}$$

Based on this solution (B.5) we proceed to obtain the explicit form of the reduced density evolution (B.4). In other words we want to derive the master equation of an optical system of a two-mode light coupled with two uncorrelated squeezed vacuum reservoirs applying the system-reservoir and the system Hamiltonians described in Eqs. (6.4) and (6.13) respectively. This optical system is considered to be a non-degenerate parametric oscillator that generates signal-idler photons when a strong photon interacts with a nonlinear crystal with in a cavity. These generated signal-idler photons are coupled with two uncorrelated squeezed vacuum reservoir modes via a partially transmitting port mirror as described in Fig. 6.1.

For obtaining the master equation of such a physical system, we use the Markov approximation in which  $\hat{\rho}(t') \rightarrow \hat{\rho}(t)$ , assume that the reservoir density operator remains constant in time ( $\hat{R}(t=0) = \hat{R}(t) = \hat{R}$ ) and the system and the reservoir modes are initially (at  $t=0$ ) uncorrelated, i.e.,

$$\hat{\chi}(0) = \hat{\rho}(0) \otimes \hat{R}(0).$$

On top of that we apply the commutation relation (1.3) and use the cyclic property of the trace:

$$\text{Tr}(\hat{A}\hat{B}\hat{C}) = \text{Tr}(\hat{C}\hat{A}\hat{B}) = \text{Tr}(\hat{B}\hat{C}\hat{A}) \quad (\text{B.6})$$

Based on these relations the time evolution the reduced density opera-

tor (B.4) could be described as

$$\begin{aligned}
\frac{d\hat{\rho}(t)}{dt} &= \frac{1}{i\hbar} [\hat{H}_s(t), \hat{\rho}(t)] + \frac{1}{i\hbar} \text{Tr}_R \left( \hat{H}_{SR}(t) \otimes \hat{\rho}(0) \otimes \hat{R} \right) \\
&- \text{Tr}_R \left( \hat{\rho}(0) \otimes \hat{R} \otimes \hat{H}_{SR}(t) \right) \\
&- \frac{1}{\hbar^2} \int_0^t dt' \text{Tr}_R \left( \left[ \hat{H}_{SR}(t), \hat{H}_{SR}(t') \right] \otimes \hat{\rho}(t') \otimes \hat{R} \right. \\
&- \left. \left[ \hat{H}_{SR}(t), \hat{\rho}(t') \otimes \hat{R} \otimes \hat{H}_{SR}(t') \right] \right) \\
&= \frac{1}{i\hbar} \left( [\hat{H}_s(t), \hat{\rho}(t)] + \langle \hat{H}_{SR}(t) \rangle_R \hat{\rho}(0) - \hat{\rho}(0) \langle \hat{H}_{SR}(t) \rangle_R \right) \\
&- \frac{1}{\hbar^2} \int_0^t dt' \left( \langle \hat{H}_{SR}(t) \otimes \hat{H}_{SR}(t') \rangle_R \hat{\rho}(t) \right. \\
&- \langle \hat{H}_{SR}(t') \otimes \hat{H}_{SR}(t) \rangle_R \hat{\rho}(t) \\
&- \hat{H}_{SR}(t) \otimes \hat{\rho}(t') \otimes \hat{R} \otimes \hat{H}_{SR}(t') \\
&- \left. \hat{\rho}(t') \otimes \hat{R} \otimes \hat{H}_{SR}(t') \otimes \hat{H}_{SR}(t) \right). \tag{B.7}
\end{aligned}$$

Based on the Hamiltonian given in (6.4) that describes the interaction of the system with the squeezed vacuum reservoirs, one gets

$$\begin{aligned}
\langle \hat{H}_{SR}(t) \rangle_R &= \text{Tr}_R (\hat{R} \otimes \hat{H}_{SR}(t)) \\
&= i\hbar \left[ \sum_j \lambda_j \left( \hat{a}^\dagger \langle \hat{A}_j \rangle_R e^{i(\omega_a - \omega_j)t} - \hat{a} \langle \hat{A}_j^\dagger \rangle_R e^{-i(\omega_a - \omega_j)t} \right) \right. \\
&+ \left. \sum_k \lambda_k \left( \hat{b}^\dagger \langle \hat{B}_k \rangle_R e^{i(\omega_b - \omega_k)t} - \hat{b} \langle \hat{B}_k^\dagger \rangle_R e^{-i(\omega_b - \omega_k)t} \right) \right] \\
&= 0 \tag{B.8}
\end{aligned}$$

since for squeezed vacuum reservoirs, as shown in Appendix (C),

$$\langle \hat{A}_j \rangle_R = \langle \hat{A}_j^\dagger \rangle_R = \langle \hat{B}_j^\dagger \rangle_R = \langle \hat{B}_j \rangle_R = 0. \tag{B.9}$$

In view of this approach, (B.7) reduces to the form

$$\begin{aligned}
\frac{d\hat{\rho}(t)}{dt} &= \frac{1}{i\hbar} \left[ \hat{H}_s(t), \hat{\rho}(t) \right] \\
&- \frac{1}{\hbar^2} \int_0^t dt' \left[ \langle \hat{H}_{SR}(t) \otimes \hat{H}_{SR}(t') \rangle_R \hat{\rho}(t) \right. \\
&- \langle \hat{H}_{SR}(t') \otimes \hat{H}_{SR}(t) \rangle_R \hat{\rho}(t) \\
&- Tr_R(\hat{H}_{SR}(t) \otimes \hat{\rho}(t) \otimes \hat{R} \otimes \hat{H}_{SR}(t')) \\
&\left. + \hat{H}_{SR}(t') \otimes \hat{\rho}(t) \otimes \hat{R} \otimes \hat{H}_{SR}(t) \right]. \tag{B.10}
\end{aligned}$$

In (B.10) we set for convenience that

$$\hat{\Gamma}_1 = \frac{1}{\hbar^2} \int_0^t dt' \langle \hat{H}_{SR}(t) \otimes \hat{H}_{SR}(t') \rangle_R \hat{\rho}(t), \tag{B.11a}$$

$$\hat{\Gamma}_2 = \frac{1}{\hbar^2} \int_0^t dt' \hat{\rho}(t) \langle \hat{H}_{SR}(t') \otimes \hat{H}_{SR}(t) \rangle_R, \tag{B.11b}$$

$$\hat{\Gamma}_3 = \frac{1}{\hbar^2} \int_0^t dt' Tr_R \left( \hat{H}_{SR}(t) \otimes \hat{\rho}(t) \otimes \hat{R} \otimes \hat{H}_{SR}(t') \right), \tag{B.11c}$$

$$\hat{\Gamma}_4 = \frac{1}{\hbar^2} \int_0^t dt' Tr_R \left( \hat{H}_{SR}(t') \otimes \hat{\rho}(t) \otimes \hat{R} \otimes \hat{H}_{SR}(t) \right). \tag{B.11d}$$

This helps us to solve the integrations in (B.10) one by one as shown in the steps below. On account of Eq. (6.4) where the explicit expression for the system-reservoir Hamiltonian is used, we get that

$$\begin{aligned}
\hat{H}_{SR}(t) \otimes \hat{H}_{SR}(t') &= -\hbar^2 \left[ \sum_j \lambda_j \left( \hat{a}^\dagger \hat{A}_j e^{i(\omega_a - \omega_j)t} - \hat{a} \hat{A}_j^\dagger e^{-i(\omega_a - \omega_j)t} \right) \right. \\
&+ \sum_k \lambda_k \left( \hat{b}^\dagger \hat{B}_k e^{i(\omega_b - \omega_k)t} - \hat{b} \hat{B}_k^\dagger e^{-i(\omega_b - \omega_k)t} \right) \left. \right] \\
&\otimes \left[ \sum_l \lambda_l \left( \hat{a}^\dagger \hat{A}_l e^{i(\omega_a - \omega_l)t'} - \hat{a} \hat{A}_l^\dagger e^{-i(\omega_a - \omega_l)t'} \right) \right. \\
&\left. + \sum_m \lambda_m \left( \hat{b}^\dagger \hat{B}_m e^{i(\omega_b - \omega_m)t'} - \hat{b} \hat{B}_m^\dagger e^{-i(\omega_b - \omega_m)t'} \right) \right]. \tag{B.12}
\end{aligned}$$

Expanding (B.12) and taking the trace over the reservoir operators only leads

to

$$\begin{aligned}
\langle \hat{H}_{SR}(t) \otimes \hat{H}_{SR}(t') \rangle_R = & - \hbar^2 \left[ \sum_{j,l} \lambda_j \lambda_l \left( \hat{a}^{\dagger 2} \langle \hat{A}_j \hat{A}_l \rangle_R e^{i(\omega_a - \omega_j)t + i(\omega_a - \omega_l)t'} \right. \right. \\
& - \hat{a}^\dagger \hat{a} \langle \hat{A}_j \hat{A}_l^\dagger \rangle_R e^{i(\omega_a - \omega_j)t - i(\omega_a - \omega_l)t'} \Big) \\
& - \sum_{j,m} \lambda_j \lambda_m \left( \hat{a}^\dagger \hat{b}^\dagger \langle \hat{A}_j \hat{B}_m \rangle_R e^{i(\omega_a - \omega_j)t + i(\omega_b - \omega_m)t'} \right. \\
& - \hat{a}^\dagger \hat{b} \langle \hat{A}_j \hat{B}_m^\dagger \rangle_R e^{i(\omega_a - \omega_j)t - i(\omega_b - \omega_m)t'} \Big) \\
& + \sum_{j,l} \lambda_j \lambda_l \left( \hat{a} \hat{a}^\dagger \langle \hat{A}_j \hat{A}_l \rangle_R e^{-i(\omega_a - \omega_j)t + i(\omega_a - \omega_l)t'} \right. \\
& - \hat{a}^2 \langle \hat{A}_j \hat{A}_l^\dagger \rangle_R e^{-i(\omega_a - \omega_j)t - i(\omega_a - \omega_l)t'} \Big) \\
& + \sum_{j,m} \lambda_j \lambda_m \left( \hat{a} \hat{b}^\dagger \langle \hat{A}_j \hat{B}_m \rangle_R e^{-i(\omega_a - \omega_j)t + i(\omega_b - \omega_m)t'} \right. \\
& - \hat{a} \hat{b} \langle \hat{A}_j \hat{B}_m^\dagger \rangle_R e^{-i(\omega_a - \omega_j)t - i(\omega_b - \omega_m)t'} \Big) \\
& - \sum_{k,l} \lambda_k \lambda_l \left( \hat{b}^\dagger \hat{a}^\dagger \langle \hat{B}_k \hat{A}_l \rangle_R e^{i(\omega_b - \omega_k)t + i(\omega_b - \omega_l)t'} \right. \\
& - \hat{b}^\dagger \hat{a} \langle \hat{B}_k \hat{A}_l^\dagger \rangle_R e^{i(\omega_b - \omega_k)t - i(\omega_a - \omega_l)t'} \Big) \\
& - \sum_{k,m} \lambda_k \lambda_m \left( \hat{b}^{\dagger 2} \langle \hat{B}_k \hat{B}_m \rangle_R e^{i(\omega_b - \omega_k)t + i(\omega_b - \omega_m)t'} \right. \\
& - \hat{b}^\dagger \hat{b} \langle \hat{B}_k \hat{B}_m^\dagger \rangle_R e^{i(\omega_b - \omega_k)t - i(\omega_b - \omega_m)t'} \Big) \\
& + \sum_{k,l} \lambda_k \lambda_l \left( \hat{b} \hat{a}^\dagger \langle \hat{B}_k \hat{A}_l \rangle_R e^{-i(\omega_b - \omega_k)t + i(\omega_a - \omega_l)t'} \right. \\
& - \hat{b} \hat{a} \langle \hat{B}_k \hat{A}_l^\dagger \rangle_R e^{-i(\omega_b - \omega_k)t - i(\omega_a - \omega_l)t'} \Big) \\
& + \sum_{k,m} \lambda_k \lambda_m \left( \hat{b} \hat{b}^\dagger \langle \hat{B}_k \hat{B}_m \rangle_R e^{-i(\omega_b - \omega_k)t + i(\omega_b - \omega_m)t'} \right. \\
& \left. \left. - \hat{b}^2 \langle \hat{B}_k \hat{B}_m^\dagger \rangle_R e^{-i(\omega_b - \omega_k)t - i(\omega_b - \omega_m)t'} \right) \right]. \quad (\text{B.13})
\end{aligned}$$

Based on the derivations given in Appendix C, the different expectation values associated with the two squeezed vacuum reservoir modes are expressible

as follows:

$$\langle \hat{A}_j \hat{A}_l \rangle_R = -M_A \delta_{l,2j_a-j}, \quad (\text{B.14a})$$

$$\langle \hat{B}_k \hat{B}_m \rangle_R = -M_B \delta_{m,2k_b-k}, \quad (\text{B.14b})$$

$$\langle \hat{A}_j^\dagger \hat{A}_l \rangle_R = N_A \delta_{j,l}, \quad (\text{B.14c})$$

$$\langle \hat{B}_k^\dagger \hat{B}_m \rangle_R = N_B \delta_{k,m}, \quad (\text{B.14d})$$

$$\langle \hat{A}_j \hat{A}_l^\dagger \rangle_R = (N_A + 1) \delta_{j,l}, \quad (\text{B.14e})$$

$$\langle \hat{B}_k \hat{B}_m^\dagger \rangle_R = (N_B + 1) \delta_{k,m}, \quad (\text{B.14f})$$

$$\langle \hat{A}_j \hat{B}_m \rangle_R = \langle \hat{A}_j \hat{B}_m^\dagger \rangle_R = \langle \hat{A}_j^\dagger \hat{B}_m \rangle_R = 0, \quad (\text{B.14g})$$

On account of these equations (B.14), (B.13) can be further expressed as

$$\begin{aligned} \langle \hat{H}_{SR}(t) \hat{H}_{SR}(t') \rangle_R = & - \hbar^2 \left[ \sum_{j,l} \lambda_j \lambda_l \left( - M_A \delta_{l,2j_a-j} e^{i(\omega_a - \omega_j)t + i(\omega_a - \omega_l)t'} \hat{a}^{\dagger 2} \right. \right. \\ & - (N_A + 1) \delta_{j,l} e^{i(\omega_a - \omega_j)t - i(\omega_a - \omega_l)t'} \hat{a}^\dagger \hat{a} \\ & - N_A \delta_{j,l} e^{-i(\omega_a - \omega_j)t + i(\omega_a - \omega_l)t'} \hat{a} \hat{a}^\dagger \\ & - M_A \delta_{l,2j_a-j} e^{-i(\omega_a - \omega_j)t - i(\omega_a - \omega_l)t'} \hat{a}^2 \left. \right) \\ & + \sum_{k,m} \lambda_k \lambda_m \left( - M_B \delta_{m,2k_b-k} e^{i(\omega_b - \omega_k)t + i(\omega_b - \omega_m)t'} \hat{b}^{\dagger 2} \right. \\ & - (N_B + 1) \delta_{k,m} e^{i(\omega_b - \omega_k)t - i(\omega_b - \omega_m)t'} \hat{b}^\dagger \hat{b} \\ & - N_B \delta_{k,m} e^{-i(\omega_b - \omega_k)t + i(\omega_b - \omega_m)t'} \hat{b} \hat{b}^\dagger \\ & \left. \left. - M_B \delta_{m,2k_b-k} e^{-i(\omega_b - \omega_k)t - i(\omega_b - \omega_m)t'} \hat{b}^2 \right) \right]. \quad (\text{B.15}) \end{aligned}$$

Now applying the properties of the Kronecker delta symbol defined as

$$\delta_{n,m} = \begin{cases} 1 & \text{for } n = m, \\ 0 & \text{for } n \neq m, \end{cases} \quad (\text{B.16})$$

into (B.15), one obtains

$$\begin{aligned}
\langle \hat{H}_{SR}(t) \hat{H}_{SR}(t') \rangle_R &= \hbar^2 \left[ \sum_j \left( \lambda_j \lambda_{2j_a-j} M_A e^{i(\omega_a-\omega_j)t+i(\omega_a-\omega_{2j_a-j})t'} \hat{a}^{\dagger 2} \right. \right. \\
&+ \lambda_j^2 (N_A + 1) e^{i(\omega_a-\omega_j)(t-t')} \hat{a}^{\dagger} \hat{a} \\
&+ \lambda_j^2 N_A e^{-i(\omega_a-\omega_j)(t-t')} \hat{a} \hat{a}^{\dagger} \\
&+ \lambda_j \lambda_{2j_a-j} M_A e^{-i(\omega_a-\omega_j)t-i(\omega_a-\omega_{2j_a-j})t'} \hat{a}^2 \left. \right) \\
&+ \sum_k \left( \lambda_k \lambda_{2k_b-k} M_B e^{i(\omega_b-\omega_k)t+i(\omega_b-\omega_{2k_b-k})t'} \hat{b}^{\dagger 2} \right. \\
&+ \lambda_k^2 (N_B + 1) e^{i(\omega_b-\omega_k)(t-t')} \hat{b}^{\dagger} \hat{b} \\
&+ \lambda_k^2 N_B e^{-i(\omega_b-\omega_k)(t-t')} \hat{b} \hat{b}^{\dagger} \\
&+ \left. \left. \lambda_k \lambda_{2k_b-k} M_B e^{-i(\omega_b-\omega_k)t-i(\omega_b-\omega_{2k_b-k})t'} \hat{b}^2 \right) \right]. \quad (\text{B.17})
\end{aligned}$$

At this level, (B.11a) can be written as

$$\begin{aligned}
\hat{\Gamma}_1 &= - (I_{1a} M_A \hat{a}^{\dagger 2} + I_{2a} (N_A + 1) \hat{a}^{\dagger} \hat{a} \\
&+ I_{3a} N_A \hat{a} \hat{a}^{\dagger} + I_{4a} M_A \hat{a}^2) \hat{\rho}(t) \\
&- (I_{1b} M_B \hat{b}^{\dagger 2} + I_{2b} (N_B + 1) \hat{b}^{\dagger} \hat{b} \\
&+ I_{3b} N_B \hat{b} \hat{b}^{\dagger} + I_{4b} M_B \hat{b}^2) \hat{\rho}(t) \quad (\text{B.18})
\end{aligned}$$

where we have set

$$I_{1a} = \int_0^t dt' \sum_j \lambda_j \lambda_{2j_a-j} e^{i(\omega_a-\omega_j)t+i(\omega_a-\omega_{2j_a-j})t'}, \quad (\text{B.19a})$$

$$I_{2a} = \int_0^t dt' \sum_j \lambda_j^2 e^{i(\omega_a-\omega_j)(t-t')}, \quad (\text{B.19b})$$

$$I_{3a} = \int_0^t dt' \sum_j \lambda_j^2 e^{-i(\omega_a-\omega_j)(t-t')}, \quad (\text{B.19c})$$

$$I_{4a} = \int_0^t dt' \sum_j \lambda_j \lambda_{2j_a-j} e^{-i(\omega_a-\omega_j)t-i(\omega_a-\omega_{2j_a-j})t'}, \quad (\text{B.19d})$$

with similar expressions for  $I_{1b}$ ,  $I_{2b}$ ,  $I_{3b}$  and  $I_{4b}$ . Upon introducing the density

of states  $g(\omega)$ , in which

$$\sum_j \lambda_j \lambda_{2j_a - j} \rightarrow \int_0^\infty d\omega g(\omega) \lambda(\omega) \lambda(2\omega_a - \omega), \quad (\text{B.20})$$

we get

$$I_{1a} = \int_0^\infty d\omega g(\omega) \lambda(\omega) \lambda(2\omega_a - \omega) \int_0^t dt' e^{i(\omega_a - \omega)(t - t')}, \quad (\text{B.21a})$$

$$I_{2a} = \int_0^\infty d\omega g(\omega) \lambda^2(\omega) \int_0^t dt' e^{i(\omega_a - \omega)(t - t')}, \quad (\text{B.21b})$$

$$I_{3a} = \int_0^\infty d\omega g(\omega) \lambda^2(\omega) \int_0^t dt' e^{-i(\omega_a - \omega)(t - t')}, \quad (\text{B.21c})$$

$$I_{4a} = \int_0^\infty d\omega g(\omega) \lambda(\omega) \lambda(2\omega_a - \omega) \int_0^t dt' e^{-i(\omega_a - \omega)(t - t')}. \quad (\text{B.21d})$$

Furthermore, setting  $t - t' = \tau$ , we see that

$$\int_0^t dt' e^{\pm i(\omega_a - \omega)(t - t')} = \int_0^t d\tau e^{\pm i(\omega_a - \omega)\tau}. \quad (\text{B.22})$$

Since the exponential function is a rapidly decaying function of time, the upper limit of integration can be extended to infinity. Thus making use of the approximation

$$\frac{1}{\pi} \int_0^\infty e^{\pm i(\omega_a - \omega)\tau} \approx \delta(\omega_a - \omega) \quad (\text{B.23})$$

one finds

$$I_{1a} = \int_0^\infty d\omega g(\omega) \lambda(\omega) \lambda(2\omega_a - \omega) \pi \delta(\omega_a - \omega), \quad (\text{B.24})$$

and applying the property of the Dirac delta function we obtain

$$I_{1a} = \pi g(\omega_a) \lambda^2(\omega_a) = \frac{\gamma_A}{2}, \quad (\text{B.25})$$

where  $\gamma_A = 2\pi g(\omega_a) \lambda^2(\omega_a)$  is the cavity damping rate for mode  $A$ . It is easy to check that

$$I_{1a} = I_{2a} = I_{3a} = I_{4a} = \frac{\gamma_A}{2}. \quad (\text{B.26})$$

Similarly, one can also show that

$$I_{1b} = I_{2b} = I_{3b} = I_{4b} = \frac{\gamma_B}{2}, \quad (\text{B.27})$$

in which  $\gamma_B = 2\pi g(\omega_b)\lambda^2(\omega_b)$  is the cavity damping rate for mode  $B$ . Substituting (B.26) and (B.27) into (B.18), we have

$$\begin{aligned} \hat{\Gamma}_1 = & - \frac{\gamma_A}{2} (M_A \hat{a}^{\dagger 2} + (N_A + 1) \hat{a}^\dagger \hat{a} + N_A \hat{a} \hat{a}^\dagger + M_A \hat{a}^2) \hat{\rho}(t) \\ & - \frac{\gamma_B}{2} (M_B \hat{b}^{\dagger 2} + (N_B + 1) \hat{b}^\dagger \hat{b} + N_B \hat{b} \hat{b}^\dagger + M_B \hat{b}^2) \hat{\rho}(t). \end{aligned} \quad (\text{B.28})$$

Moreover, using the fact that

$$\int_0^t dt' \hat{H}_{SR}(t) \hat{H}_{SR}(t') = \int_0^t dt' \hat{H}_{SR}(t') \hat{H}_{SR}(t), \quad (\text{B.29})$$

one readily gets the result

$$\begin{aligned} \hat{\Gamma}_2 = & - \frac{\gamma_A}{2} \hat{\rho}(t) (M_A \hat{a}^{\dagger 2} + (N_A + 1) \hat{a}^\dagger \hat{a} + N_A \hat{a} \hat{a}^\dagger + M_A \hat{a}^2) \\ & - \frac{\gamma_B}{2} \hat{\rho}(t) (M_B \hat{b}^{\dagger 2} + (N_B + 1) \hat{b}^\dagger \hat{b} + N_B \hat{b} \hat{b}^\dagger + M_B \hat{b}^2). \end{aligned} \quad (\text{B.30})$$

Applying once more Eq. (6.4), expression (B.11c) can be rewritten as

$$\begin{aligned} \hat{\Gamma}_3 = & - \int_0^t dt' \text{Tr}_R \left[ \sum_j \lambda_j \left( \hat{a}^\dagger \hat{A}_j e^{i(\omega_a - \omega_j)t} - \hat{a} \hat{A}_j^\dagger e^{-i(\omega_a - \omega_j)t} \right) \right. \\ & + \sum_k \lambda_k \left( \hat{b}^\dagger \hat{B}_k e^{i(\omega_b - \omega_k)t} - \hat{b} \hat{B}_k^\dagger e^{-i(\omega_b - \omega_k)t} \right) \left. \right] \hat{\rho}(t) \hat{R} \\ & \otimes \left[ \sum_l \lambda_l \left( \hat{a}^\dagger \hat{A}_l e^{i(\omega_a - \omega_l)t'} - \hat{a} \hat{A}_l^\dagger e^{-i(\omega_a - \omega_l)t'} \right) \right. \\ & \left. + \sum_m \lambda_m \left( \hat{b}^\dagger \hat{B}_m e^{i(\omega_b - \omega_m)t'} - \hat{b} \hat{B}_m^\dagger e^{-i(\omega_b - \omega_m)t'} \right) \right], \end{aligned} \quad (\text{B.31})$$

from which follows

$$\begin{aligned}
\hat{\Gamma}_3 = & - \int_0^t dt' Tr_R \left[ \sum_{j,l} \lambda_j \lambda_l \left( \hat{a}^\dagger \hat{\rho}(t) \hat{a}^\dagger \hat{A}_j \hat{R} \hat{A}_l e^{i(\omega_a - \omega_j)t + i(\omega_a - \omega_l)t'} \right. \right. \\
& - \hat{a}^\dagger \hat{\rho}(t) \hat{a} \hat{A}_j \hat{R} \hat{A}_l^\dagger e^{i(\omega_a - \omega_j)t - i(\omega_a - \omega_l)t'} \Big) \\
& + \sum_{j,m} \lambda_j \lambda_m \left( \hat{a}^\dagger \hat{\rho}(t) \hat{b}^\dagger \hat{A}_j \hat{R} \hat{B}_m e^{i(\omega_a - \omega_j)t + i(\omega_b - \omega_m)t'} \right. \\
& + \hat{a}^\dagger \hat{\rho}(t) \hat{b} \hat{A}_j \hat{R} \hat{B}_m^\dagger e^{i(\omega_a - \omega_j)t - i(\omega_b - \omega_m)t'} \Big) \\
& - \sum_{j,l} \lambda_j \lambda_l \left( \hat{a} \hat{\rho}(t) \hat{a}^\dagger \hat{A}_j^\dagger \hat{R} \hat{A}_l e^{-i(\omega_a - \omega_j)t + i(\omega_a - \omega_l)t'} \right. \\
& - \hat{a} \hat{\rho}(t) \hat{a} \hat{A}_j^\dagger \hat{R} \hat{A}_l^\dagger e^{-i(\omega_a - \omega_j)t - i(\omega_a - \omega_l)t'} \Big) \\
& - \sum_{j,m} \lambda_j \lambda_m \left( \hat{a} \hat{\rho}(t) \hat{b}^\dagger \hat{A}_j^\dagger \hat{R} \hat{B}_m e^{-i(\omega_a - \omega_j)t + i(\omega_b - \omega_m)t'} \right. \\
& - \hat{a} \hat{\rho}(t) \hat{b} \hat{A}_j^\dagger \hat{R} \hat{B}_m^\dagger e^{-i(\omega_a - \omega_j)t - i(\omega_b - \omega_m)t'} \Big) \\
& + \sum_{k,l} \lambda_k \lambda_l \left( \hat{b}^\dagger \hat{\rho}(t) \hat{a}^\dagger \hat{B}_k \hat{R} \hat{A}_l e^{i(\omega_b - \omega_k)t + i(\omega_b - \omega_l)t'} \right. \\
& - \hat{b}^\dagger \hat{\rho}(t) \hat{a} \hat{B}_k \hat{R} \hat{A}_l^\dagger e^{i(\omega_b - \omega_k)t - i(\omega_a - \omega_l)t'} \Big) \\
& + \sum_{k,m} \lambda_k \lambda_m \left( \hat{b}^\dagger \hat{\rho}(t) \hat{b}^\dagger \hat{B}_k \hat{R} \hat{B}_m e^{i(\omega_b - \omega_k)t + i(\omega_b - \omega_m)t'} \right. \\
& - \hat{b}^\dagger \hat{\rho}(t) \hat{b} \hat{B}_k \hat{R} \hat{B}_m^\dagger e^{i(\omega_b - \omega_k)t - i(\omega_b - \omega_m)t'} \Big) \\
& - \sum_{k,l} \lambda_k \lambda_l \left( \hat{b} \hat{\rho}(t) \hat{a}^\dagger \hat{B}_k^\dagger \hat{R} \hat{A}_l e^{-i(\omega_b - \omega_k)t + i(\omega_a - \omega_l)t'} \right. \\
& - \hat{b} \hat{\rho}(t) \hat{a} \hat{B}_k^\dagger \hat{R} \hat{A}_l^\dagger e^{-i(\omega_b - \omega_k)t - i(\omega_a - \omega_l)t'} \Big) \\
& - \sum_{k,m} \lambda_k \lambda_m \left( \hat{b} \hat{\rho}(t) \hat{b}^\dagger \hat{B}_k^\dagger \hat{R} \hat{B}_m e^{-i(\omega_b - \omega_k)t + i(\omega_b - \omega_m)t'} \right. \\
& \left. \left. - \hat{b} \hat{\rho}(t) \hat{b} \hat{B}_k^\dagger \hat{R} \hat{B}_m^\dagger e^{-i(\omega_b - \omega_k)t - i(\omega_b - \omega_m)t'} \right) \right]. \tag{B.32}
\end{aligned}$$

Applying the cyclic property of the trace and making use of relations (B.14),

(B.16) and (B.21), expression (B.32) takes the form

$$\begin{aligned}
\hat{\Gamma}_3 = & - \left[ I_{1a} M_A \hat{a}^\dagger \hat{\rho}(t) \hat{a}^\dagger + I_{2a} (N_A + 1) \hat{a}^\dagger \hat{\rho}(t) \hat{a} \right. \\
& + \left. I_{3a} N_A \hat{a} \hat{\rho}(t) \hat{a}^\dagger + I_{4a} M_A \hat{a} \hat{\rho}(t) \hat{a} \right] \\
& - \left[ I_{1b} M_B \hat{b}^\dagger \hat{\rho}(t) \hat{b}^\dagger + I_{2b} (N_B + 1) \hat{b}^\dagger \hat{\rho}(t) \hat{b} \right. \\
& + \left. I_{3b} N_B \hat{b} \hat{\rho}(t) \hat{b}^\dagger + I_{4b} M_B \hat{b} \hat{\rho}(t) \hat{b} \right]
\end{aligned} \tag{B.33}$$

so that, in view of (B.26) and (B.27), we have

$$\begin{aligned}
\hat{\Gamma}_3 = & - \frac{\gamma_A}{2} \left( M_A \hat{a}^\dagger \hat{\rho}(t) \hat{a}^\dagger + (N_A + 1) \hat{a}^\dagger \hat{\rho}(t) \hat{a} \right. \\
& + \left. N_A \hat{a} \hat{\rho}(t) \hat{a}^\dagger + M_A \hat{a} \hat{\rho}(t) \hat{a} \right) \\
& - \frac{\gamma_B}{2} \left( M_B \hat{b}^\dagger \hat{\rho}(t) \hat{b}^\dagger + (N_B + 1) \hat{b}^\dagger \hat{\rho}(t) \hat{b} \right. \\
& + \left. N_B \hat{b} \hat{\rho}(t) \hat{b}^\dagger + M_B \hat{b} \hat{\rho}(t) \hat{b} \right).
\end{aligned} \tag{B.34}$$

Similarly, one can easily establish that

$$\begin{aligned}
\hat{\Gamma}_4 = & - \frac{\gamma_A}{2} \left( M_A \hat{a}^\dagger \hat{\rho}(t) \hat{a}^\dagger + (N_A + 1) \hat{a}^\dagger \hat{\rho}(t) \hat{a} \right. \\
& + \left. N_A \hat{a} \hat{\rho}(t) \hat{a}^\dagger + M_A \hat{a} \hat{\rho}(t) \hat{a} \right) \\
& - \frac{\gamma_B}{2} \left( M_B \hat{b}^\dagger \hat{\rho}(t) \hat{b}^\dagger + (N_B + 1) \hat{b}^\dagger \hat{\rho}(t) \hat{b} \right. \\
& + \left. N_B \hat{b} \hat{\rho}(t) \hat{b}^\dagger + M_B \hat{b} \hat{\rho}(t) \hat{b} \right).
\end{aligned} \tag{B.35}$$

Now combining expressions (B.28), (B.30), (B.34) and (B.35) we arrive at the required master equation which is already given on page 68 by Eq. (6.15).



# Appendix C

## Expectation Values of Squeezed Vacuum Reservoir Modes

In this Appendix we derive the expectation values of squeezed vacuum reservoir modes in a detail way. This enables us understand clearly the calculations of the fluctuations associated with squeezed states of light. For this purpose we consider the optical system described in Fig. 6.1 in which two uncorrelated squeezed vacuum modes are coupled with the NDPO via the mirror from the right side of the cavity through which light is assumed to enter or leave in a single direction.

A squeezed light of single reservoir mode  $k$  can be described by the squeeze operator  $\hat{S}_k(\xi)$  as

$$\hat{S}_k(\xi) = \exp\left(-\frac{\xi}{2}\hat{A}_k^{\dagger 2} + \frac{\xi^*}{2}\hat{A}_k^2\right), \quad (\text{C.1})$$

where  $\xi$  an arbitrary complex number and  $\hat{A}_k/\hat{A}_k^\dagger$  are the annihilation/creation photonic operators of the squeezed vacuum state. Using (C.1) along with the squeezed vacuum state

$$|\xi\rangle = \hat{S}_k(\xi)|0\rangle, \quad (\text{C.2})$$

the density operator of the squeezed vacuum could be expressed as

$$\hat{\rho}_k(r) = \hat{S}_k(r)|0_k\rangle\langle 0_k|\hat{S}_k^\dagger(r), \quad (\text{C.3})$$

where in this case  $r$  is the squeezing parameter as described before in Sec. 6.3 and is replacing  $\xi$  in the squeeze operator (C.1). Introducing the operator defined by

$$\hat{A}_k(r) = \hat{S}_k^\dagger(r)\hat{A}_k\hat{S}_k(r), \quad (\text{C.4})$$

we proceed to look for its expectation value as

$$\langle \hat{A}_k(r) \rangle = Tr \hat{\rho}_k \hat{A}_k(r) = \langle 0_k | \hat{A}_k(r) | 0_k \rangle. \quad (\text{C.5})$$

Applying (C.4) it is possible to express

$$\frac{d\hat{A}_k(r)}{dr} = -\frac{1}{2} [\hat{A}_k(r), \hat{A}_k^{\dagger 2}(r)] = -\hat{A}_k^{\dagger}(r) \quad (\text{C.6})$$

and

$$\frac{d\hat{A}_k^{\dagger}(r)}{dr} = -\hat{A}_k(r). \quad (\text{C.7})$$

In view of (C.6) and (C.7) we get

$$\frac{d^2\hat{A}_k^{\dagger}(r)}{d^2r} = \hat{A}_k(r). \quad (\text{C.8})$$

The solution of (C.8) could be expressed as

$$\hat{A}_k(r) = \hat{c}_1 e^r + \hat{c}_2 e^{-r} \quad (\text{C.9})$$

which leads to

$$\hat{A}_k(r=0) = \hat{c}_1 + \hat{c}_2 = \hat{A}_k \quad (\text{C.10})$$

and

$$\left. \frac{d\hat{A}_k(r)}{dr} \right|_{r=0} = \hat{c}_1 - \hat{c}_2 = \hat{A}_k^{\dagger}. \quad (\text{C.11})$$

Combining (C.10) and (C.11) we obtain that

$$\hat{c}_1 = \frac{1}{2}(\hat{A} + \hat{A}^{\dagger}) \quad (\text{C.12})$$

and

$$\hat{c}_2 = \frac{1}{2}(\hat{A} - \hat{A}^{\dagger}). \quad (\text{C.13})$$

Substituting expressions (C.12) and (C.13) into (C.9) we arrive at

$$\hat{A}_k(r) = \hat{A}_k \cosh r - \hat{A}_k^{\dagger} \sinh r. \quad (\text{C.14})$$

Now making use of (C.14) in (C.5), the expectation value of the operator  $\hat{A}_k(r)$  turns out to

$$\begin{aligned} \langle \hat{A}_k(r) \rangle &= \langle 0_k | \hat{A}_k \cosh r - \hat{A}_k^{\dagger} \sinh r | 0_k \rangle \\ &= \langle 0_k | \hat{A}_k | 0_k \rangle \cosh r - \langle 0_k | \hat{A}_k^{\dagger} | 0_k \rangle \sinh r \\ &= 0 \end{aligned} \quad (\text{C.15})$$

as  $\langle 0_k | \hat{A}_k^{\dagger}(r) | 0_k \rangle = \langle 0_k | \hat{A}_k | 0_k \rangle = 0$ .

We want now to determine the expectation value of the photon number  $\hat{A}_k^{\dagger}(r) \hat{A}_k(r)$  and other related averages of the squeezed vacuum reservoir

modes. Since the reservoir modes are considered to be uncorrelated with each other, we see that, for  $k \neq k'$

$$\langle \hat{A}_k^\dagger(r) \hat{A}_{k'}(r) \rangle = \langle \hat{A}_k^\dagger(r) \rangle \langle \hat{A}_{k'}(r) \rangle = 0. \quad (\text{C.16})$$

However for  $j = j'$ , one can obtain that

$$\langle \hat{A}_k^\dagger(r) \hat{A}_{k'}(r) \rangle = \langle \hat{A}_k^\dagger(r) \hat{A}_k(r) \rangle = \langle 0_k | \hat{A}_k^\dagger(r) \hat{A}_k(r) | 0_k \rangle. \quad (\text{C.17})$$

At this stage inserting (C.14) into (C.17), we get

$$\begin{aligned} \langle \hat{A}_k^\dagger(r) \hat{A}_k(r) \rangle &= \langle 0_k | \left[ \hat{A}_k^\dagger \hat{A}_k \cosh^2 r + \hat{A}_k \hat{A}_k^\dagger \sinh^2 r \right. \\ &\quad \left. - \cosh r \sinh r \left( \hat{A}_k^\dagger \hat{A}_k^\dagger + \hat{A}_k \hat{A}_k \right) \right] | 0_k \rangle. \end{aligned} \quad (\text{C.18})$$

Applying (6.51), it is a direct forward to show that  $\langle \hat{A}_k \hat{A}_k \rangle = \langle \hat{A}_k^\dagger \hat{A}_k^\dagger \rangle = 0$ . Assuming that the photonic operators satisfy the commutation relation

$$[\hat{A}_k, \hat{A}_{k'}^\dagger] = \delta_{k,k'} \quad (\text{C.19})$$

and using the identities  $\hat{A}_k \hat{A}_k^\dagger = 1 + \hat{A}_k^\dagger \hat{A}_k$ ,  $\cosh^2 r + \sinh^2 r = 0$  and  $\cosh^2 r - \sinh^2 r = 1$ , we arrive at the general expression for the expectation value or simply the mean photon number for the squeezed vacuum reservoir:

$$\langle \hat{A}_k^\dagger(r) \hat{A}_k(r) \rangle = \sinh^2 r \delta_{j,j'} = N(r) \delta_{k,k'} = N \delta_{k,k'}, \quad (\text{C.20})$$

where

$$N(r) = N = \sinh^2 r. \quad (\text{C.21})$$

In view of (C.19) and (C.20) one can easily express

$$\langle \hat{A}_k(r) \hat{A}_{k'}^\dagger(r) \rangle = (N(r) + 1) \delta_{k,k'} = \cosh^2 r \delta_{k,k'}. \quad (\text{C.22})$$

A similar approach leads to

$$\langle \hat{A}_k(r) \hat{A}_{k'}(r) \rangle = -M(r) \delta_{k,k'}, \quad (\text{C.23})$$

where

$$M(r) = \cosh r \sinh r e^{i\varphi} = |M(r)| e^{i\varphi} \quad (\text{C.24})$$

and

$$|M(r)| = M = \sqrt{N(N+1)} \quad (\text{C.25})$$

characterizes the phase of the squeezed vacuum reservoir mode via the phase of the squeezed state  $\varphi$  which could be taken to be zero for pure squeezed states [12].

Note that in order to apply (C.23) in the derivation of the master equation (Appendix B), the wave vector  $k$  associated with the Kronecker delta,  $\delta_{k,k'}$ , should be approximated by a valid expression. Assuming that  $k \sim k_0$ , where  $k_0$  is the central wave number of the reservoir mode we can express  $k \approx 2k_0 - k$  which leads (C.23) to

$$\langle \hat{A}_k(r) \hat{A}_{k'}(r) \rangle = -M(r) \delta_{2k_0 - k, k'}. \quad (\text{C.26})$$

In addition it is important to stress that the results given by the expressions (C.15), (C.20) and (C.26) are valid when the squeezed vacuum reservoir mode is coupled to the system or is incident on it only from one direction. When it is incident on the system from different directions one needs to replace  $k$ ,  $k_0$ ,  $k'$  by their corresponding vectors  $\mathbf{k}$ ,  $\mathbf{k}_0$  and  $\mathbf{k}'$ .

# Appendix D

## Acknowledgements

First and foremost, I would like to express my heartfelt thanks and gratitude to my supervisor Prof. Dr. Maciej Lewenstein for his excellent, sustainable and enthusiastic supervision. I would like also to express the same, to my Co-advisor Prof. Dr. Anna Sanpera. Specially Prof. Sanpera has taught me all the numerics and she has been helping me continuously all along. The two were not only my mentors in the academia but also were always on my side in many aspects in my everyday life during all my study time. Without their unreserved support and continuous advise I would not have had reached this stage. It was also a golden opportunity for me to be able to join Prof. Lewenstein's group. I have had the chance to participate in several workshops and summer schools all over Europe which has helped me quite a lot in consolidating my knowledge and also my experience in the international forum of scholars. For this and all, I lack words to express my appreciations and thanks to Maciej and Anna but to simply say: "it was extremely cool to work with both of you and study the field of ultracold atomic gases which is one of the coolest fields in physics currently."

Joining Prof. Lewenstein's group has also enabled me to be acquainted with other great persons from whom I have benefited a lot. Prof. Dr. Luis Santos is the next person whom I must have to thank most. I have been getting additional advise from him since the beginning of my study while he was a Postdoc researcher with Prof. Lewenstein. His return as a full professor to the University of Hannover was a great opportunity for me. He has helped me quite a lot particularly in shaping the final form of the Thesis. I am also highly indebted to Prof. Dr. Jan Arlt for his sustainable assistance in elaborating me the experimental aspects associated with my works. I highly appreciate his valuable comments on my Thesis. I am also highly indebted for Dr. Veronica Ahufniger for her sustained cooperation from which I have benefited significantly.

On the course of doing this PhD work, I have had the chance of interacting with many other people who have had one way or the other a contribution to my Thesis: I am highly indebted to my friends and colleagues Dr. Philip Hyllus, Dr. Henning Fehrmann, Dr. Helge Kreuzmann, Dr. K. Eckert, Prof. Dr. Dagmar Bruss, Dr. L. Sanchez-Palencia, Klaus Osterloh, Carsten Luckmann and Alex Cojuhovski and all the group members of Prof. Dr. W. Ertmer of the IQO of the University of Hannover for the many discussions we have had over the years. I am also grateful to all the employees of the ITP of the same University where I have been hosted during my study for their continuous cooperations and sense of friendship. Particularly Dr. Philip Hyllus, who has introduced me with Prof. Lewenstein, my supervisor, and shared with me a room for more than a year, and Klaus Osterloh who have been on my side on my occasions, were and are very special for me and I would like to applaud them for their interesting sociability and sense of humor.

I would like also to express my gratitude to the group members of Prof. M. Lewenstein at the ICFO, and to the group members and colleagues of Prof. A. Sanpera at the IFAE, both in Barcelona, Spain, for their cordial reception during my frequent visits to Barcelona. My visit to Barcelona was not only an academic one but also I have had experienced a very great joy and special memory to the city and its friendly weather which resembles in many ways to that of my home town Adigart in Northern Ethiopia where I was born and grown up.

I am very much thankful Dr. Fesseha Kassahun, my former advisor during my MSc. study, for helping me quite a lot to be prepared to this stage. I am also thankful to Prof. Dr. J. Dalibard and former members of his group, Dr. C. Roos and Prof. Dr. D. Guéry-Odelin for their generosity to give me their molecular dynamics code which I have used it as a basis for the molecular dynamics simulation.

My special thanks are for Frau Christel Franko and her husband Dr. Wolfgang Franko for their hospitality and their friendship. Mrs. Franko was my special tutor on different social issues particularly during my early time in the Institute.

On the financial aspect, which was very important for me, and all the aspects associated with my and my family's travel to Germany I am sincerely thankful and grateful to the Deutscher Akademischer Austausch Dienst (DAAD). The DAAD is for me a highly efficient and respected organisation. It was not only covering all my expenses but also was very flexible to entertain almost all my demands all over the time. I am specially particularly highly indebted to Frau Vera Osnski of the DAAD for her unreserved efforts to facilitate the visa to my family which was very crucial for me. I also

acknowledged the financial support from the Institute of Theoretical Physics of the University of Hannover during the last year of my PhD. In this regard I am highly indebted to my Supervisor and Prof. Dr. Dragon, director of the Institute.

I would like as well to thank my home University, the Mekelle University, for granting me a study leave during my stay here for my studies.

Last but not the least, I would like to thank my beloved wife Mulu Hailu and my daughters Meaza and Eden for accompanying me all the years and provided me all what was necessary for me, my parents and my friends for their moral assistance all over the time.

Alem Mebrahtu,  
October 2006, Hannover Germany



# Appendix E

## Dedication

I dedicate this work to my beloved wife Mulu, our daughters Meaza and Eden. Mulu has been incredibly supportive all the time and rendering me and of course our children endless help that we were in need of. Our kids were also the source of my pleasure and recreation. Their wonderful performances in the new German school by quickly and easily coping to the new language and environment was something that has made me proud of them and was energising me all the time particularly when they did come with excellent results in their exams. It was not an easy task to master the language in such a short time and both to be able join the best school in the German education system: The Gymnasium School.



# Appendix F

## List of Publications

1. V. Ahufinger, A. Mebrahtu, R. Corbalán, A. Sanpera, Quantum Switches and Memories for Matter Wave Lattice Solitons (submitted to New Journal of Physics).
2. A. Mebrahtu, A. Sanpera, M. Lewenstein, Splitting and Merging an Elongated Bose-Einstein Condensate at Finite Temperature, Phys. Rev. A **73**, 033601 (2006).
3. A. Mebrahtu, Parametric Oscillation with Squeezed Vacuum Reservoirs, J. Mod. Opt. **52**, 813 (2005).



# Appendix G

## Curriculum Vitae

### Personal data

Name	Alem Mebrahtu Tesfamariam
Date of Birth	28.03.1969
Place of Birth	Adigrat, Tigray, Ethiopia
Family Status	Married and have two dependents
Address	Hannover, Germany

### Education

Since 2003	PhD Student at ITP University of Hannover under the supervision of Prof. Dr. Maciej Lewenstein and Prof. Dr. Anna Sanpera Title: “Fluctuations in Quantum Optical Systems: From Bose-Einstein Condensates to Squeezed States of Light”
Apr 2002-Jan 2003	PhD Student at ITP University of Hannover
1997-1998	Master of Science in Physics (Quantum Optics), Addis Ababa University, Addis Ababa , Ethiopia
1986-1990	Bachelor of Science in Physics, Addis Ababa University, Addis Ababa , Ethiopia
1980-1986	High School (Agazi Comprehensive Secondary School, Adigrat, Ethiopia)
1975-1980	Primary School (Agoro Elementary School, Adigrat, Ethiopia)

## Working Experience

- 1998-2001 Physics Lecturer, at Mekelle University, Tigray, Ethiopia  
1993-1996 Science Radio Program Producer and Coordinator,  
Tigray Education Bureau, Ethiopia  
1990-1993 Physics High School teacher at different schools and  
states in Ethiopia

## Grants awarded

Oct 2001-Jun 2006 Deutsche Akademischer Austausch Dinst: DAAD

## Memberships

Ethiopian Physical Society  
German Physical Society (DPG)

# Bibliography

- [1] A. Anderson and J. J. Halliwell, *Phys. Rev. D* **48**, 2753 (1993).
- [2] J. J. Sakurai, *Modern Quantum Mechanics*, Addison-Wesley, New York (1994).
- [3] M. G. Raymer, *Amer. J. Phys.* **62**, 986 (1994).
- [4] C. Fabre 1997 *Quantum Fluctuations* ed S. Reynaud, E. Giacobino, and J Zinn-Justin (Amsterdam: North-Holland) p 181.
- [5] M. H. Anderson, J. R. Ensher, M. R. Mathews, C. E. Wieman, and E. A. Cornell, *Science* **269**, 198 (1995).
- [6] K. B. Davis, M. O. Mewes, M. R. Andrews, N. J. van Druten, D. S. Durfee, D. M. Kurn, and W. Ketterle, *Phys. Rev. Lett.* **75**, 3969 (1995).
- [7] C. C. Bradley, C. A. Sackett, J. J. Tollett, and R. G. Hulet, *Phys. Rev. Lett.* **75**, 1687 (1995).
- [8] D. F. Walls, *Nature* **306**, 141 (1983).
- [9] R. E. Slusher, B. Yurke, P. Grangier, A. Laporta, D. F. Walls, and M. Reid, *J. opt. Soc. Am.* **B4**, 1453 (1987).
- [10] L. Wu, H. J. Kimble, J. L. Hall, and H. Wu, *Phys. Rev. Lett.* **57**, 2520 (1986).
- [11] R. E. Slusher, L. W. Hollberg, B. Yurke, J. C. Mertz, and J. F. Valley, *Phys. Rev. Lett.* **55**, 2409 (1985).
- [12] C. W. Gardiner, 1991, *Quantum Noise* (Berlin: Springer-Verlag).
- [13] J. Oh and G. Ahlers, *Phys. Rev. Lett.* **91**, 094501 (2003).
- [14] D. Abbotta, *Chaos*, **11**, 526 (2001).

- 
- [15] P. D. Drummond, K. Dechoum, and S. Chaturvedi, *Phys. Rev. A* **65**, 033806 (2002).
- [16] K. Dechoum, P. D. Drummond, S. Chaturvedi, and M. D. Reid, *Phys. Rev. A* **70**, 053807 (2004).
- [17] S. Dettmer, D. Hellweg, P. Ryytty, J. J. Arlt, W. Ertmer, K. Sengstock, D. S. Petrov, G. V. Shlyapnikov, H. Kreutzmann, L. Santos, and M. Lewenstein, *Phys. Rev. Lett.* **87**, 160406 (2001).
- [18] H. D. Politzer, *Phys. Rev. A* **54**, 5048 (1996).
- [19] M. Gajda and K. Rzazewski, *Phys. Rev. Lett.* **78**, 2686 (1997).
- [20] S. Giorgini, L. P. Pitaevskii, and S. Stringari *Phys. Rev. Lett.* **80**, 5040 (1998).
- [21] Z. Idziaszek, M. Gajda, P. Navez, M. Wilkens, and K. Rzazewski *Phys. Rev. Lett.* **82**, 4376 (1999).
- [22] R. Graham, *Phys. Rev. A* **62**, 023609 (2000).
- [23] D. Hellweg, S. Dettmer, P. Ryytty, J. J. Arlt, W. Ertmer, K. Sengstock, D. S. Petrov, G. V. Shlyapnikov, H. Kreutzmann, L. Santos, and M. Lewenstein, *Appl. Phys. B: Lasers Opt.* **73**, 781 (2001).
- [24] D. S. Petrov, G. V. Shlyapnikov, and J. T. M. Walraven, *Phys. Rev. Lett.* **87**, 050404 (2001).
- [25] L. Pitaevskii and S. Stringari, *Phys. Rev. Lett.* **87**, 180402 (2001).
- [26] S. Richard, F. Gerbier, J. H. Thywissen, M. Hugbart, P. Bouyer, and A. Aspect, *Phys. Rev. Lett.* **91**, 010405 (2003).
- [27] A. Yu. Cherny, *Phys. Rev. A* **71**, 043605 (2005).
- [28] Z. Idziaszek, *Phys. Rev. A* **71**, 053604 (2005).
- [29] D. C. Roberts and Y. Pomeau, *cond-mat/0503757* (2005).
- [30] R. Gati, B. Hemmerling, J. Fölling, M. Albiez, and M. K. Oberthaler, *Phys. Rev. Lett.* **96**, 130404 (2006).
- [31] N. D. Mermin and H. Wagner, *Phys. Rev. Lett.* **22**, 1133 (1966).
- [32] P. C. Hohenberg, *Phys. Rev.* **158**, 383 (1967).

- 
- [33] M. Greiner, O. Mandel, T. Esslinger, T. W. Hänsch, and I. Bloch, *Nature (London)* **415**, 39 (2002).
- [34] K. A. Milton, *J. Phys. A* **37**, 209(R) (2004).
- [35] H. J. Carmichael and H. Nha *J. Opt. B: Quantum Semiclass. Opt.* **6** S645 (2004).
- [36] H. B. G. Casimir, *Proc. Kon. Ned. Akad. Wet.* **51**, 793 (1948).
- [37] S. Lamoreaux, *Phys. Rev. Lett.* **78**, 5 (1997).
- [38] L. Pitaevskii and S. Stringari, *Phys. Rev. Lett.* **81**, 4541 (1999).
- [39] J. M. Vogels, K. Xu, and W. Ketterle, *Phys. Rev. Lett.* **89**, 020401 (2002).
- [40] G. A. Bird, *Molecular Gas Dynamics and the Direct Simulation of Gas Flow*, Clarendon, Oxford (1994).
- [41] H. Wu and C. Foot, *J. Phys. B*, **29** L321 (1996).
- [42] D. Guéry-Odelin, J. Söding, P. Desbiolles, and J. Dalibard, *Optics Express* **2**, 323 (1998).
- [43] C. F. Roos, P. Cren, D. Guéry-Odelin, and J. Dalibard, *Europhys. Lett.* **61**, 187 (2003).
- [44] Y. Castin, J. I. Cirac, and M. Lewenstein, *Phys. Rev. Lett.* **80**, 5305 (1998).
- [45] T. W. Hänsch and A. L. Schawlow, *Opt. Commun.* **13**, 68 (1975).
- [46] H. J. Metcalf and P. van der Straten, 1999, *Laser Cooling and Trapping* (New York: Springer-Verlag).
- [47] S. Stenholm, *Rev. Mod. Phys.* **58**, 699 (1986).
- [48] V. S. Letokhov and V. G. Minogin, *Phys. Rep.* **73** 1 (1981).
- [49] J. Dalibard and C. Cohen-Tannoudji, Laser cooling below the Doppler limit by polarization gradients: simple theoretical models, *J. Opt. Soc. Am. B* **6** (1989) 2023.
- [50] R. Grimm, M. Weidemüller, and Yu. B. Ovchinnikov, *Adv. At. Mol. Opt. Phys.* **42**, 95 (2000).

- 
- [51] A. L. Migdall, J. V. Prodan, W. D. Phillips, T. H. Bergeman, and H. J. Metcalf, Phys. Rev. Lett. **54**, 2596 (1985).
- [52] E. L. Raab, M. Prentiss, A. Cable, S. Chu, and D. E. Pritchard, Phys. Rev. Lett. **59**, 2631 (1987); S. Loutzenheiser and C. E. Wieman, Opt. Lett. **21**, 290 (1996).
- [53] L. Santos, On Laser-driven Ultracold Atomic Samples, Universidad De Salamanca, PhD Thesis (unpublished) (1998).
- [54] H. F. Hess, Phys. Rev. B **34**, 3476 (1986).
- [55] W. Ketterle and N.J. van Druten, Adv. At. Mol. Opt. Phys. **37**, 181 (1996).
- [56] O. J. Luiten, M. W. Reynolds, and J. T. M. Walraven, Phys. Rev. A **53**, 381 (1996).
- [57] E. Carboneschi, C. Menchini, and E. Arimondo, Phys. Rev. A **62**, 0136061 (2000).
- [58] S. Boussen, N. Hoang, S. Guibal, N. Zahzam, L. Pruvost, D. Marescaux, J. Pinard, and P. Pillet, Eur. Phys. J. D **28**, 259 (2004).
- [59] We have reproduced the analytical results shown by Roos *et al.* [43] and plotted them in Figs. 2.3(a), 2.4(a) and 2.5(a) in order to verify that the  $U_{rad}/k_B = 274\mu\text{K}$  is the optimal transverse trap depth. Our work differs from them in that we have additionally carried out simulations on the time evolution of  $N(t)$ ,  $T(t)$ ,  $\text{PSD}(t)$ ; and  $\eta_{rad}(t)$  and  $\eta_{ax}(t)$  among others.
- [60] S. Inouye, M. R. Andrews, J. Stenger, H.-J. Miesner, D. M. Stamper-Kurn, and W. Ketterle, Nature (London) **392**, 151 (1998).
- [61] M. Lewenstein, Li You, J. Cooper, and K. Burnett, Phys. Rev. A **50** 2207 (1994).
- [62] C. J. Pethick and S. Smith, 2002, Bose-Einstein Condensation in Dilute Gases, (Cambridge University Press, UK).
- [63] W. Ketterle, Rev. Mod. Phys. **74**, 1131 (2004).
- [64] S. N. Bose, Z. Phys. **26**, 178 (1924).
- [65] A. Einstein, Sitzungsberichte der Preussische Akademie der Wissenschaften Physikalisch-mathematische Klasse 261 (1925).

- 
- [66] F. London, *Phys. Rev.* **54**, 947 (1938).
- [67] K. Darrow, *Rev. Mod. Phys.* **12**, 257 (1940).
- [68] A. J. Leggett, *Rev. Mod. Phys.* **71** S318 (1999).
- [69] C. E. Hecht, *Physica* **25**, 1159 (1959).
- [70] D. G. Fried, T. C. Killian, L. Willmann, D. Landhuis, S. C. Moss, D. Kleppner, and T. J. Greytak, *Phys. Rev. Lett.* **81**, 3811 (1998).
- [71] S. L. Cornish, N. R. Claussen, J. L. Roberts, E. A. Cornell, and C. E. Wieman, *Phys. Rev. Lett.* **85**, 1795 (2000).
- [72] A. Robert, O. Sirjean, A. Browaeys, J. Poupard, S. Nowak, D. Boiron, C. I. Westbrook, and A. Aspect, *Science* **292**, 461 (2001).
- [73] G. Modugno, G. Ferrari, G. Roati, R. J. Brecha, A. Simoni, and M. Inguscio, *Science* **294**, 1320 (2001).
- [74] T. Weber, J. Herbig, M. Mark, H. Nägerl, and R. Grimm *Science* **299**, 232 (2003).
- [75] Y. Takasu, K. Maki, K. Komori, T. Takano, K. Honda, M. Kumakura, T. Yabuzaki, and Y. Takahashi, *Phys. Rev. Lett.* **91**, 040404 (2003).
- [76] A. Griesmaier, J. Werner, S. Hensler, J. Stuhler, and T. Pfau, *Phys. Rev. Lett.* **94**, 160401 (2005).
- [77] S. Jochim, M. Bartenstein, A. Altmeyer, G. Hendl, S. Riedl, C. Chin, J. H. Denschlag, and R. Grimm, *Science* **302**, 2101 (2003).
- [78] M. Greiner, C. A. Regal, and D. S. Jin, *Nature (London)*, **426**, 537 (2003).
- [79] L. P. Pitaevskii, *Sov. Phys.-JETP* **13**, 451 (1961).
- [80] E. P. Gross. *Nuovo Cimento* **20**, 454 (1961).
- [81] E. P. Gross, *J. Math. Phys.* **4**, 195 (1963).
- [82] A. Griffin, *Phys. Rev. B* **53**, 9341 (1995).
- [83] K. Huang, *J. Res. Natl. Inst. Stand. Technol.* **101**, 435 (1996).
- [84] N. N. Bogoliubov, *J. Phys. USSR* **11**, 23 (1947).

- 
- [85] R. Wynar, R. S. Freeland, D. J. Han, C. Ryu, and D. J. Heinzen, *Science* **287**, 1016 (2000).
- [86] M. W. Zwierlein, C. A. Stan, C. H. Schunck, S. M. F. Raupach, S. Gupta, Z. Hadzibabic, and W. Ketterle, *Phys. Rev. Lett.* **91**, 250401 (2003).
- [87] S. Dürr, T. Volz, A. Marte, and G. Rempe, *Phys. Rev. Lett.* **92**, 020406, (2004).
- [88] V. A. Yurovsky and A. Ben-Reuven, *Phys. Rev. A* **72**, 053618 (2005).
- [89] C. A. Regal, M. Greiner, and D. S. Jin, *Phys. Rev. Lett.* **92**, 040403 (2004).
- [90] M. Köhl, T. W. Hansch, and T. Esslinger, *Phys. Rev. A* **65**, 021606(R) (2002).
- [91] P. W. H. Pinkse, T. Fischer, P. Maunz, and G. Rempe, *Nature (London)* **404**, 365 (2000).
- [92] A. P. Chikkatur, Y. Shin, A. E. Leanhardt, D. Kielpinski, E. Tsikata, T. L. Gustavson, D. E. Pritchard, and W. Ketterle, *Science* **296**, 2193 (2002).
- [93] T. H. Maiman, *Nature (London)* **187**, 493 (1960).
- [94] W. Yi and L.-M. Duan, *Phys. Rev. A* **72**, 043607 (2005).
- [95] Z. Hadzibabic, S. Stock, B. Battelier, V. Bretin, and J. Dalibard, *Phys. Rev. Lett.* **93**, 180403 (2004).
- [96] Y. Shin, M. Saba, T. A. Pasquini, W. Ketterle, D. E. Pritchard, and A. E. Leanhardt, *Phys. Rev. Lett.* **92**, 050405 (2004).
- [97] L. Pezzé, L. A. Collins, A. Smerzi, G. P. Berman, and A. R. Bishop, *Phys. Rev. A* **72**, 043612 (2005).
- [98] T. Schumm, S. Hofferberth, L. M. Andersson, S. Wildermuth, S. Groth, I. Bar-Joseph, J. Schmiedmayer, and P. Krüger, *Nature* **1**, 57 (2005).
- [99] J. Javanainen and M. Wilkens, *Phys. Rev. Lett.* **78**, 4675 (1997).
- [100] A. J. Leggett and F. Sols, *Phys. Rev. Lett.* **81**, 1344 (1998).
- [101] B. Paredes, A. Widera, V. Murg, O. Mandel, S. Fölling, I. Cirac, G. V. Shlyapnikov, T. W. Hansch, and I. Bloch, *Nature* **429**, 277 (2004).

- [102] T. Kinoshita, T. Wenger, and D. S. Weiss, *Science* **305** 1125 (2004).
- [103] D. S. Petrov, G. V. Shlyapnikov, and J. T. M. Walraven, *Phys. Rev. Lett.* **85**, 3745 (2000).
- [104] A. Görlitz, J. M. Vogels, A. E. Leanhardt, C. Raman, T. L. Gustavson, J. R. Abo-Shaeer, A. P. Chikkatur, S. Gupta, S. Inouye, T. Rosenband, and W. Ketterle, *Phys. Rev. Lett.* **87**, 130402 (2001).
- [105] W. Ketterle and N. J. van Druten, *Phys. Rev. A* **54**, 656 (1996).
- [106] H. Moritz, T. Stöferle, M. Köhl, and T. Esslinger, *Phys. Rev. Lett.* **91**, 250402 (2003).
- [107] T. Stöferle, H. Moritz, C. Schori, M. Köhl, and T. Esslinger, *Phys. Rev. Lett.* **92**, 130403 (2004).
- [108] A. I. Safonov, S. A. Vasilyev, I. S. Yasnikov, I. I. Lukashevich, and S. Jaakkola, *Phys. Rev. Lett.* **81**, 4545 (1998).
- [109] D. S. Petrov, M. Holzmann, and G. V. Shlyapnikov, *Phys. Rev. Lett.* **84**, 2551 (2000).
- [110] Yu. Kagan, V. A. Kashurnikov, A. V. Krasavin, N. V. Prokof'ev, and B. V. Svistunov, *Phys. Rev. A* **61**, 43608 (2000).
- [111] L. Pitaevskii and S. Stringari, 2003, *Bose-Einstein Condensation*, (Oxford Science Publications, London).
- [112] M. Girardeau, J., *Math. Phys.* **1**, 156 (1960); *Phys. Rev.* **139**, B500 (1965).
- [113] C. Menotti and S. Stringari, *Phys. Rev. A* **66**, 043610 (2002).
- [114] K. V. Kheruntsyan, D. M. Gangardt, P. D. Drummond, and G. V. Shlyapnikov, *Phys. Rev. Lett.* **91**, 040403 (2003).
- [115] P. Pedri and L. Santos, *Phys. Rev. Lett.* **91**, 110401 (2003).
- [116] F. Gerbier, J. H. Thywissen, S. Richard, M. Hugbart, P. Bouyer, and A. Aspect, *Phys. Rev. A* **67**, 051602(R) (2003).
- [117] H. Kreutzmann, A. Sanpera, L. Santos, M. Lewenstein, D. Hellweg, L. Cacciapuoti, M. Kottke, T. Schulte, K. Sengstock, J. J. Arlt, and W. Ertmer, *Appl. Phys. B: Lasers Opt.* **76**, 165 (2003).

- 
- [118] F. Dalfovo, S. Giorgini, L. P. Pitaevskii, and S. Stringari, *Rev. Mod. Phys.* **71**, 463 (1999).
- [119] M. J. Davis, R. J. Ballagh, and K. Burnett, *J. Phys. B* **34**, 4487 (2001).
- [120] D. Kadio, M. Gajda, and K. Rzążewski, *Phys. Rev. A* **72**, 013607 (2005).
- [121] M. J. Davis, S. A. Morgan, and K. Burnett, *Phys. Rev. Lett.* **87**, 160402 (2001).
- [122] M. J. Davis, S. A. Morgan, and K. Burnett, *Phys. Rev. A* **66**, 053618 (2002).
- [123] M. J. Davis and S. A. Morgan, *Phys. Rev. A* **68**, 053615 (2003).
- [124] M. Brewczyk, P. Borowski, M. Gajda, and K. Rzążewski, *J. Phys. B* **37**, 2725 (2004).
- [125] K. Góral, M. Gajda, and K. Rzążewski, *Opt. Express* **8**, 92 (2001).
- [126] K. Góral, M. Gajda, and K. Rzążewski, *Phys. Rev. A* **66**, 051602(R) (2002).
- [127] H. Schmidt, K. Góral, F. Floegel, M. Gajda, and K. Rzążewski, *J. Opt. B: Quantum Semiclassical Opt.* **5**, S96 (2003).
- [128] R. Bach and K. Rzążewski, *Phys. Rev. A* **70**, 063622 (2004).
- [129] R. Bach and K. Rzążewski, *Phys. Rev. Lett.* **92**, 200401 (2004).
- [130] E. Altman, E. Demler, and M. D. Lukin, *Phys. Rev. A* **70**, 013603 (2004).
- [131] M. Olshanii, *Phys. Rev. Lett.* **81**, 938 (1998).
- [132] Y. Shin, C. Sanner, G. B. Jo, T. A. Pasquini, M. Saba, W. Ketterle, D. E. Pritchard, M. Vengalattore, and M. Prentiss, *Phys. Rev. A* **72**, 021604(R) (2005).
- [133] S. I. Shevchenko, *Sov. J. Low. Temp. Phys.* **18**, 223 (1992).
- [134] For a recent review see for instance, O. Morsch, and M. Oberthaler, *Rev. Mod. Phys.* **78**, 179 (2006); V. A. Brazhnyi and V. V. Konotop, *Mod. Phys. Lett. B* **18**, 627 (2004).

- [135] For reviews see for instance, I. Bloch, and M. Greiner, *Adv. At. Molec. Opt. Phys.* **52**, 1 (2005); M. Lewenstein, A. Sanpera, V. Ahufinger, B. Damski, A. Sen, and U. Sen, cond-mat/0606771 (2006).
- [136] L. Khaykovich, F. Schreck, G. Ferrari, T. Bourdel, J. Cubizolles, L. D. Carr, Y. Castin, and C. Salomon, *Science* **296**, 1290 (2002).
- [137] K. E. Strecker, G. B. Partridge, A. G. Truscott, and R. G. Hulet, *Nature* **417**, 150 (2002).
- [138] S. Burger, K. Bongs, S. Dettmer, W. Ertmer, K. Sengstock, A. Sanpera, G. V. Shlyapnikov, and M. Lewenstein, *Phys. Rev. Lett.* **83**, 5198 (1999).
- [139] J. Denschlag, J. E. Simsarian, D. L. Feder, C. W. Clark, L. A. Collins, J. Cubizolles, L. Deng, E. W. Hagley, K. Helmerson, W. P. Reinhardt, S. L. Rolston, B. I. Schneider, and W. D. Phillips, *Science* **287**, 97 (2000).
- [140] V. A. Brazhnyi, V. V. Konotop, and L. P. Pitaevskii *Phys. Rev. A* **73**, 053601 (2006).
- [141] B. Eiermann, Th. Anker, M. Albiez, M. Taglieber, P. Treutlein, K.-P. Marzlin, and M. K. Oberthaler, *Phys. Rev. Lett.* **92** 230401 (2004).
- [142] O. Zobay, S. Pötting, P. Meystre, and E. M. Wright, *Phys. Rev. A* **59**, 643 (1999).
- [143] A. Trombettoni and A. Smerzi, *Phys. Rev. Lett.* **86**, 2353 (2001).
- [144] V. Ahufinger, A. Sanpera, P. Pedri, L. Santos, and M. Lewenstein, *Phys. Rev. A* **69**, 053604 (2004).
- [145] V. Ahufinger and A. Sanpera, *Phys. Rev. Lett.* **94**, 130403 (2005).
- [146] F. Kh. Abdullaev, B. B. Baizakov, S. A. Darmanyan, V. V. Konotop, and M. Salerno, *Phys. Rev. A* **64**, 043606 (2001).
- [147] P. J. Y. Louis, E. A. Ostrovskaya, C. M. Savage, and Y. S. Kivshar, *Phys. Rev. A* **67**, 013602 (2003).
- [148] H. Sakaguchi and B. A. Malomed, *J. Phys. B: Mol. Opt. Phys.* **37**, 1443 (2004).
- [149] P. J. Y. Louis, E. A. Ostrovskaya, and Y. S. Kivshar, *J. Opt. B: Quantum Semiclass. Opt.* **6**, S309 (2004).

- 
- [150] B. B. Baizakov, V. V. Konotop, and M. Salerno, *J. Phys. B: At. Mol. Opt. Phys.* **35**, 5105 (2002).
- [151] E. A. Ostrovskaya and Y. S. Kivshar, *Phys. Rev. Lett.* **90**, 160407 (2003).
- [152] B. B. Baizakov, B. A. Malomed, and M. Salerno, *Europhys. Lett.* **63**, 642 (2003).
- [153] H. Sakaguchi and B. A. Malomed, *J. Phys. B: Mol. Opt. Phys.* **37**, 2225 (2004).
- [154] A. M. Dudarev, R. B. Diener, and Q. Niu, *J. Opt. B: Quantum Semi-class. Opt.* **6** S231 (2004).
- [155] V. A. Brazhnyi, V. V. Konotop, and V. Kuzmiak, *Phys. Rev. A* **70**, 043604 (2004).
- [156] P. J. Y. Louis, E. A. Ostrovskaya, and Y. S. Kivshar, *Phys. Rev. A* **71**, 023612 (2005).
- [157] P. G. Kevrekidis, D. J. Frantzeskakis, R. Carretero-González, B. A. Malomed, G. Herring, and A. R. Bishop, *Phys. Rev. A* **71**, 023614 (2005).
- [158] M. A. Porter, P. G. Kevrekidis, R. Carretero-González, and D. J. Frantzeskakis, *Phys. Lett. A* **352** 210 (2006).
- [159] V. A. Brazhnyi, V. V. Konotop, and V. M. Pérez-García, *Phys. Rev. Lett.* **96**, 060403 (2006).
- [160] J. Cuevas, B. A. Malomed, and P. G. Kevrekidis, *Phys. Rev. E* **71**, 066614 (2005).
- [161] F. Kh. Abdullaev and J. Garnier, *Phys. Rev. A* **72**, 061605 (2005).
- [162] Y. S. Kivshar and B. A. Malomed, *Rev. Mod. Phys.* **61**, 763 (1989).
- [163] R. Balakrishnan, *Phys. Rev. A* **32**, 1144 (1985).
- [164] Y. S. Kivshar, A. M. Kosevich, and O.A. Chubykalo, *Phys. Lett. A* **125**, 35 (1987).
- [165] D. I. Pushkarov and R. D. Atanasov, *Phys. Lett. A* **149**, 287 (1990).
- [166] X. D. Cao and B. A. Malomed, *Phys. Lett. A* **206**, 177 (1995).

- 
- [167] R. H. Goodman, P. J. Holmes, and M. I. Weinstein, *Physica D* **192**, 215 (2004).
- [168] V. V. Konotop, D. Cai, M. Salerno, A. R. Bishop, and N. G.-Jensen, *Phys. Rev. E* **53**, 6476 (1996).
- [169] R. H. Goodman, R. E. Slusher, M. I. Weinstein, *J. Opt. Soc. Am. B* **19**, 1635 (2002).
- [170] K. Forinash, M. Peyrard, and B. malomed, *Phys. Rev. E* **49**,3400 (1994).
- [171] H. Frauenkron and P. Gassberger, *Phys. Rev. E* **53**, 2823 (1996).
- [172] K. T. Stoychev, M. T. Primatarowa, and R. S. Kamburova, *Phys. Rev. E* **70**, 066622 (2004).
- [173] M. T. Primatarowa, K. T. Stoychev, and R. S. Kamburova, *Phys. Rev. E* **72**, 036608 (2005).
- [174] D. J. Frantzeskakis, G. Theocharis, F. K. Diakonov, P. Schmelcher, and Y. S. Kivshar, *Phys. Rev. A* **66**, 053608 (2002).
- [175] G. Herring, P. G. Kevrekidis, R. Carretero-González, B. A. Malomed, D.J. Frantzeskakis, and A. R. Bishop, *Phys. Lett. A* **345**, 144 (2005).
- [176] C. Lee and J. Brand, *Europhys. Lett.* **73**, 321 (2006).
- [177] J. Garnier and F. Abdullaev, *cond-mat/0605261* (2006).
- [178] R. Loudon, and P. L. Knight, *J. Mod. Opt.* **34**, 709 (1987).
- [179] M. I. Kolobov, *Rev. Mod. Phys.* **71**, 1539 (1999).
- [180] V. V. Dodonov, *J. Opt. B: Quantum Semiclass. Opt.* **4**, 1 (2002).
- [181] V. Buzek and P. L. Knight, *Opt. Commun.* **81**, 331 (1991).
- [182] P. Meystre and M. Sargent III, 1999, *Elements of quantum optics*, 2<sup>ed</sup> ed. (Berlin: Springer-Verlag).
- [183] W. P. Schleich, 2001, *Quantum optics in phase space* (Berlin: WILEY-VCH Verlag GmbH).
- [184] D. F. Walls and G. J. Milburn, 1991, *Quantum Optics* (Berlin: Springer-Verlag).

- 
- [185] S. J. Carter, P. D. Drummond, M. D. Reid, and R. M. Shelby, *Phys. Rev. Lett.* **58**, 1841 (1987).
- [186] H. Takahashi, 1965, in *Advances in Communication Systems: Theory and Applications*, edited by A. V. Balakrishnan (New York: Academic Press), Vol. **1**, p. 227.
- [187] J. Anwar and M. S. Zubairy, *Phys. Rev. A* **45**, 1804 (1992).
- [188] J. J. Slosser and G. J. Milburn, *Phys. Rev. A* **50**, 793 (1994).
- [189] K. J. McNeil, *Phys. Rev. A* **28**, 1560 (1983).
- [190] W. J. Munro and M. D Reid, *Quantum Opt.* **4**, 181 (1992).
- [191] L. Wu, M. Xia, H. J. Kimble, *J. opt. Soc. Am.* **B4**, 1465 (1987).
- [192] M. Raginsky and P. Kumar, *J. Opt. B: Quantum Semiclass. Opt.* **3**, 1 (2001).
- [193] C. M. Caves, K. S. Thorne, R. W. P. Drever, V. D. Sandberg, and M. Zimmermann, *Rev. Mod. Phys.* **52**, 341 (1980).
- [194] A. Abramovici, W. E. Althouse, R. W. P. Drever, Y. Gursel, S. Kawamura, F. J. Raab, D. Shoemaker, L. Sievers, R. E. Spero, K. S. Thorne, R. E. Vogt, R. Weiss, S. E. Whitcomb, M. E. Zucker, *Science* **256**, 325 (1992).
- [195] J. Harms, Y. Chen, S. Chelkowski, A. Franzen, H. Vahlbruch, K. Danzmann, and R. Schnabel, *Phys. Rev. D* **68**, 042001 (2003).
- [196] R. Schnabel, J. Harms, K. A. Strain, and K. Danzmann, *Classical Quant. Grav.* **25**, 1045 (2004).
- [197] C. M. Caves *Phys. Rev. D* **23**, 1693 (1981).
- [198] M. Xiao, L. A. Wu, and H. J. Kimble, *Phys. Rev. Lett.* **59**, 278 (1987).
- [199] E. S. Polzik, J. Carri, and H. J. Kimble, *Phys. Rev. Lett.* **68**, 3020 (1992).
- [200] R. J. Glauber, *Phys. Rev.* **131**, 2766 (1963).
- [201] A. Wunsche, *J. Opt. B: Quantum. Semiclass. Opt.* **6**, 159 (2004).
- [202] K. Fesseha, *J. Math. Phys.* **33**, 2179 (1992).

# Index

- $^{87}\text{Rb}$  ..... v, 6, 9, 29, 41, 54
- 1D-BEC ..... 32
  - splitting and merging
    - at T finite ..... 46
    - at T=0 ..... 44
- adiabatic splitting and merging 45
- anisotropic trap ..... 6
- anti-normal operator ordering . 84,  
85
- approximation
  - Markov ..... 70
  - mean-field ..... 32
  - Thomas-Fermi ..... 35
  - weak coupling ..... 69
- aspect ratio ..... 39
- atom laser ..... 51
- atomic trapping ..... 9
- BdG ..... *see* equation, 40
- BEC ..... 2, 6
  - 1D
    - splitting and merging .37, 93
  - elongated ..... 37
  - low-D ..... 38
- Bose ..... 29
- Bose gas ..... 24, 34, 39
- Bose-Einstein Condensation
  - see* BEC ..... 23
- Bose-Einstein distribution function ..... 24
- coherence ..... 41
- coherence length ..... 38
- coherent state ..... 2, 3, 5, 67
- commutation relation ..... 31
- condensate ..... *see* BEC
  - quasi ..... 39
- coupling constant
  - 1D BEC ..... 36, 41, 54
  - 3D BEC ..... 31
- de Broglie wavelength ..... 2, 30
- density fluctuations ..... 48
- Dirac delta function ..... 71
- DPO ..... 82, 83
- Einstein ..... 29
- equation
  - Bogoliubov-de Gennes .. 33, 95
  - Fokker-Planck ..... 74, 75
  - Gross-Pitaevskii ..... 32, 33
  - master ..... 68, 73, 94
- evaporative cooling ... 9, 19, 37, 93
- Feshbach resonance ..... 23
- fluctuations ..... 1
  - quantum .... 1–4, 6, 39, 67, 93
  - thermal ..... 1, 3, 5, 39
  - vacuum ..... 1, 6
- GPE ..... *see* equation, 40
  - 1D-BEC ..... 41, 54
- harmonic oscillator ..... 27
- Initial 1D BEC ..... 44
- isothermal process ..... 38
- Jacobi transformation ..... 80
- Kronecker delta symbol ..... 70

- 
- laser cooling ..... 9
  - macro-atom ..... 13
  - magnetic trap ..... 10
  - mean-field theory ..... 30
  - Merged 1D BEC ..... 44
  - minimum uncertainty state ..... 5
  - molecular dynamics ..... 12, 93
  - molecular dynamics simulation . 12
  - NDPO ..... 7, 68, 72, 87
  - noise ..... 67
  - non-linear crystal ..... 68, 73
  - nonclassical states of light ..... 67
  - normal operator ordering ..... 74
  - order parameter ..... 33
  - parametric amplifier
    - degenerate ..... 67, 91
    - non-degenerate .. 67, 82, 90, 91
  - parametric oscillator
    - degenerate ..... 82, 86, 91
    - non-degenerate ..... 68, 91
  - phase fluctuations ..... 48
  - phase space density .. 9, 16, 21, 93
  - phase transition ..... 23
    - classical ..... 4
    - quantum ..... 6
  - photon number distribution .... 91
  - potential
    - barrier ..... 66
    - double-well ..... 38, 42, 43
    - trapping ..... 30
    - well ..... 61, 63
  - propagator method ..... 76, 91
  - Q-function ..... 74, *see* NDPO
    - DPO ..... 82
    - initial ..... 80
    - NDPO ..... 81
    - propagator ..... 78, 80
  - quadrature squeezing ..... 83
    - DPO ..... 83
    - NDPO ..... 87
    - single-mode ..... 86
    - two-mode ..... 87
  - quantum
    - memory ..... 63, 66, 93
    - switch ..... 58, 66, 93
  - quantum fluctuations ..... *see* fluctuations
  - quantum phase transitions ..... 4
  - s-wave scattering length ..... 23
  - signal-idler modes ..... 72, 74, 94
  - solitons
    - bright ..... 53, 66
    - dark ..... 53
    - defect ..... 66
    - reflection ..... 60
    - transmission ..... 66
  - Split 1D BECs ..... 44
  - squeeze operator ..... 109
  - squeezed states ..... 1, 2, 4, 67, 94
  - squeezed vacuum reservoirs .... *see* USVR, 86
  - squeezed vacuum state ..... 5
  - squeezing parameter ..... 109
  - standard quantum limit .. 4, 67, 89
  - strong-field seeker ..... 11
  - temperature
    - absolute zero ..... 27
    - critical ..... 24, 27
    - degeneracy ..... 40
    - finite ..... 39
  - thermal fluctuations ..... *see* fluctuations
  - Thomas-Fermi radius ..... 42, 47
  - truncation parameters ..... 9
    - axial ..... 16
    - radial ..... 21
  - ultracold atomic gases ..... 4, 23

- 
- uncertainty principle 1, 3–5, 67, 91  
USVR ..... 68  
vacuum fluctuations ..... *see*  
    fluctuations  
vacuum state ..... 2, 80  
weak-field seeker ..... 11  
Zeeman sublevels ..... 10